SINGLE MOLECULE KINETICS IN FAMILIAL HYPERTROPHIC CARDIOMYOPATHY TRANSGENIC HEART

DISSERTATION

Presented to the Graduate Council of the

Graduate School of Biomedical Sciences

University of North Texas Health Science Center at Fort Worth

In Partial Fulfillment of the Requirements

For the Degree of

Doctor of Philosophy

By

Yalla Vara Prasad Mettikolla, M.S

Fort Worth, Texas

May 2010

ACKNOWLEDGEMENTS

I would like to thank my advisor, Dr. Julian Borejdo for his guidance and supervision during my research work. I sincerely pay my tribute to him for his patience in understanding and helping through out my PhD work. Apart from advisor, he is a great person with a friendly nature and warm smile. It is not exaggerating to say that with out his unwavering support it would have been difficult for me to reach this stage.

I sincerely acknowledge my committee members- Dr. Ignacy Gryczynski, Dr. Nils Calander and Dr. Douglas Root, as well as my university member, Dr. Robert Mallet for all their time and help. Their timely comments and healthy criticism helped to complete all the tasks in my PhD in a timely manner.

A special thanks to Dr. Jamboor K. Vishwanatha, former graduate advisor of biomedical sciences, for his support and advices during the initial stage of my PhD.

I would like to express my special gratitude to Dr. Priya Muthu, former gradate student in the laboratory. She is a gem of a personality with helping nature and continuous support during the tough times of my research work. Special thanks to Dr. Karol Gryczynski, Dr. Rafal Luchowski, Pabak Sarkar, Krishna Midde, Dr. Irina Akopova, Shashank Bharill and Amol Rajmane for their support the entire time. I am also grateful to Dr. Szczesna Cordary and her lab members for their readiness in providing us with samples and their helpful correspondence.

I want to take this opportunity to thank my parents for the unending support and unconditional love they showered on me throughout my life and especially during my PhD tenure. I would like to express my thanks to my sister and her family as well as my brother.

There is no better occasion than this to express my special gratitude to my wife, Anila for her unwavering support and patience.

I would like to thank all my friends who helped me through the tough times of my life.

Above all, I would like to thank God for blessing me in every step and giving me this opportunity to do my PhD.

TABLE OF CONTENTS

LIST OF ILLUSTRATIONS

Chapter I

Chapter III

Chapter IV

LIST OF TABLES

LIST OF ABBREVIATIONS

t_I – the time cross-bridge is unable to interact with actin

t_A – the time cross-bridge is able to interact with actin

t_{ON} – the time cross-bridge is strongly attached to actin

t_{OFF} – the time cross-bridge is detached from actin

Ψ – Duty Cycle of the cross-bridge

τ - Average fluorescence lifetime of actin

AP – Alexa488-Phalloidin

APD – Avalanche Photodiode

DTT -- Cleland's reagent

EDC -- 1-ethyl-3-(3'-dimethylaminopropyl) carbodiimide

FCS – Fluorescence Correlation Spectroscopy

FHC - Familial Hypertrophic Cardiomyopathy

HS – Half Sarcomere

RP – Rhodamine-Phalloidin

SMD – Single Molecule Detection

SPCE - Surface plasmon coupled emission

Tg-WT - Transgenic Wild Type

TIRFM - Total internal reflection fluorescence microscope

UP – Unlabeled-Phalloidin

PEER-REVIEWED PUBLICATIONS

Mettikolla P, Luchowski R, Calander N, Gryczynski I, Gryczynski Z and Borejdo J; Observing Cycling of a few Cross-bridge During Isometric Contraction of Skeletal Muscle. Cytoskeleton, 2010(In Press)

P.Mettikolla, R. Luchowski, I. Gryczynski, Z. Gryczynski, D. Szczesna-Cordary, and J. Borejdo; Fluorescence Lifetime of Actin in the Fhc TransgenicHeart. Biochemistry, 2009:48 (6), 1264-1271

P.Muthu,P.Mettikolla , R. Luchowski, I. Gryczynski, Z. Gryczynski, D. Szczesna-Cordary, and J. Borejdo; Single Molecule Kinetics in the Familial Hypertrophic Cardiomyopathy D166V Mutant Mouse Heart. J Mol Cell Cardiol. 2010 May;48(5):989-98

Mettikolla P, R. Luchowski, I. Gryczynski, Z. Gryczynski, D. Szczesna-Cordary, and J. Borejdo; Faster Cross-bridge Kinetics Caused by the Familial Hypertrophic Cardiomyopathy R58Q Mutation in the Regulatory Light Chain of Myosin. Submitted to: Biophysical Journal, May 2010

Mettikolla P, R. Luchowski, I. Gryczynski, Z. Gryczynski, D. Szczesna-Cordary, and J. Borejdo; Single Molecule Kinetics in the Familial Hypertrophic Cardiomyopathy A13T Mutant Mouse Heart. In progress

Mettikolla P, Calander N, Luchowski R, Gryczynski I., Gryczynski Z and J.Borejdo; Kinetics of a Single Cross-Bridge in FHC muscle Measured by Reverse Kretschmann Fluorescence. J. Biomed. Opt. 15, 017011.

CHAPTER I

INTRODUCTION

Cardiovascular diseases are the predominant cause of death in the United States and most of the European countries. Familial hypertrophic cardiomyopathy (FHC) is a serious heart disease that often leads to a sudden cardiac death (SCD) at a young age. It is an autosomal dominant disease characterized by left ventricular, septal hypertrophy and myofibrillar disarray. One of the most common causes of FHC is single-point-mutation in a gene that encodes for the ventricular myosin regulatory light chain (RLC). Heart muscle contraction results from periodic interaction of myosin cross-bridges with actin, during which myosin delivers force impulses to the thin filament.

The purpose of this study is to define FHC muscle kinetics at the level of a single molecule. This study will help in understanding the disease pathology, improve risk assessment and may ultimately lead to the development of cardiomyocyte and myosin light chain specific treatments. The results of our studies may significantly contribute to the development the targeted cellular therapeutics to treat FHC related cardiac dysfunction. In addition, the single molecule experiments and methods employed will have numerous applications in monitoring ligand receptor interactions in live cells, involvement of protein molecules in internalization of bacteria by cells, conformational fluctuations of DNA and in detection of viruses at an early phase of infection.

FAMILIAL HYPERTROPHIC CARDIOMYOPATHY

Familial hypertrophic cardiomyopathy (FHC) is a serious heart disease that often leads to a sudden cardiac death (SCD) at young age (1). Clinical advances in cardiovascular therapeutics have no effect on the mortality rates in persons suffering from FHC (9). FHC is one of the pathological manifestations of the heart resulting from its inability to adequately pump blood, thus leading to premature fatigue, dyspnea, hypertrophy and cardiac failure. One of the most common causes of FHC is single-point-mutation in a gene that encodes for the ventricular myosin regulatory light chain (RLC). FHC is characterized by ventricular hypertrophy, myofibrillar disarray, abnormal ECG findings and sudden cardiac death (1).

FHC is the leading cause of sudden death in athletes and young people. FHC is a heritable condition characterized by abnormal thickening of myocardium and histological manifestations of myocyte disarray. FHC is transmitted as an autosomal dominant disease caused by mutations in genes that encode for the major contractile proteins of the heart. It has an estimated prevalence of about 0.2% (1 in 500) in general population (3, 9, 32).

Genetic analysis has identified 270 mutations in nine sarcomeric protein genes (3). These were caused by missense mutations of β-myosin heavy chain, myosin-binding protein C, myosin regulatory light chain (RLC), myosin essential light chain (ELC), troponin T, troponin I, α-tropomyosin, actin, and titin genes (9, 37, 44). The relative frequency and distribution of these sarcomeric protein mutations linked with FHC are summarized in the table.

Table 1: Distribution of sarcomeric protein mutations linked to FHC (52, 54, 65).

Protein	Gene	# of confirmed Mutations	% of Total Mutations
βMyHC	MYH7	116	43%
Reg. LC	MYL2	10	3.7%
Ess.LC	MYL3	3	1%
cTnT	TNNT2	27	10%
cTnI	TNNI3	24	9%
TM	TPM1	10	3.7%
Actin	ACTC	5	2%
MyBP-C	MYBPC3	72	27%
Titin	TTN	1	<1%
	Total=	270	

FHC has a variable presentation with regard to degree, severity, and extent of myocardial disarray depending on the affected gene and the site of the mutation. A severe presentation is often associated with mutation in RLC (29, 33, 51). RLC mutations D166V and R58Q have been associated with malignant FHC phenotype and sudden cardiac death (53, 61). Another mutation A13T has been shown to be associated with a particular subtype of FHC defined by mid-left ventricular obstruction.

Although genetic studies have yielded compelling evidences that myosin mutations are responsible for FHC, not much is known about this disease at the molecular level (39, 44). There is diverse variety of theories implicated including abnormal cellular calcium fluxes, abnormal sympathetic stimulation, abnormalities of intramural vasculature, and primary structural abnormalities (35). Early attempts suggest that incorporation of mutant sarcomeric proteins impairs the contractile function and effects cardiac performance which ultimately leads to hypertrophy (38). Some cases showed reduced mechanical force and filament translocation (22). Other studies showed enhanced motor activity in myosin cardiomyopathy (66). Some of the FHC mutations in Troponin I, troponin T, tropomyosin and RLC cause increased Ca^{+2} sensitivity force (22, 66, 68). These studies suggest that depression in contractile function and the resulting compensatory reaction of heart cause FHC. Crucial studies on morphology and time progression of FHC argue against the compensatory hypothesis. This lack of consistent contractile abnormalities suggests that cardiac cell has an increased energy demand due to inefficient ATP utilization (5).

Myocyte dysfunction results from failure of the cell to maintain energy levels necessary for contraction and critical function such as Ca^{+2} uptake. Increased rate of cross-bridge detachment might be the cause of this dysfunction. Early detachment of myosin heads from actin implies consumption of ATP without contributing to force generation. This early detachment before power stroke completed implies decreased efficiency, which might be the root cause of FHC mutations (5).

We tested this by comparing the kinetics of single actin and myosin molecules in transgenic mouse hearts which carry disease-causing mutations in the Regulatory RLC against healthy controls. We conclude that a change in the kinetics of cross bridge interaction with actin would

alter the kinetics of cross bridge motion, thereby affecting the efficiency of utilization of ATP during contraction, ultimately leading to FHC.

STRUCTURE AND FUNCTION OF MUSCLE:

Striated muscles are of two types, namely Skeletal and cardiac muscle. Cardiac muscle shares similarities with skeletal muscle with regard to its striated appearance and contraction. Due to presence of many aligned sarcomeres gives it more striations in appearance for cardiac muscle than skeletal muscle (http:en.wikipedia.org/wiki/muscle, 58).

Cardiac muscle cells are known as Cardiac myocytes. These cells are relatively small in size averaging 10–20 μm in diameter and 50–100 μm in length. Skeletal muscle has an extensive and well organized sarcoplasmic reticulum (SR) network, abutting the narrow T-tubules. In contrast, the SR of cardiac muscle is rather sparse and less organized, and surrounded with T-tubules of much larger diameter. Most of the cells have single nucleus, but there are some cells which have more than one nucleus. Cardiac muscle contains intercalated discs, which are mainly responsible for force transmission during muscle contraction. Intercalated discs also support the rapid spread of action potentials and the synchronized contraction of the myocardium (29, 32).

Fig 1.Schematic drawing of cardiac muscle and skeletal muscle

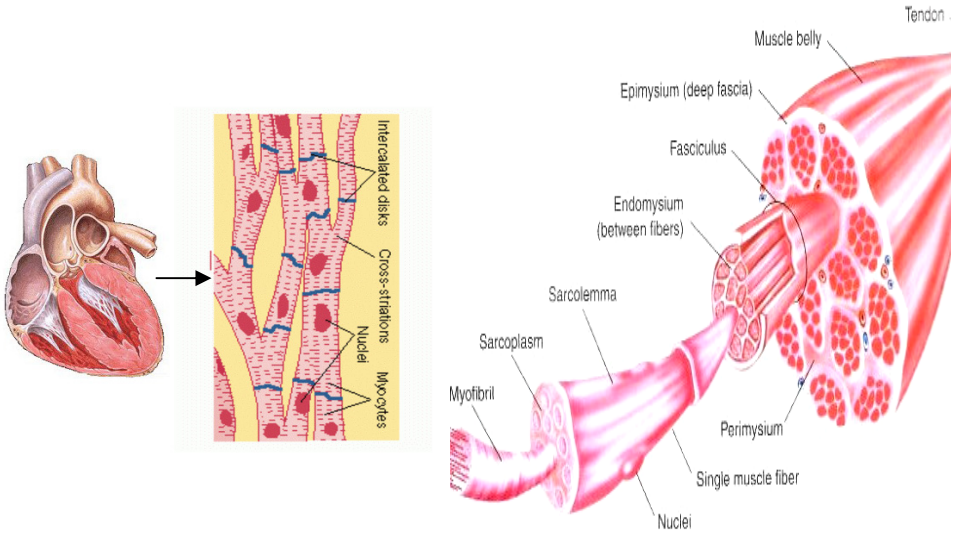

The muscle is composed of many subunits called fascicles. Fascicles are bundles of individual muscle fibers. Each individual fiber consists of a membrane (Sarcolemma) and can be further broken down into thousands of myofibrils. Myofibrils are in turn made of many sarcomere subunits that are attached end to end. Each myofibril is composed of repeating sarcomere units separated by Z disks (52). Sarcomeres are the basic contractile subunit of myofibrils. The sarcomere is composed of both thick (assembly of myosin molecules) and thin filaments (actin, troponin and tropomyosin). Myosin has tiny globular heads protruding from it at regular intervals, called as cross- bridges. These cross bridges plays an important role during muscle contraction (2, 57).

Fig 2.Schematic drawing of sarcomere structure (44)

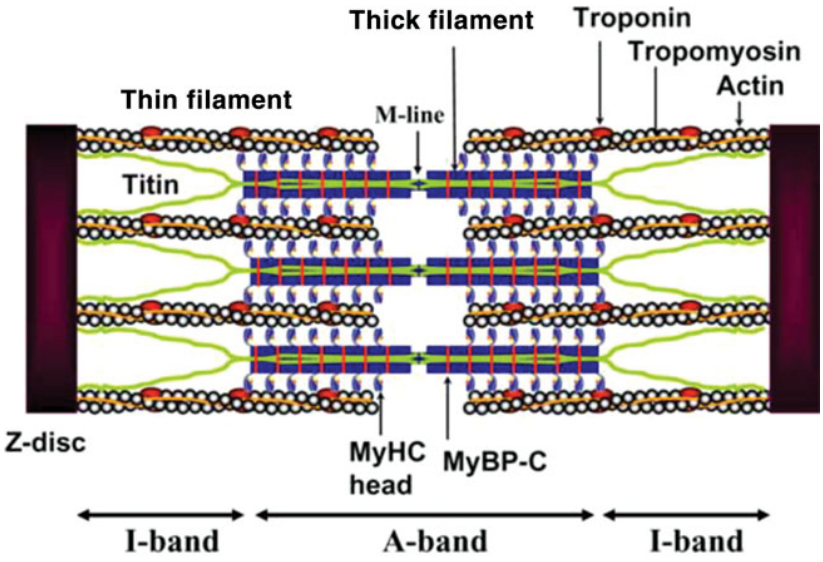

Myosin: Myosin is a major protein of thick filaments of striated muscles. Myosin along with actin plays an essential role in force generation (69). It has three major and functionally different domains: motor domain, lever arm domain and tail region. Myosin presence is not only restricted to muscle, various isoforms of myosin are present in cytoplasm and various membranes. The most common type or conventional myosin is myosin II. This class of myosins is present in the smooth, cardiac and skeletal muscle (56).

The myosin motor domain contains a catalytic site, also called as ATP binding site and an actin binding region. It is a hexamer with molecular weight of 520kD. It has two heavy chains of 220kD each and four light chains of 20KD each (56). Each of the amino-termini of the myosin heavy chains form a globular domain called myosin head or subfragment (S_1), and contains a

pair of regulatory and essential light chains. RLC localized in the head-rod junction of the myosin heavy chain and plays important role during contraction. RLC together with ELC stabilizes the helical neck of the myosin head (52, 58).

Fig 3.Three- dimensional representation of human cardiac myosin (58, 61)

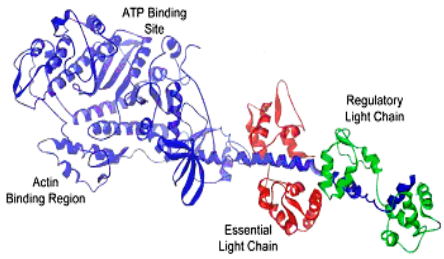

Excitation-Contraction Coupling (23, 29, 61)

The general excitation-contraction of striated muscle is similar even though some functional differences exist between skeletal and cardiac muscle. Electrical excitation leads to generation of action potential across surface membrane. Action potential propagates along the surface and T-Tubules as wave. The depolarization of the T-tubule overlying the terminal cisternae of the SR induces the release of Ca^{2+} from SR. Ca^{2+} binds to Troponin C on the actin containing thin filaments and leads to allosteric modulation of tropomyosin. These modulations open the binding sites for myosin on the thin filament. Myosin along with ADP and inorganic phosphate binds to the newly opened thin filament in the strong binding state. The release of ADP and inorganic phosphate are tightly coupled to the power stroke along with shortening of the sarcomere. ATP binding leads to detachment of myosin from actin. Myosin heads contain an ATP binding pocket and an ATPase (30, 36). When ATP binds to the ATP-binding pocket, the ATPase hydrolyzes ATP forming ADP and inorganic phosphate. The cycle continues as long as Ca^{2+} and ATP are present (30, 36).

Cellular Ca^{2+} movement in the heart is somewhat complex because of the presence of Ca^{2+} channels and transport system in the sarcolemma. Cardiac muscle contraction depends on both Ca^{2+} entry across the sarcolemma and Ca^{2+} release from the SR (61).

Muscle Contraction: Muscle contraction results from the cyclical interactions of actin and myosin filaments. During this interaction myosin cross-bridge delivers force impulses to actin. Isometric force is the time average of those impulses (50).

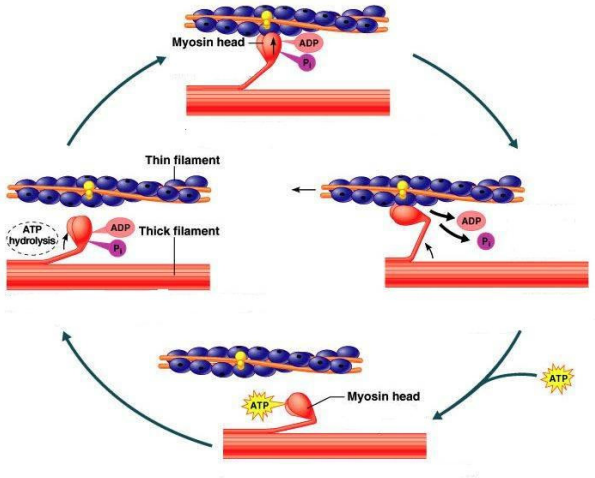

Fig 4.Schematic representation of muscle contraction

(((faculty.irsc.edu/…/AP1/AP%201%20resources.htm))

The impulse begins when dissociated cross-bridge, containing products of hydrolysis of ATP, attaches to actin (29). It is believed that a cross-bridge is strongly bound to actin for a period of time t_{ON} (ON-time) during which it generates contractile force. The binding and force generation is followed by a release of phosphate, the dissociation of ADP and the onset of rigor state. In rigor state a cross-bridge assumes a well defined orientation (11). The end of an impulse is marked by the binding of a fresh molecule of ATP and dissociation of myosin from actin (31,

64). Cross-bridge remains detached from actin for a period of time t_{OFF} (OFF-time) during which it is idle and disordered. Finally, ATP is hydrolyzed to ADP and phosphate, and the cycle repeats with the period $t_{ON}+t_{OFF}$. The fraction of a total cycle time that a cross-bridge remains attached to actin is known as the duty cycle, $\Psi = t_{ON} /(t_{ON}+t_{OFF})$ (12, 47, 48, 49, 58).

Role of RLC in striated muscle Contraction (58)

Myosin Regulatory light chain role in smooth muscle contraction is well understood but their role in striated muscle contraction is not well known. Recent studies have demonstrated the phosphorylation and Ca^{2+} binding to RLC plays significant role in muscle contraction. Another important aspect about RLC as sarcomeric proteins is their association with an autosomal dominant disease, Familial hypertrophic cardiomyopathy (FHC) (58, 59).

RLC localized in the head-rod junction of the myosin heavy chain and, together with ELC, stabilizes the helical neck of the myosin head. N-terminal domain of striated muscle contains phosphorylation site, Serine, 15. There are different isoforms of RLC available in both skeletal and cardiac muscle. The localization of RLC in helical neck of the myosin head emphasize their role in proper structural maintenance as well as cross bridge cycling in muscle contraction. This region has been postulated to undergo conformational changes that are crucial for working muscle during contraction. Recent studies revealed RLC binding domain of myosin undergoes repetitive tilt and twist conformational changes and play major role in force generation of contracting muscle (55). In skeletal muscle the structural significance of RLC has been demonstrated by reduction in rate of force generation by factor of two upon removal of RLC and reversed upon reincorporation of RLC (58). *In vitro* motility studies of reduction in sliding velocity of actin on myosin coated surface upon removal of RLC and restoration upon

reincorporation of RLC indicates their crucial role in regulation of muscle contraction (58, 60, 61).

Increase in $Ca2^{+}$ concentration during muscle contraction leads to activation of Ca^{2+}/Calmodulin(CAM) dependent myosin light chain kinase (MLCK) and phosphorylation of RLC. There are contradictory statements on effect of RLC phosphorylation on muscle contraction. Extensive literature supports the idea that RLC phosphorylation leads to decreased rate of cross bridge cycling. However few studies indicated the importance of RLC phosphorylation by MLCK in force development, Ca^{2+}sensitivity and ATPase activity (58, 2, 63).

RLC mutations associated with FHC

Recent studies have revealed that the ventricular isoform of myosin RLC is one of the sarcomeric proteins associated with FHC. To date 10 RLC mutations have been linked with FHC (58).

Fig 5.Three- dimensional representation of human cardiac RLC (61)

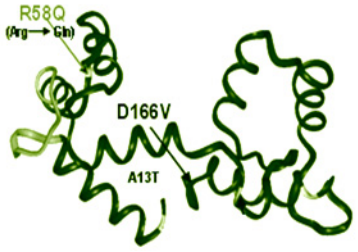

A13T, E22K and P95A are the first identified mutations associated with FHC. These mutations are linked with subtype of hypertrophy named as mid left ventricular obstruction. Later identified mutations F18L and R58Q are associated with increased left ventricular wall thickness and abnormal ECG findings, characteristics of FHC symptoms. There is high sequence homology

among various species according to amino acid sequence analysis for FHC mutations (15, 19, 58).

RLC mutations D166V and R58Q, which have been associated with malignant FHC phenotype and sudden cardiac death, were exclusively used to study cross bridge kinetics along with one other mutation, A13T, which has been shown to be associated with a particular subtype of FHC defined by mid-left ventricular obstruction (24).

Clinical studies have revealed D166V and R58Q, RLC mutations are associated with malignant FHC phenotype and sudden cardiac death (58). Recent studies revealed that the Aspartate to Valine substitution in Tg-D166V mice and Arginine to Glutamine in Tg-R58Q mice result in a decreased phosphorylation of RLC (58). Hydrophobic and branched valine replacing negatively charged aspartic acid may restrict conformations that main chain can adapt. R58Q mutation of replacing arginine to glutamine leads to a loss of a positive charge results in electric charge modification of the domain and may disrupt the ionic interactions. The mutated amino acid may have implications in the calmodulin dependent phosphorylation of the RLC chain. Recent studies suggest that phosphorylation of RLC plays an important role in regulating cardiac function and its deficit may contribute to malignant FHC phenotypes (24, 58).

Another mutation, A13T is localized near the functionally important RLC site, Ser15, a target for Ca^{+2} calmodulin activated myosin light chain kinase (MLCK). A13T associated with a particular subtype of cardiac hypertrophy defined by mid left ventricular obstruction.

Recent studies of substitution of the A to T residue resulted surprisingly large increase in the α-helical content monitored by UV-CD spectroscopy since alanine's predisposition for stabilizing α-helical structures. Recent studies on phosphorylation effects of A13T demonstrated a 15-fold greater affinity for Ca^{2+} than phosphorylated WT, while nonphosphorylated A13T bound Ca^{2+}

with a 3-fold lower affinity than nonphosphorylated WT. Therefore, the consequences of the FHC mutation (A13T) were

most profound in conditions where the protein became phosphorylated (24, 61).

One more interesting data from the recent studies about Ca^{2+} binding to A13T decreased their α-helical content that was initially increased by the FHC mutation, and phosphorylation of A13T restored the amount of the α-helical content to the level of WT. This data suggests that phosphorylation of RLC during contraction could act as a backup mechanism attenuating the physiological consequences of the FHC mutation in the working heart.

Kinetics of Muscle contraction (10, 11, 12, 13)

Studying cross-bridge kinetics is complicated in muscle as each contractile event is different than other. Kinetics of cross-bridge depends on the relative position of actin and myosin. This position is not constant, even during isometric contraction because of internal elasticity of a sarcomere. Averaging of information or signal is a predominant problem in such situation. However, the extent of averaging is inversely related to the number of molecules under observation. Therefore, when only a few molecules are observed, the true kinetic information of cross-bridge can be obtained, In addition, it is important to perform experiments in muscle tissue. This is because the concentration of proteins in muscle is extremely high, the proteins tend to form aggregates at such high concentration which allow access only to small solutes. As a result, certain regions of a cell are over hydrated and behave differently than parts that are normally hydrated.

Fig 6.Schematic illustration to show importance of Single molecule measurement

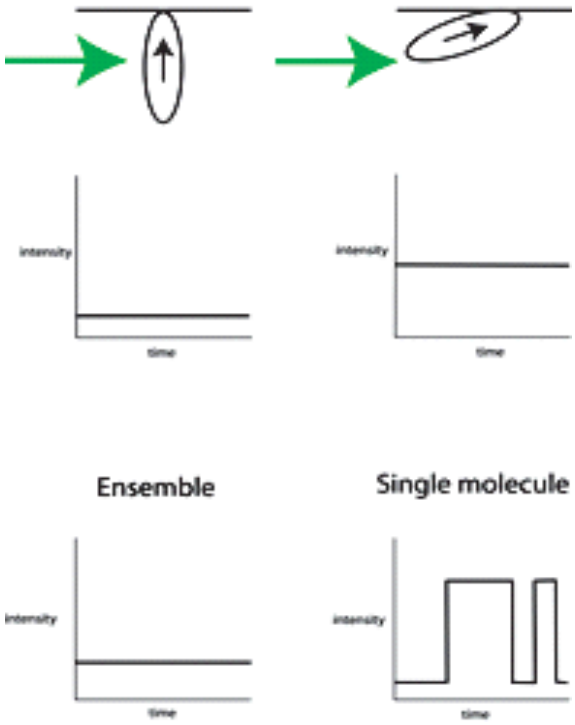

Additional reason why the cross-bridge kinetics in cardiac muscle must be studied at single cross bridge as human patients are heterozygous for FHC mutations which mean their thick filaments composed of wild type myosin heads interspersed with mutant heads. Any large observational volume contains mixture of both populations can not distinguish the kinetics of healthy versus diseased. However kinetic information can be extracted from stochastic fluctuations of the signal from small ensemble of molecules by the use of Fluorescence Correlation Spectroscopy (FCS) (18, 27).

The FCS was first introduced in the early 1970s by Magde, Elson, and Webb. Since then, the technique has been developed into a powerful tool in analytical chemistry and biological

research. The elegance of FCS lies in its ability to measure the kinetics of chemical reactions under zero perturbation conditions (18). FCS can extract a wealth of molecular and environmental information from a weak fluorescence signal that is comparable with the background noise, using correlation analysis of the fluorescence fluctuations of very small samples of molecules at nanomolar concentrations. The Fluctuations will be processed to yield an autocorrelation function from which rates of diffusion, convection, chemical reaction, and other processes can be extracted. Unique information about the local concentration, aggregation and molecular interaction can be obtained from FCS using amplitude of fluctuation and cross-correlation methods (7, 20).

The objective of our study is elucidating the molecular mechanisms involved in triggering of hypertrophic processes in the individuals carrying FHC mutations in myosin RLC. The following chapters are pursued in order to address the overall goal.

In Chapter III, we have used skeletal muscle to study the kinetics of muscle contraction by computing the correlation function. This can extract contribution of individual molecules from stochastic variations. Correlation function at a given delay time τ is a sum of the products of a signal multiplied by a signal shifted by a delay time τ. Thus if τ is small and there is any correlation between signal and its value at time τ later, the correlation function will be large. As the value of τ increases, however, a signal has drifted from the original point that it is now of the opposite sign and the product will be negative. As a consequence a correlation function will be small. If there is no correlation between signal and its value at time τ later, the correlation function will be zero. Thus the shape of correlation function reveals the shape of the underlying event (6, 18, 20).

Chapter IV is an independent way to measure the kinetics of a single myosin cross bridge by following the changes in the environment as it under goes a cycle of binding and dissociation from actin using the fluorescence lifetime of the flurophore attached to actin (21). As the fluorescence lifetimes are sensitive to change in environment, the time course of change in lifetime will give us information of ON-time (t_{ON}) and OFF-time (t_{OFF}).

Chapters V and VI studied and compared kinetic parameters between Tg-WT (transgenic wild-type) and Tg-M (transgenic mutant) ventricular muscle. The information obtained are 1) the time a cross-bridge is strongly attached to actin (tON), 2) the time the cross-bridge detached from actin (tOFF), and 3) the duty cycle Ψ- the fraction of overall cycle time that a cross- bridge is strongly attached to actin (10, 11, 42, 43, 45). The information obtains the molecular mechanisms involved in triggering of hypertrophic processes in the individuals carrying FHC mutations in myosin RLC.

Chapter VII addressed the typical problems encountered in FCS measurements like back ground observational volume as well reflected excitation light from the surface with Surface Plasmon Assisted Microscope (SPAM) (10, 26). SPAM allows observing few molecules by producing extremely thin optical sectioning and by providing excellent background rejection. The axial dimension decrease is a consequence of the fact that the SPCE takes advantage of strongly restricted range for near field interactions (8). In SPCE the axial dimension is made small (ca 50 nm) by placing a sample on a thin metal film and illuminating it with the laser beam directly called reverse Kretschmann (RK) configuration (14, 25, 34, 40, 42).

CHAPTER II

Materials and methods

Chemicals and solutions. Alexa488 (AP)- and rhodamine-phalloidin (RP) were from Molecular Probes (Eugene, OR). All other chemicals including 1-ethyl-3-(3'-dimethylaminopropyl) carbodiimide (EDC), dithiotreitol (DTT), creatine phosphate and creatine kinase were from Sigma. EDTA-rigor solution contained 50 mM KCl, 2 mM EDTA, 1 mM DTT, 10 mM Tris-HCl buffer pH 7.5. Ca-rigor solution contained 50 mM KCl, 4 mM $MgCl_2$, 0.1 mM $CaCl_2$, 1 mM DTT, 10 mM Tris-HCl buffer pH 7.5. Mg-rigor solution contained 50 mM KCl, 4 mM $MgCl_2$, 1 mM DTT, 10 mM Tris-HCl buffer pH 7.5. Contracting solution was the same as Ca-rigor, except that it contained also 5 mM ATP. When low concentrations of ATP were used, *the* contracting solution contained 20 mM creatine phosphate and 10 units/mL creatine kinase (~1 mg/mL).

Preparation of myofibrils. Thin strips of glycerinated rabbit psoas muscle were incubated in EDTA rigor solution until they turned white (~1 hr). The fiber bundle was then homogenized using a Heidolph Silent Crusher S homogenizer for 20 sec (with a break to cool after 10 s) in Mg^{2+}-rigor solution (it was important that the fibers were not homogenized in the EDTA rigor buffer to avoid foaming). Myofibrils were always freshly prepared for each experiment. Labeled myofibrils (25 μl) were applied to a coverslip (Menzel-Glaser 20x20 mm #1 or Corning #1 25x60 mm). The sample was left on a coverslip for 3 minutes to allow the myofibrils to adhere to the glass. The bottom cover slip was covered with a small coverslip (to prevent drying) and the two were separated by Avery Hole Reinforcement Stickers. Labeled myofibrils were washed

with 5 volumes of the Ca^{2+}-rigor solution by applying the solution to the one end of the channel and absorbing with #1 filter paper at the other end.

Muscle. After euthanasia, the hearts from 6 month old Tg-D166V and Tg-WT mice were quickly removed and rinsed briefly (no more than 30 sec) with ice-cold 0.9% NaCl. Muscle strips from left ventricles and papillary muscles were dissected at 4°C/in a cold room in ice-cold pCa 8 solution (10^{-8} M [Ca^{2+}], 1mM [Mg^{2+}], 7mM EGTA, 2.5 mM [$MgATP^{2+}$], 20 mM MOPS, pH 7.0, 15 mM creatinine phosphate, ionic strength = 150 mM adjusted with potassium propionate) containing 30 mM BDM and 15% glycerol (62). After dissection, muscle strips were transferred to pCa 8 solution mixed with 50% glycerol and incubated for 1 hr on ice. Then the muscle strips were transferred to fresh pCa 8 solution mixed with 50% glycerol and containing 1% Triton X-100 for 24 hr at 4°C. Muscle strips were finally transferred to a fresh batch of pCa 8 solution mixed 1:1 with glycerol and kept at -20°C until used for the preparation of myofibrils (62).

Preparation of cardiac myofibrils. Myofibrils from Tg-WT and Tg-D166V mouse papillary muscles and left ventricles were prepared from glycerinated fiber bundles stored at -20°C in glycerinating solution. The muscle fibers were first incubated in EDTA rigor solution until they turned white (~1 hr). The fiber bundle was then homogenized using a Heidolph Silent Crusher S homogenizer for 20 sec (with a break to cool after 10 sec) in Mg^{2+}-rigor solution. It was important that the fibers were not homogenized in the EDTA rigor buffer to avoid foaming. Myofibrils were always freshly prepared for each single molecule experiment. Labeled myofibrils (25 µl) were applied to a 20 mm diameter (19 mm x 19 mm) glass bottom coverslip (Menzel-Glaser 20x20 mm #1). The sample was then incubated on the coverslip for 3 min to allow the myofibrils to adhere to the glass. The bottom cover slip was covered with a small (5

mm in diameter) top glass coverslip separated from each other by Avery Hole Reinforcement Stickers. Labeled myofibrils were washed with at least 5 volumes of the Ca^{2+}-rigor solution by applying the solution to the one end of the sandwhich and absorbing with #1 filter paper at the other end.

Cross-linking. To prevent *the* shortening of muscle in *the* contracting solution *the* myofibrils (1 mg/mL) were incubated with 20 mM EDC for 10 min at room temperature according to procedure of Herrmann (31). The reaction was stopped by 20 mM DTT. Cross-linking did not affect ATPase. The lack of shortening was checked by comparing the length of a myofibril before and 100 sec after inducing contraction in a TIRF microscope. Within the limits of measuring accuracy on the computer screen (~1%), the length always remained unchanged. The same result was obtained earlier using a confocal microscope (10). Cross-liked myofibrils are a good model for muscle fiber ATPase and the kinetics of Ca(2+)-activated activity (Herrmann et al. 1994). The large P(i) bursts and kcat values were the same in cross-linked myofibrils and muscle fibers (31). Those results were confirmed by (36).

ATPase measurements. 200 μL of 1 mg/mL myofibrillar suspension was incubated in 0.1 mM ATP for 30, 60, 90 and 120 s. After the specified time, the reaction was stopped by 700 μL of 1 mM HCl. The samples were filtered through *a* cotton ball in *a* 1 mL pipette tip. 100 μL of Malachite Green (MG) reagent from the SensoLyte Phosphatase assay kit (AnaSpec, San Jose, CA) was added and incubated for 5 minutes. 10 μL of phosphate contained in the kit was dissolved in 190 μL of deionized water along with 700 μL HCl and 100 μL MG reagent and used

as a standard. 1 mL of 10 μM of standard contained 10^{-9} moles of phosphorus. *The* concentration of phosphate was measured at 650 nm. 200 μL of Ca^{2+}- rigor containing 700 μL HCl and 100 μL MG reagent was used as a blank. [P_i] was calculated as mol/ 1 mol/min= Abs (sample)* [standard mol]/Abs (standard)/ [myosin mol]/minutes. The amount of myosin in 200 μL of 1 mg/mL myofibrils was taken as $0.2*10^{-9}$ mol. The mean ± SD of 4 measurements were 3.1 ± 0.8 s^{-1} .

Labeling. 1 mg/mL myofibrils (~ 4 μM actin) were mixed with 0.1 nM Alexa488-phalloidin+10 μM unlabeled-phalloidin or with 0.1 nM rhodamine-phalloidin+10 μM unlabeled-phalloidin. Unlabeled phalloidin was necessary to prevent uneven labeling. If it was not there, *the* sarcomeres closest to the tip of the pipette used to add the label would have contained more chromophores than sarcomeres further away from the tip. The degree of labeling was 10 μM/0.1 nM = 100,000, i.e. on the average 1 actin protomer in 10^5 was fluorescently labeled.

Microscope slides. Glass or sapphire microscope slides were covered with metal by vapor deposition by EMF Corp. (Ithaca, NY). A 48-nm layer of gold was deposited on the slides. A 2-nm chromium undercoat was used as an adhesive background. NA=1.45 objective was used with gold coated glass slides, and NA=1.65 objective with gold coated sapphire slides.

Data collection. The experiments were done using Micro Time 200 (PicoQuantGmbH, Berlin, Germany) confocal system coupled to Olympus IX 71 microscope. The objective was water immersion NA=1.2, 60x. The excitation was by a 470-nm laser pulsed diode, and the observation was through a 500-nm long pass filter. *The* confocal pinhole was 30 μm. The instrument

measured fluorescence lifetimes as well as anisotropies. Whenever indicated, the data was collected by ISS-Alba-FCS (ISS Co, Urbana, IL). The excitation was by a 532 nm CW laser. *The* confocal pinhole was 50 μm. Fluorescence was collected every 10 μs. Orthogonally linearly polarized analyzers were placed before Avalanche PhotoDiodes (APD's). The laser was polarized vertically (on the microscope stage). *The* myofibrils *were* also vertical.

Data analysis. The signal was smoothed by adding photons over small time intervals. The smoothed signal was fitted to an exponential that was subsequently subtracted from the signal. From this the autocorrelation function was calculated. The autocorrelation function was fitted to a train of triangular waves by a least squares fit. It was assumed that the "hidden signal" to look for was a rectangular wave. The programming and calculations were done in Matlab. The autocorrelation functions were calculated in the Fourier domain by taking the Fast Fourier transform of the signal padded with an equal number of zeros in order to not have the last points in the signal to correlate with the first.

Measuring anisotropy in solution. Fluorescence anisotropies were measured by time-domain technique using FluoTime 200 fluorometer (PicoQuant, Inc.). The excitation was by a 475-nm laser pulsed diode, and the observation was through a monochromator at 590 nm with a supporting 590-nm long wave pass filter. The FWHM of pulse response function was 68 ps (measured by PicoQuant, Inc.). Time resolution was better than 10 ps. The intensity decays were analyzed in terms of a multi-exponential model using FluoFit software (PicoQuant, Inc.).

Lifetime measurements. Fluorescence lifetimes were measured by the time-domain technique using a MicroTime 200 instrument coupled to an Olympus IX71 microscope (PicoQuant, GmbH, Berlin, Germany). Excitation was achieved using a 470-nm pulsed laser diode, and the observation was made through a 500-nm long wave pass filter. FWHM??? of pulse response function was 68 psec (measured by PicoQuant, Inc.) while the time resolution was better than 10 psec. The intensity decays were analyzed in terms of a multi-exponential model using SymPhoTime v. 4.3 software (PicoQuant, Inc.). The intensity average lifetime was calculated as $\bar{\tau} = \sum_i f_i \tau_i$ where $f_i = \frac{\alpha_i \tau_i}{\sum_i \alpha_i \tau_i}$ and α_i is the fractional contribution of the i-th lifetime, τ_i. The amplitude average lifetime was calculated as $\langle \tau \rangle = \sum_i \alpha_i \tau_i$. The lifetimes of free and bound Alexa488-phalloidin in water and glycerol were measured with/in a FluoTime 200 fluorometer (PicoQuant Inc) equipped with a microchannel plate (MCP) and 470 nm pulsed laser diode (76 ps half-width). This instrument provides an exceptional resolution in the sub-nanosecond range (45,47).

Rotation of Rhodamine-phalloidin bound to F-actin**.** For the quantitative measurement of orientation, it is important to know whether the probe is immobilized by the protein so that the transition dipole of the fluorophore reflects the orientation of the protein. For this reason we compared *the* decay of *the* anisotropy of RP and of RP on F-actin. The decay of *the* anisotropy of RP was best fitted by a single exponent. 100% of the signal decay was contributed by the decay time of 0.519 ns, consistent with *the* rotation of a molecule with M_w=1,250. No independent rotation of rhodamine moiety was observed. The decay of anisotropy of RP coupled to thin filaments was best fitted by the two exponents with correlation times of 0.665 and 36.8 ns with the relative contributions of 13.7 and 86.3%, respectively. The short correlation time is due to the

rotation of rhodamine moiety independent of phalloidin moiety which remains bound to F-actin. It is not due to rotation of free rhodamine-phalloidin, because binding of phalloidin to F-actin is extremely strong. The long correlation time is due to rotation of F-actin oligomers. Thus over 86% of fluorescent phalloidin is immobilized by F-actin. This is consistent with the fact that *the* probes attached to proteins through interactions that stretch over large surface areas, such as hydrophobic or Van der Waals interactions are attached more rigidly than probes that are attached by covalent links.

Steady-state Force Development. Transgenic mutant mice used in these experiments were ~5 month old males that were age and gender matched with Tg-WT controls. A bundle of fibers of the approximate diameter of 100-150 μm was isolated from a batch of glycerinated mouse papillary fibers and attached by tweezer clips to a force transducer. The fibers were relaxed in a 1 ml of pCa 8 solution and then tested for maximal steady state force in pCa 4 solution (composition identical to pCa 8 solution except the $[Ca^{2+}] = 10^{-4}$ M). Steady state force development was monitored for the Tg-R58Q fibers and compared to control, Tg-WT fibers.

Ca^{2+} Dependence of Force Development. After the initial steady state force was determined, the fibers were relaxed in pCa 8 solution and then exposed to solutions of increasing Ca^{2+} concentrations (from pCa 8 to pCa 4). The maximal force was measured in each "pCa" solution followed by a short relaxation of the fibers in pCa 8 solution. Data were analyzed using the following equation: % Change in Force = $100 \times [Ca^{2+}]^{nH}/([Ca^{2+}]^{nH}+[Ca^{2+}_{50}]^{nH})$ where "$[Ca^{2+}_{50}]$" is the free Ca^{2+} concentration which produces 50% force and "n_H" is the Hill coefficient.

CHAPTER III

Observing cycling of a single cross-bridge during isometric contraction of skeletal muscle

Introduction

Muscle contraction results from the cyclical interactions of actin and myosin. During this interaction myosin cross-bridges cyclically deliver force impulses to actin. Force, stiffness and ATPase are related to the time average of those impulses . Kinetic constants characterizing contraction can be determined by measuring averages together with the rate constant of force redevelopment. Although it is a compelling and successful approach, it involves the application of a specific model (e.g. (17)) of muscle action. A more direct approach is not having to rely on any specific model. If it was possible to observe a single molecule, no averaging would occur and the dynamics of a cross-bridge could be directly observed. At the same time it is important to perform experiments *in-* or *ex-vivo*, because muscle proteins are arranged in well-ordered arrays where relative position of actin and myosin are important. Moreover, the concentration of proteins in muscle is very high (of the order of 100 μM) and at such high concentrations the excluded volume effect come into play. For example, the access to contractile proteins may be limited to only small solvents and as a result certain regions of a muscle cell may become over hydrated and behave differently than isolated proteins in solution.

A signal originating from a single flurophore is weak. This has been overcome by recent advances in single molecule detection in vitro (68). In the application to muscle Warshaw and collaborators measured the orientation of a single molecule of smooth myosin II (70) and Goldman & Selvin et al. measured orientation of a single molecule of myosin V (67). In addition to being weak, a signal from single molecule in a tissue is dominated by autofluorescence. This work deals with our efforts to overcome this problem. There are two key aspects to our approach: The first is to measure the autocorrelation function of the signal (the intensity of polarized fluorescence), rather than the signal itself. Autocorrelation diminishes noise because the white noise is not correlated with itself. Measuring a signal directly is much more difficult. For example, recently we compared the fluorescence lifetime of cardiac myofibrils from healthy and diseased hearts carrying a point mutation that leads to the expression of cardiac hypertrophy phenotype (43). We were unable to detect any differences in this signal between healthy and diseased hearts. But when we measured correlation function, we detected significant decrease in myosin kinetics in diseased muscle. The second key is to observe actin rather than myosin. Observing actin has five essential advantages. First, labeling actin with phalloidin preserves the regular structure of a myofibril, unlike the less gentle labeling of myosin. Second, phalloidin does not alter the enzymatic properties of muscle (13). Third, phalloidin labels actin specifically and stoichiometrically, which allows strict control of the degree of labeling. Fourth, phalloidin attaches to actin very rigidly because it involves hydrophobic and Van der Waals links. Finally, labeling actin with phalloidin allows observing events that occur only in the area where actin and cross-bridges interact. This is because in skeletal muscle (in contrast to cardiac muscle) phalloidin initially labels only the ends of thin filaments (Overlap zone, O-band) (60) precisely

the region where filaments overlap and interact. Observing actin is a valid way of observing the effect of cross-bridges, because it has been known for a long time that actin changes orientation in response to cross-bridge binding and that those changes parallel changes of orientation of a cross-bridge (12).

The common way to determine kinetics is to follow orientation changes of actin or myosin by measuring polarization of fluorescence (P) of a fluorophore attached to either moiety. P is a sensitive indicator of orientation (16, 41). For fluorophores in solution, P is defined as the ratio of parallel and perpendicular polarized intensities: $P=(I_V-I_H)/(I_V+I_H)$, where I_V and I_H are the orthogonal intensities of fluorescence obtained using vertical and horizontal polarization of exciting light, respectively. In the case of muscle, where the fluorophores assume fixed orientation with respect to muscle axis, there are two polarizations, $P_H=(I_{HV}-I_{HH})/(I_{HV}+I_{HH})$ and $P_V=(I_{VV}-I_{VH})/(I_{VV}+I_{VH})$. Following the original notation of Tregear & Mendelson the first subscript indicates the direction of polarization of the exciting light with respect to the laboratory frame of reference, and the second subscript indicates direction of polarization of the emitted light with respect to the laboratory frame of reference. In this work muscle axis was always vertical (V) and the direction of polarization of the laser was also always vertical (V), so we measured I_{VV} or I_{VH} which allowed us to determine P_V. But in the actual calculations of correlation function we did not use P_V. We used one of the two orthogonal components, either I_{VV} or I_{VH}. The reason for this was that polarized fluorescence is the ratio of two noisy signals. Consequently, its correlation function is noisy and it cannot be carefully analyzed. In the earlier work we calculated polarization of fluorescence (11), but it was demonstration of principle, and correlation function was not computed. But to extract kinetic parameters from the data the

correlation function must be calculated. We have shown experimentally that over short period of time (where laser instabilities, motion of the microscope etc are minimized) correlation function of one orthogonal component behaves like correlation function of polarized fluorescence (45). Gratton's group demonstrated the same thing theoretically (7). A good demonstration that correlation function of one component of polarization retains characteristic of correlation of the entire polarization function is a comparison of correlation of one orthogonal intensity (**Fig. 9A**) with correlation of the corresponding polarization of fluorescence. The comparison (data not shown) reveals that although correlation of polarization retains many essential details, some details (like substructure of the correlation peaks) are lost in the noise.

We were able to select a single actin molecule for measurements by labeling one in 100,000 actins with rhodamine-phalloidin, and by selecting small detection volume by using confocal detection. The changes in orientation were characterized by periods of activity during which myosin cross-bridges interacted normally with actin, interspersed with periods of inactivity during which actin and myosin were unable to interact. The periods of activity lasted on average 1.2 ± 0.4 s and were separated on average by 2.3 ± 1.0 s. During active period, actin orientation oscillated between the two extreme values with the ON and OFF times of 0.4±0.2 and 0.7±0.4 s, respectively. When the contraction was induced by a low concentration of ATP both active and inactive times were longer and approximately equal.

Results

Imaging**.** A typical lifetime image of a rigor myofibril is shown in **Fig. 7A.** (Lifetime image is shown here because it was superior to conventional intensity image. The various bands are best identified with the aid of image of myofibrils more heavily labeled with phalloidin (10 nM RP +

10 µM UP; **Fig. 7C**). This image clearly shows that that there are two bright overlap bands (O-bands) in a center of each sarcomere (i.e. fluorescence does not originate from the I-bands) and that each is separated by a dark I-band and H-zone. This is consistent with earlier findings that phalloidin originally labels the ends of actin filaments (60). After this initial binding phalloidin redistributes itself to the I-band, a process which takes several hours (4). As a result, only those actin protomers that are located in the region where interactions with myosin occur, are initially labeled.

Fig 7

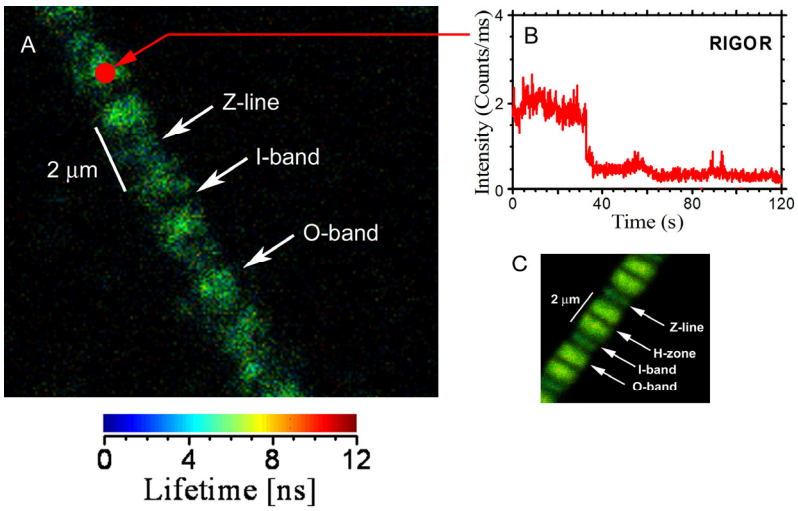

Fig. *7. **(A)**: The image of a myofibril in rigor sparsely labeled with fluorescent phalloidin. The location of various bands is indicated by white arrows. The red arrow points to the area (0.5 µm in diameter) from which the microscope collects the data. Myofibril irrigated with 0.1 nM Alexa488-phalloidin + 10 µM unlabeled phalloidin. **(B)**: Sudden drop of I_V intensity to the level of the background in rigor muscle – behavior characteristic of single molecule bleaching. The rate of arrival of fluorescent photons was estimated as 4 (see text). **(C)**: Lifetime image of a*

myofibril irrigated with higher concentration of the dye (10 nM Alexa488-phalloidin + 10 μM unlabeled phalloidin to pinpoint location of fluorescence in different bands more clearly. Cross-linked myofibril, excitation at 470 nm, emission viewed through 500 nm long-pass filter. Laser power 2μW. 60x, NA=1.2 water immersion objective.

Number of detected actin molecules. The red circle in Fig. 1A indicates the projection of the confocal aperture on the image plane. The diameter of this projection (0.5 μm) is equal to the diameter of the confocal pinhole (30 μm) divided by the magnification of the objective (60x). Fig. 1B shows the time course of the parallel polarized signal (I_V) collected from the Detection Volume (DV). The trace exhibits a classical symptoms of bleaching of a few molecules - a sudden stepwise drop of intensity to the background level. The major part of a decline, attributed to bleaching of a single molecule, consisted of a decrease in the vertical component of the intensity fluorescence rate (δI_V) of ~1,000 photons/s. The perpendicular component (I_H) of the signal was ~2 photons/ms. The total loss of fluorescence rate due to bleaching of a single molecule was $\delta I_V + \delta 2*G*\delta I_H \approx 3$ photons/ms, where G is the correction factor (=1.06). This number carries significant uncertainty. The time course and the time before photobleaching were different for each spot. This is not surprising because different fluorophores reside at different distances from the focus of the illuminating laser beam. They are thus subjected to different illuminating light intensities and take varying amount of time to absorb the number of photons required for photobleaching. Overall, a single fluorophore contributed photons at a rate of 3 - 10/ms. Knowing this rate makes it possible to estimate the number of detected molecules: **Fig. 8A** shows a typical signal of contracting muscle. The perpendicular (I_H) and parallel (I_V) intensities are shown in the red and blue, respectively. The decay of the signal during the first 4 s

is due to photobleaching of some of the fluorophores. The contributions of these fluorophores were rejected in analysis, and the data was analyzed only when the signal reached steady-state (4-10 s range in this case). The fluorophores that remained unbleached after 4 sec of illumination cannot be bleached within 20-30 s. The average counts from I_V and I_H channels after 4 s were 4.4 and 1.8 counts/ms, respectively. The inset to **Fig. 8A** shows the signal from an empty area immediately adjacent to a myofibril. The average counts from I_H and I_V channels of background were I_{Hb}= 0.4±6 and I_{Vb}= 0.7±9 photons/ms, respectively. The total photon rate during 4-10 s interval was $I_{Tot}=(I_V-I_{Vb}) +2*G*(I_H-I_{Hb})$ = 9.8 photons/ms. This corresponds to a single molecule of actin.

We wish to point out that another way to determine the number of fluorophores in the DV is to use the well known dependence of the maximum value of correlation function, G(0), on the number of molecules N: G(0)=1+1/N.

Autocorrelation of polarized fluorescence of contracting muscle**.** In principle, when a single molecule is observed, it should be possible to distinguish individual impulses by inspection of the intensity traces. In practice this was not possible because of the noise. **Fig 8B** shows I_{VH} intensity trace during steady-state on a magnified scale. Any periodicity is lost in a noise. A standard way to reduce the contribution of white noise to a periodic signal is to compute its autocorrelation function. The correlation function at a given delay time τ is the sum of the products of a signal multiplied by a signal shifted by a delay time τ. Thus if τ is small the correlation function will be large. If τ is equal to the period of a signal, the product will also be large because there is correlation between the signal and its value one period later. But the situation is different with white noise. Now the only correlation present is between the initial value and the value a short time τ later. As τ increases, a high frequency white noise assumes

the value of the opposite sign to that of the original point. The product of such pairs will be negative and the sum of the products will be smaller. If τ is sufficiently large, the sum will be zero. The relation between the signal, correlation function and its power spectrum is shown in **Fig. 8C**. The autocorrelation corresponding to the signal of **Fig. 8B** is shown in **Fig. 8D**. The periodicities are now clearly visible.

Fig 8

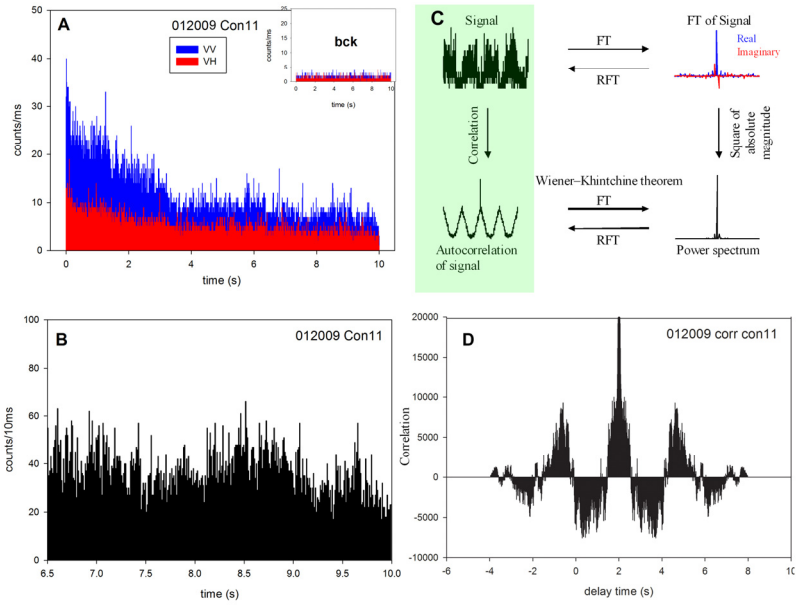

Fig. 8. ***(A)****: The time course of polarized intensity of contracting myofibril. Myofibrillar axis is Vertical on the microscope stage. Laser polarization is Vertical on the microscope stage. Counts in H channel (red) and V channel (blue) are the fluorescence intensities polarized perpendicular and parallel to the myofibrillar axis, respectively. Inset: Signal from an empty area immediately adjacent to the myofibril. Excitation 470 nm, emission>500 nm. Laser power = 2 μW, light flux ~7 μW/μm^2. **(B)**: The same signal with the first 6.5 s removed. Note that the vertical scale is magnified 10x. The fluctuations during 6.5-10 s are contributed by a single molecule of actin.*

*(**C**): The schematic representation of a relation between signal, correlation function and power spectrum. Amplitude power spectrum is a Fourier Transform (FT) of the signal. Absolute square of amplitude spectrum is the power spectrum, whose Reverse Fourier Transform (RFT) is the correlation function. In practice one computes correlation function from signal by first computing Amplitude and Power Spectrum. (**D**): the autocorrelation function of the signal in **B**. The intensity data was fitted to the exponential function, the exponential was subtracted from the data to get zero average value and correlation function was computed. In order to get correlations only between corresponding points, padded zeros have been added before the correlation calculation.*

Inspection of **Fig. 8D** reveals that the correlation function contains two types of periodicities: a slow one, characterized by a sudden bursts of activity every couple of seconds, and a fast one, characterized by rapid bursts within the main peaks. **Fig. 9** shows a typical example of an experiment which was analyzed for slow oscillations. **A** shows the original signal from the contracting muscle. **B** is a negative control, showing no activity whatever in rigor muscle. The same negative result was obtained from non-crosslinked myofibrils bathed in contracting solution that were prepared from fibers that were pre-stretched beyond overlap in a relaxing solution. The correlation functions are shown in **C** & **D**. The red line in Fig. **3C** shows the least square fit of the slow oscillations to a piecewise linear train of triangles. The reason it is fit to a series of triangles is that a waveform which gives rise to triangular correlation function is a train of rectangular waves. The train of rectangular waves is the simplest time course of orientation change during muscle contraction. We recognize that a simple ON-OFF mechanism is an oversimplification of the actual events, but there is no doubt that the main cyclical events giving rise to orientation change (binding and dissociation of a myosin cross-bridge) are correctly

represented (see Discussion). The binding of a cross-bridge most likely leads to a reduction in the number of the bending modes of actin rather than the reorientation of the actin monomer, because the work of Yangida and collaborators implied the lack of any gross rotational motion of a monomer (71) (**Fig. 13B**). Conversely, the dissociation of a cross-bridge probably leads to the increase in the number of bending modes. The time during which the signal is high and low indicates the ability or inability of cross-bridges to access thin filament. We call these times t_A and t_I. t_A was extracted by measuring the time from 0 until the correlation function first changed slope. t_I was measured from the time the correlation function changed slope to the next maximum. These times are tabulated in **Table 2** for all 17 independent experiments on 6 different myofibrillar preparations.

Fig 9

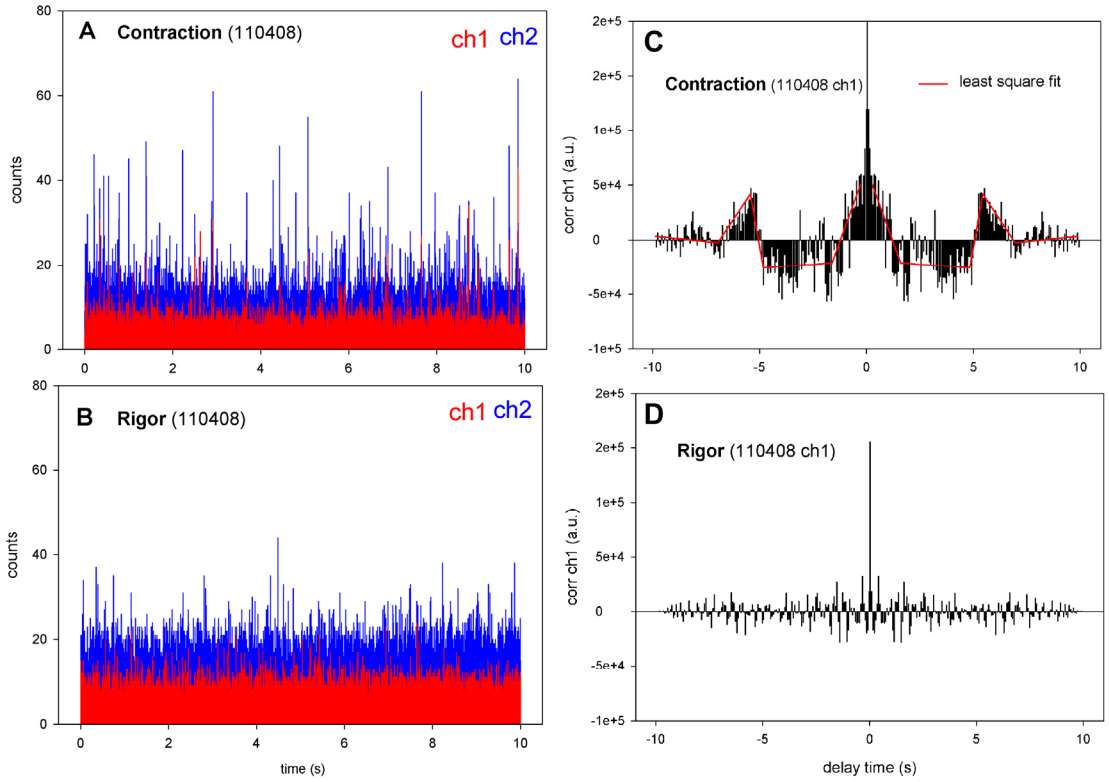

Fig. 9. *(**A**): The time course of polarized intensity of contracting myofibril. Counts in horizontal channel1 (red) and vertical channel2 (blue) are the fluorescence intensities polarized perpendicular and parallel to the myofibrillar axis, respectively. Vertical axis - counts during 1 ms. (**B**): The time course of polarized intensity of rigor myofibril. (**C**): The autocorrelation function of counts in channel 1 of for the signal in **A**. Red line - the best fit of the experimental autocorrelation function to piecewise triangular waveform. (**D**): the autocorrelation function of rigor muscle (the signal in **B**). Myofibrillar axis is Vertical on the microscope stage. Laser polarization is Vertical on the microscope stage. Excitation 470 nm, emission>500 nm. Laser power = 2 μW, light flux ~7 μW/μm^2. Data collected with PicoQuant MT200.*

Fig. 10 shows a typical example of an experiment which was analyzed for fast oscillations. **A** and **B** show the original signal. The correlation functions are shown in **C** & **D**. The green line in **C** shows the fit of the fast periodicities in the experimental correlation function to a piecewise linear train of triangles. The time during which the signal is high and low indicates the ability or inability of cross-bridges to bind the thin filament. When a cross-bridge strongly attaches to actin the anisotropy is high because during this time the rotational freedom of a whole actin filament is low. The opposite is true for detached cross-bridge. We call these times t_{ON} and t_{OFF}. **Fig. 11** demonstrates how the times were extracted from the correlation function. t_{ON} was extracted by measuring the time from 0 until the correlation function first changed slope. t_{OFF} was measured from the time the correlation function changed slope to the next maximum. The inset shows the autocorrelation function with X-axis plotted on log scale. These times , measured at high (5mM) ATP, are summarized in **Table 2**.

Table 2. *Accessible-Inaccessible and ON-OFF times obtained from contractions induced by high and low ATP concentrations. N is the number of independent experiments.*

[ATP]	t_A (s)	t_I (s)	N	t_{ON} (s)	t_{OFF} (s)	N
5 mM	1.2 ± 0.40	2.3 ± 1.0	17	0.4±0.2	0.7±0.4	10
10 µM	3.1 ± 0.7	3.2 ± 0.7	11	-	-	10

Fig 10

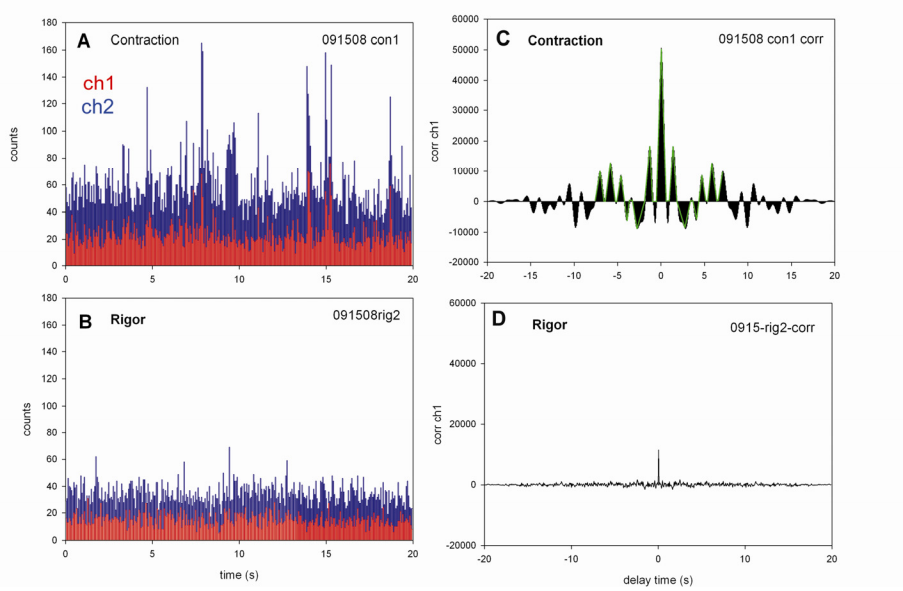

Fig. 10. *Example of a signal which gives correlation function with clear substructure in slow oscillating peaks. The time course of polarized intensity of contracting (**A**) and rigor (**B**) myofibril. Vertical axis - counts during 1 ms. The autocorrelation function of counts in channel 1 (**C**). Green line - fit of the experimental autocorrelation function to piecewise triangular waveform. The autocorrelation function of rigor muscle (**D**). Data collected with ISS Alba.*

Fig 11

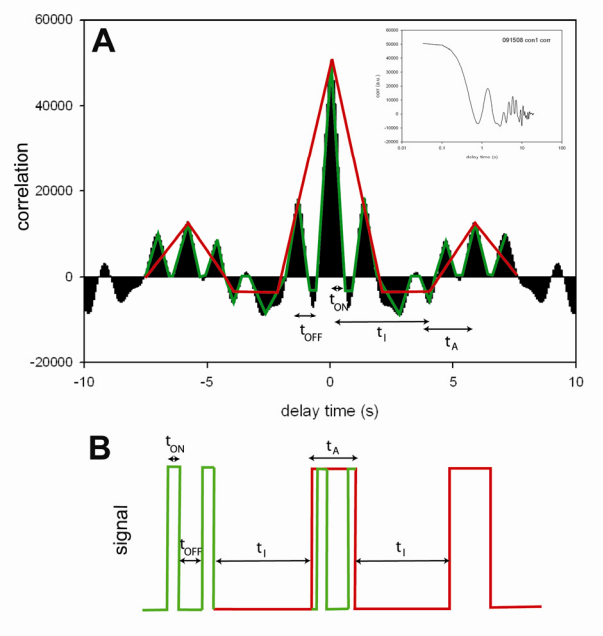

Fig. 11. A *- The autocorrelation function was fitted by a slowly oscillating (red) and rapidly oscillating (green) train of triangles.* t_A *and* t_{ON} *are defined as times from the peak of the slow or rapid triangles to zero, respectively.* t_I *and* t_{OFF} *are the times remaining to complete a cycle. The inset shows the autocorrelation function with X-axis plotted on log scale. The initial decay is characteristic of rapid oscillations.* ***B*** *- the signal corresponding to the autocorrelation function in A.*

Contraction induced by low [ATP]. It is known that in the presence of low [ATP] the rate of actin motion in the in vitro motility assay is low and that the decrease in the concentration of ATP causes the duration of the strongly bound state of skeletal myosin to increase (6). **Fig. 12A** shows a typical record of the time course of polarized fluorescence of a myofibril whose contraction was induced by 10 µM ATP. The autocorrelation function is shown in **Fig. 12B**. It is clear that the major change was an increase in t_A and t_I .We carried out 10 experiments using 10 µM ATP to induce contraction. The average value of t_A and t_I are given in **Table 2**. The

differences in means are statistically significant for both times (t=7.03, P<0.001 for t_A and t=2.30, P=0.042 for t_I).

Fig 12

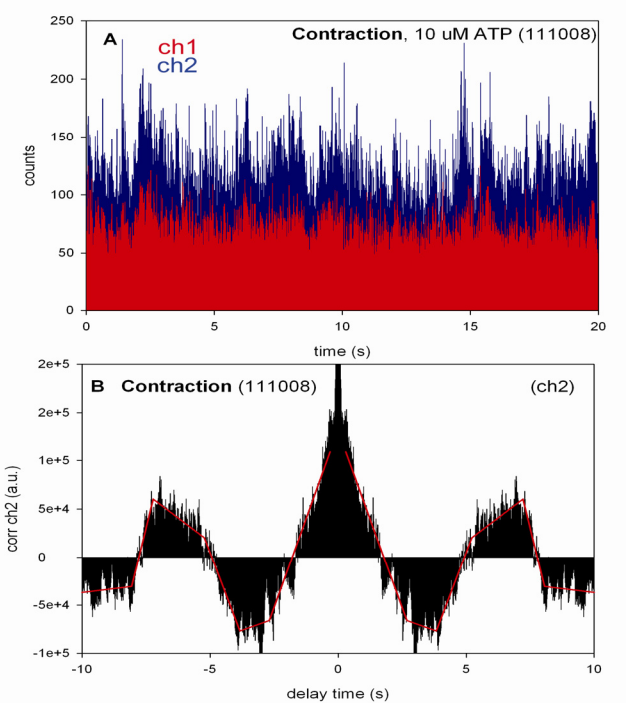

Fig. 12. A *– The raw signal from muscle contracting in the presence of 10 μM ATP. Ch1 (red) and ch2 (blue) are the fluorescence intensities polarized perpendicular and parallel to the myofibrillar axis, respectively. The number of detected molecules in low [ATP] experiment is estimated from the intensity of the signal as before: average of* I_V *and* I_H *signal: 117 and 69 photons/66ms. Total signal=* $I_V+2*G*I_H$*=255 photons/66 ms=3.8K photons/s. Background=1.9K photons/s. Therefore the signal (1.9K photons/s) originates from ~1 fluorophore.* ***B*** *- The correlation function of the blue signal. Data was fitted to the exponential function, the exponential was subtracted from the data to get zero average value and correlation function was computed. The red line is the least square fit to the correlation. In order to get correlations only between corresponding points, padded zeros have been added before the*

correlation calculation. 1000 points averaging was used. Excitation 532 nm, emission>590 nm. The data was collected every 10 μs. The vertical scale is the number of counts during 66.7 ms. Myofibrillar axis is vertical on the microscope stage. Laser polarization is vertical on the microscope stage. Data collected with ISS Alba.

Discussion

We've used intensity of polarized fluorescence to measure the kinetics of the binding of myosin cross-bridges to actin. Anisotropy is a ratio of two noisy signals and its autocorrelation function is very noisy. We have therefore measured the correlation of one of its intensity components. This is justified, because we have previously shown that parallel and perpendicular fluorescence intensities behave similar to anisotropy (45). Moreover, as already mentioned, Barcellona et al. (7) have shown that the autocorrelation function of P approximates the autocorrelation function of polarized intensity.

The kinetics was measured from a single molecule of actin. Although there were originally several molecules in DV, as shown in **Fig. 7A**, the majority of fluorophores become bleached out. A single fluorescent molecule remaining after bleaching out could not be destroyed in a few seconds (the remaining molecule is probably located further from the focus of the laser beam than the bleachable ones). This fitted our purpose well, because it gave rise to undiminished fluorescence for at least 10-20 s necessary to perform the experiment. While we have provided, what is in our opinion, a convincing argument that the signal is coming from a single molecule, it is possible that we have inadvertently underestimated the number of molecules, and the data does not originate from a single molecule but from a small assembly of several molecules. But the

nature of argument does not change even if we have underestimated number of detected molecules. As long as the number falls within mesoscopic regime, i.e. stochastic fluctuations become important, the same kinetic information is extracted from fluctuations even when more than one molecule contributes to the signal. The size of fluctuations is largest when one molecule is observed (18), but the autocorrelation function is the same whether 1 or 10 molecules are observed.

Not surprisingly, a signal from a single molecule was very noisy - it originated from a single actin molecule among 200,000 present in a Half Sarcomere (HS). To reduce noise, we constructed the correlation function of the signal. Correlation function reduces the white noise because there is no correlation between the noise at a given time and the noise any time later. This reduction comes at a heavy price - the degeneracy of the correlation function. The phase information is lost by squaring the amplitude power spectrum (or, in the case where correlation is computed directly, by multiplying signal by itself). **Fig. 13A** illustrates the fact that there are many waveforms giving the same correlation function. For example, crystallographic studies, single-molecule studies, spectroscopic experiments, and X-ray diffraction experiments on muscle fibers suggest that in addition to ON and OFF conformations, cross-bridge lever arm assumes an additional -- weak binding -- conformation (50). This leads to a conclusion that polarized intensity of actin monomer assumes 3 different values, as illustrated in the bottom left column of **Fig. 13A**. If the duration of each step were equal, the result would lead to a correlation function of the same shape as 2-step process. Because of this degenerative property of the Fourier Transform, our results cannot provide evidence for such a state.

This degeneracy makes is necessary to presume a shape of the signal giving rise to the observed correlation function. The simplest signal giving rise to the observed correlation function (a linear train of triangles) is a linear train of rectangles. As we said earlier, this is an oversimplification, but the one that most likely correctly reflects the main events occurring during contraction. It is interesting to note that the correlation function is comprised of two periodic processes. They both give rise to a rectangular signal of the same shape, but with a different period (**Fig. 11B**). The first, a slow process, probably reflects the ability of a cross-bridge to bind to actin. The period of this process was 3.5 s. It implies that cross-bridges bind to actin in bursts. During the time t_I no binding occurs. During this time the cross-bridges may be unable to reach actin because they may have restricted access or because their axial position does not allow the power stroke to take place. During the time t_A cross-bridges undergo normal interaction with actin. The cycle of events is illustrated in **Fig. 13C. Fig. 13D** shows the assumed shape of the corresponding correlation function: Cross-bridges carrying the products of the hydrolysis of ATP bind strongly

to actin leading to a decrease in the number of bending modes of the thin filament and presumably resulting in high anisotropy. The dissociation of Pi leads to force generation followed by the dissociation of ADP and the formation of rigor complex. The attached state ends when the myosin cross-bridge binds to a new molecule of ATP. The strongly attached state lasts t_{ON} seconds. The cross-bridge detachment results in increase in the number of the bending modes of thin filament and leads presumably to a low anisotropy. This state lasts t_{OFF} seconds. The average cycle time determined in the present work $t_C=t_{ON} + t_{OFF}=1.1$ s, is longer than determined from the maximal ATPase activity measured in isometric myofibrils here (~300 ms) and in

glycerinated muscle fibers (120-100 ms). This is most likely caused by the fact that the ATPase measurements in muscle fibers are not equivalent to measurements of changes in the orientation of the phalloidin-actin protomer. The former reflects a gross phenomenon, while the SMD polarization measurements report on a local orientation change. It is likely that a hydrolysis event by a distant cross-bridge is not sensed by the actin molecule under observation. The binding signal propagates only over a few actin monomers and the nearest cross-bridge on the same actin filament is 38.5 nm away.

Fig 13

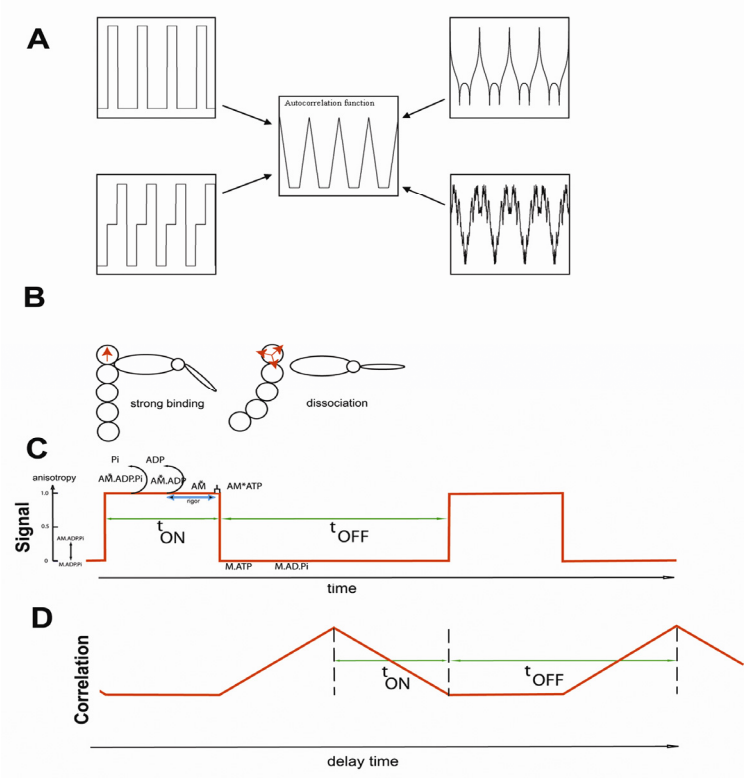

Fig. 13. A - *Examples of degeneracy of autocorrelation function. Many waveforms have the same autocorrelation function. The relationship between molecular events (**B**), the observed signal calculated from the autocorrelation function (**C**). The fact that anisotropy is high when*

*myosin is strongly bound to actin and low when it is dissociated from it is an assumption. (**D**) correlation function.*

Duty ratio**.** A useful measure of the myosin cross-bridge kinetics is the duty cycle - a fraction of the total cycle time that a cross-bridge remains attached to actin. A cross-bridge is in a strongly attached state for a period of time t_{ON}, while the total cycle time is t_I+t_A. The duty ratio of the entire isometric cycle, $\Psi = t_{ON} /(t_I+t_A)$ was ~11%. This is smaller than data obtained earlier by Cooke et al (Cooke et al. 1982) by electron spin resonance, and by Duong and Reisler by measuring tryptic digestion at the 50/20 kD junction of the myosin heavy chain. The value of Ψ obtained here is also smaller than the value of ~0.3 obtained by Cooper at al. A different measure of the activity of cross-bridges is the "accessible" duty cycle - a fraction of the accessible time that a cross-bridge remains attached to actin. This ratio was $\Psi' = t_{ON} /(t_{ON}+t_{OFF})$=36%.

The most obvious change in the pattern of contraction induced by low concentration of ATP was in t_A and t_I. The values of t_A and t_I increased 160 and 40%, respectively. The entire kinetics of contraction became different, as demonstrated by the fact that Ψ became now ~ 50%. These results are consistent with the earlier results on isolated single myosin molecules in vitro.

Relaxed muscle. We did not systematically analyze relaxed muscle. The reason was that in a few experiments the signals from active and relaxed muscle were similar. This was because cross-linking caused damage to the regulatory proteins. Herrmann et al. (31) estimated that ~8% of the myosin cross-bridges were cross-linked to actin using 2 mM EDC. This was apparently sufficient to permanently turn on the system. The problem is even more severe in our case because 2 mM

EDC was not sufficient in our hands to completely prevent shortening. We had to increase the concentration of EDC to 20 mM to assure that no shortening whatever occurred. With such high [EDC], the degree of cross-linking (in heart papillary muscle) was 30% (43). We conclude that the extensive cross-linking that we needed to employ to completely eliminate shortening, permanently turned on the system and made experiments on relaxed muscle not reliable.

CHAPTER IV

Fluorescence Lifetime of Actin in the FHC Transgenic Heart

The fluorescence lifetime is the average rate of decay of a fluorescent species from its excited state. The fundamental feature of the fluorescence lifetime is that it depends on a variety of environmental factors such as general solvent effects due to the interaction of the dipole of the fluorophore with environment, specific solvent effects due to fluorophore-solvent interactions, formation of internal charge transfer states and viscosity and probe-probe interactions (34).

Analysis of the crystal structures, X-ray diffraction patterns and spectroscopic experiments confirmed the original idea of Huxley (17) that during isometric muscle contraction the myosin cross-bridges assume at least two distinct conformations, when they are strongly attached to- and dissociated from- thin filaments (50, 64). It is believed that strongly attached cross-bridges produce contractile force. The environment of a strongly attached cross-bridge is different from the environment of a dissociated cross-bridge. In this work we compare environments during isometric contraction of transgenic wild type (Tg-WT) mouse ventricle and transgenic ventricle carrying the D166V point mutation (Tg-D166V). A convenient way to get information about the environment is to measure the fluorescence lifetime of a fluorophore attached to a molecule of interest, in our case of actin. The fluorescence lifetime is generally longer when fluorophores are bound to immobile structures than when they are free in aqueous solution. Lifetime is independent of fluorophore concentration, a critical advantage in systems where photobleaching

is significant. These advantages were recognized by Ferenczi and his collaborators who first used fluorescence lifetimes to detect actomyosin states in mammalian muscle sarcomeres (21). In addition to fluorescence lifetime, a meaningful indicator of the state of muscle is its duty cycle. A cross-bridge is in a strongly attached state for a period of time t_s, while it remains in a dissociated or a weakly attached state for a period of time, t_d. The ratio $\Psi = t_s /(t_d+t_s)$ is defined as the duty cycle. To measure Ψ one can follow the changes in the environment of a cross-bridge while it undergoes a cycle of binding and dissociation from actin.

From the relative frequency of occurrence of a given lifetime it was estimated that during contraction the lifetimes and duty cycle of Tg-WT and Tg-D166V hearts were not different. Independently performed measurements in skinned papillary muscle fibers showed a large decrease in the cross-bridge turnover rate (g) in Tg-D166V preparations compared to controls (personal communication of Dr. D. Szczesna-Cordary). The cross-bridge turnover rate ($g \approx 1/t_s$) was calculated by taking the ratio of fiber ATPase/concentration of cross-bridges attached at all levels of force activation. For the duty cycle Ψ to remain constant, with a large decrease in g, one has to observe a parallel decrease in $f \approx 1/t_d$, i.e. our measurements suggest that the rate of attachment of D166V cross-bridges to thin filaments is lower than in WT cross-bridges. This is consistent with prolonged force transients combined with no change in Ca^{2+} transients observed in Tg-D166V intact papillary muscle compared to Tg-WT fibers (personal communication of Dr. D. Szczesna-Cordary).

RESULTS

Preventing shortening of contracting muscle. Our task was to compare the fluorescence lifetimes of actin in Tg-WT and Tg-D166V myofibrils during rigor, relaxation and contraction. There is no difficulty in measuring lifetime of rigor myofibrils. However, it is impossible to do so during contraction, because myofibrils shorten. Myofibrils often shorten in relaxing solution as well, due to the damage to troponin or tropomyosin, which become ineffective in preventing contraction even in the absence of Ca^{2+}. To measure the lifetime of a relaxed or contracting muscle, it is therefore necessary to prevent myofibrils from shortening. This was done by cross-linking with the water-soluble cross-linker EDC (31). Cross-linking does not affect force development (12, 31). Myofibrils were cross-linked for 20 minat room temperature with 2 mM EDC. The lack of shortening was checked by following the changes in the image in a microscope as described in (11).

Distribution of lifetimes during contraction of Tg-WT muscle. **Fig. 14** shows a typical lifetime image of rigor, relaxed and contracting cardiac Tg-WT myofibrils labeled with Alexa488-phalloidin. In, skeletal muscle myofibrils, phalloidin labels only the overlap zone because of nebulin (60). The enlarged image of a relaxed myofibril (right) clearly shows that in cardiac muscle the entire I-bands are labeled. This is consistent with the finding that binding of phalloidin in skeletal muscle is regulated by nebulin (4). Cardiac muscle has no nebulin.

Fig 14

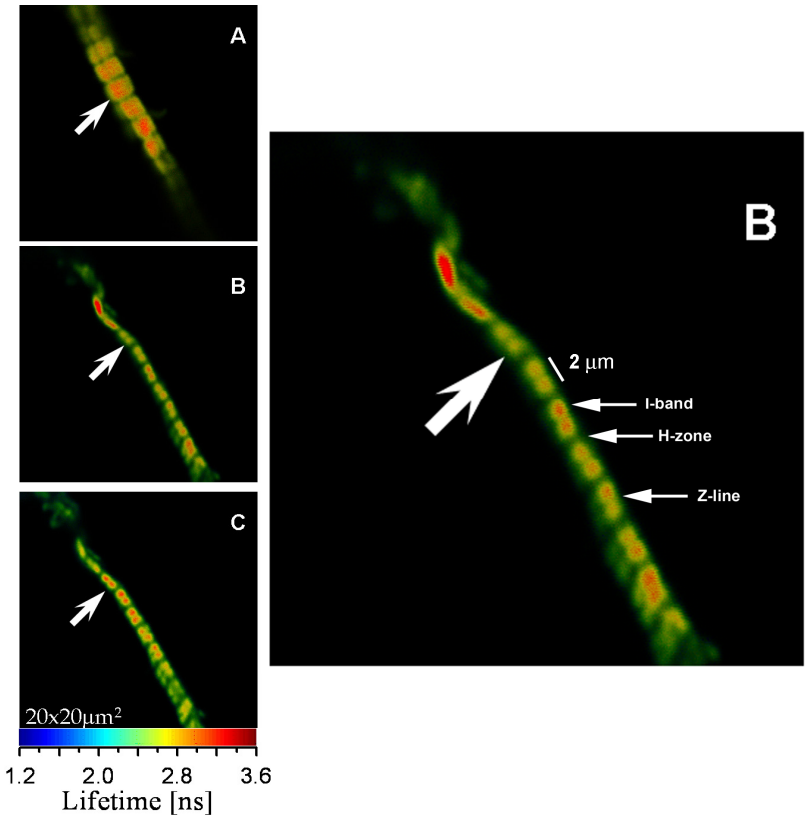

Fig. 14*. Lifetime images of rigor (A), relaxed (B) and contracted (C) Tg- WT myofibrils of cardiac papillary muscle. The color bar at the bottom is the lifetime scale. The enlarged image of a relaxed myofibril is shown on the right. As in Fig. 8 myofibrils were cross-linked to avoid shortening. Excitation was at 470 nm, emission was viewed through a 500 nm long-pass filter.*

The lifetime was measured by positioning the laser beam at the center of the I-band pointed to by the arrow. The laser beam was not scanned. **Fig. 15** shows the lifetime data collected during 60 sec. The fluorescence intensity decay was best fit (black line) with a double exponential function with slow (τ_1) and fast (τ_2) decaying components. The fractional contributions of slow and fast decaying components were approximately constant at 0.6 and 0.4, respectively. The excellent quality of the fit is demonstrated by a small χ^2 value of the fit (the residuals are shown in the

bottom figure of each panel). An equivalent strategy was to measure the lifetime 1,200 times every 50 msec for a total of 60 sec. The 50 msec interval is the approximate time necessary to collect enough photons in a sparsely labeled muscle to accurately calculate lifetime.

Fig 15

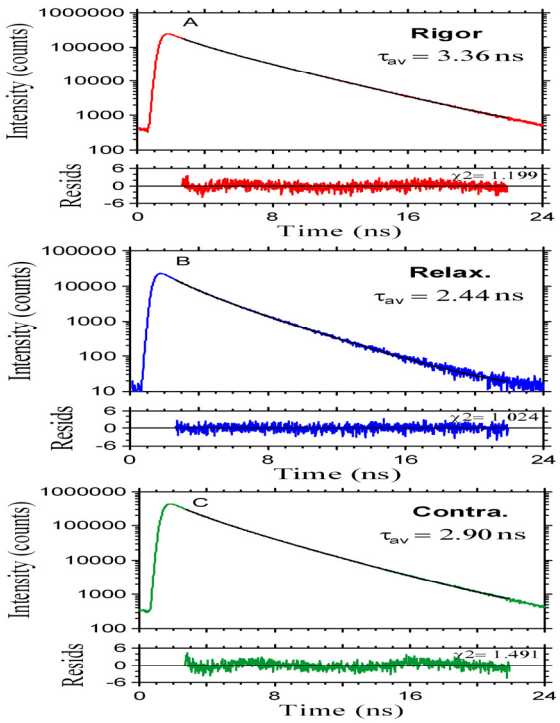

Fig. 15. *Intensity decays of fluorescence of pixels in the middle of the I-band pointed to by the arrows in* ***Fig. 14****. Colored lines – experimental decays, black lines – data fitted by two exponentials. Data collected for 60 sec, excitation with a 470 nm pulse of light, emission through LP500 filter.*

Fig. 16 shows a typical time-course of the intensity averaged lifetime of a single pixel of rigor (A), relaxed (B) and contracting (C) Tg-D166V muscle monitored every 100 msec. It can be seen that the average value of the lifetime remained constant in spite of the fact that photobleaching occurred.

Fig 16

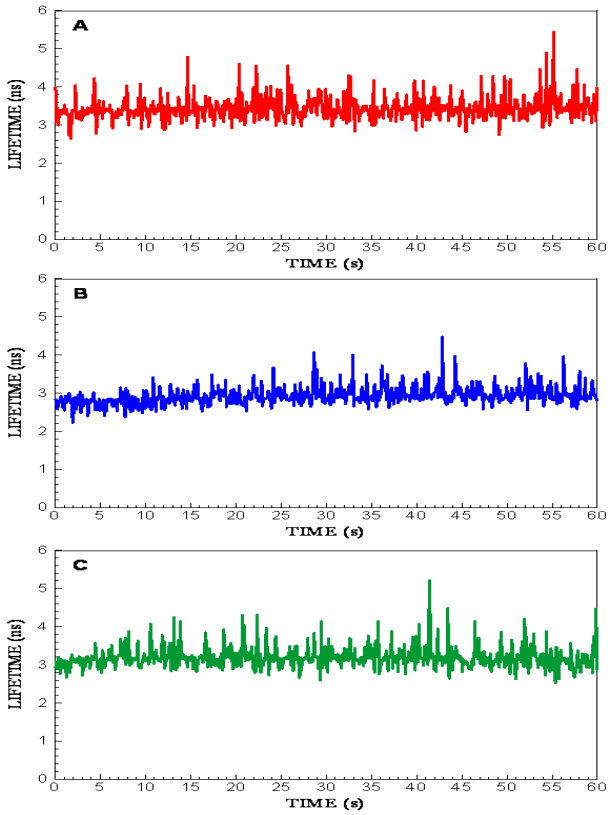

Fig. 16. *The time-course of changes of τ_2 of contracting Tg-D166V muscle. A –rigor, B – relaxation, C- contraction. Data obtained every 1 msec, but the points are plotted every 100 msec.*

The normalized distributions of lifetimes of rigor, relaxed and contracting Tg-WT muscle (1,200 measurements) are plotted in **Fig. 17**. The histogram of slow decay times τ_1 is shown in pink, the histogram of fast decay times τ_2 in violet and the histogram of the intensity averaged decay times in gray. The intensity averaged lifetimes for Tg-WT muscle were 3.31±0.21, 2.59±0.19 and 2.89±0.10 nsec for rigor, relaxed and contracted muscle, respectively. This data is summarized in **Table 3**. As shown, an increase in mobility of the fluorophore occurs in the following order: $\tau_{rig}>\tau_{con}>\tau_{rel}$ for both Tg-WT and Tg-D166V.

The duty cycle was calculated assuming that 100% of cross-bridges were bound to actin in rigor and that 0% during relaxation. Thus, under ideal conditions the distribution of lifetimes during contraction should be biphasic: it should assume the values characteristic of either relaxation or rigor. In practice, the distribution was smeared: the observed (apparent) lifetime τ_{con} was intermediate between rigor and relaxation $\tau_{con} = (N_{rel} \cdot \tau_{rel} + N_{rig} \cdot \tau_{rig})/ (N_{rel} + N_{rig})$, where N_{rel} and N_{rig} are the number of times that relaxed and rigor lifetimes appeared during the experiment. We think that this is because the peaks corresponding to the averaged values of τ_{rig} and τ_{rel} cannot be resolved. It is therefore reasonable to assume that the duty cycle is $\Psi = (\tau_{con}-\tau_{rel})/(\tau_{rig}-\tau_{rel})$ x 100%. From the intensity averages in **Fig. 17** the duty cycle $\Psi = (\tau_{con}-\tau_{rel})/(\tau_{rig}-\tau_{rel})$ x 100% for Tg-WT muscle was calculated as 45%. Only in some cases the distribution of τ_2 was biphasic (e.g. violet trace in **Fig. 17C**). The advantage of this is that Ψ can be estimated only from the contraction data, i.e. it does not rely on measurements of τ_{rig} and τ_{rel}. The lifetime τ_2 always behaved oppositely to τ_1: whereas for τ_1 $\tau_{rig}>\tau_{con}>\tau_{rel}$, the opposite was true for τ_2, i.e. $\tau_{rig}<\tau_{con}<\tau_{rel}$. From the violet curves in **Fig 17C** it can be seen that some contraction lifetimes have τ_2 characteristic of rigor and some have lifetime characteristic of relaxation. The ratio of the two was estimated as 1.5, suggesting that the duty cycle during contraction of Tg-WT muscle is $(1+1/1.5)^{-1} \approx 60\%$.

Fig17

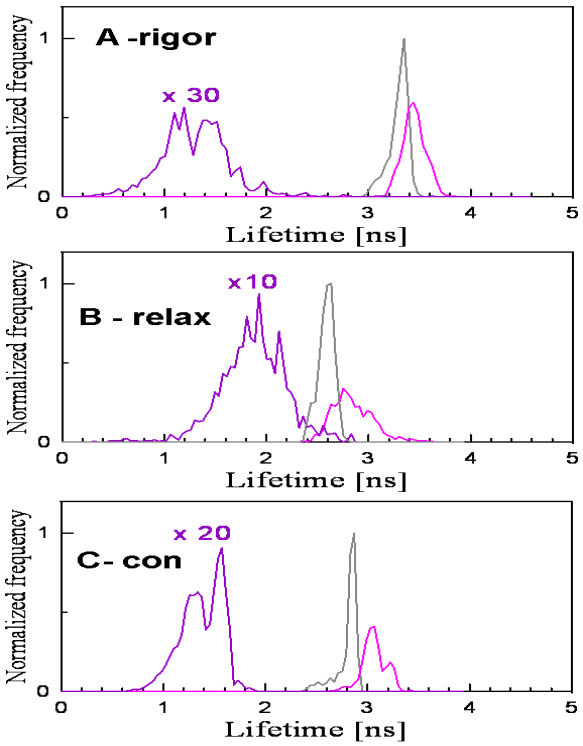

Fig. 17*. Normalized histogram of single-point lifetimes taken every 50 msec during a 60 sec of data collection in rigor (A), relaxed (B) and contracted (C) Tg-WT muscle. The histogram of slow decay time* τ_1 *is shown in pink, the histogram of fast decay time* τ_2 *in violet and the histogram of intensity average decay times in gray.*

Distribution of lifetimes during contraction of Tg-D166V muscle. **Fig. 18** shows a typical lifetime image of a rigor, relaxed and contracting cardiac Tg-D166V myofibril. As before, the decay could be best fit with a double exponential function. The fractional contributions of slow and fast decaying components were approximately constant at 0.6 and 0.4.

Fig18

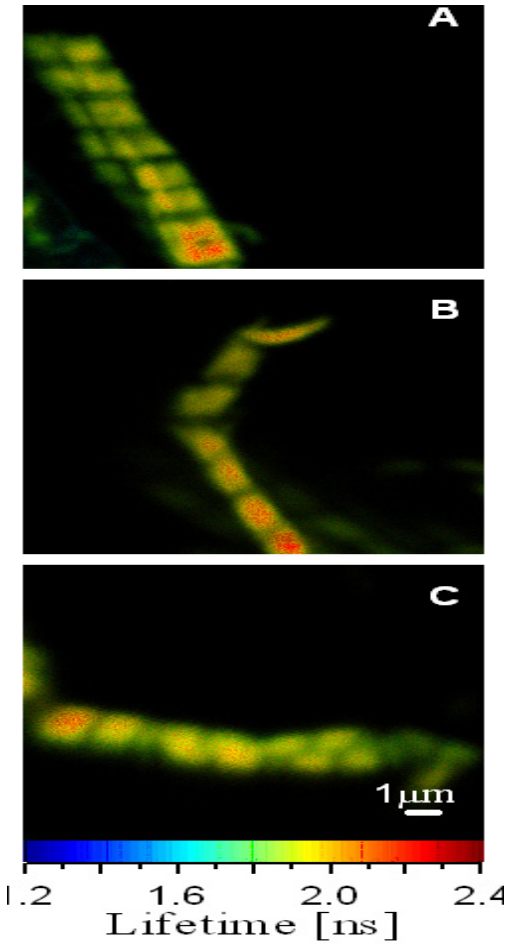

Fig. 18*.Lifetime images of rigor (A), contracted (B) and relaxed (C) Tg-D166V myofibril. The color bar at the bottom is the lifetime scale. Excitation was at 470 nm, emission was viewed through a 500 nm long-pass filter.*

The normalized histograms are plotted in **Fig. 19**. The intensity averaged lifetimes (gray) and their variations were τ_{rig}= 3.30 ± 0.20, τ_{rel}= 2.81 ± 0.18 nsec and τ_{con}= 3.15 ± 0.19 nsec for 60 sec data collected from muscle in rigor, relaxation and contraction, respectively. This data is summarized in **Table 3**. The differences between WT and mutated muscle were not statistically

significant (t_{rig}=0.062, t_{rel}=1.57, t_{con}=1.605, P<0.184 in all cases). The duty cycle $\Psi = (\tau_{con}-\tau_{rel})/(\tau_{rig}-\tau_{rel})$ x 100% was 69%.

Table 3

Temporal average of lifetimes of actins located in the center of the I-band of rigor, relaxed and contracted muscle in Tg-WT and Tg-D166V myofibrils.

Muscle	Tg-WT	Tg-D166V
τ_{rig} (nsec)	3.31±0.21	3.30±0.20
τ_{rel} (nsec)	2.59±0.19	2.81±0.18
τ_{con} (nsec)	2.89±0.10	3.15±0.19

Fig 19

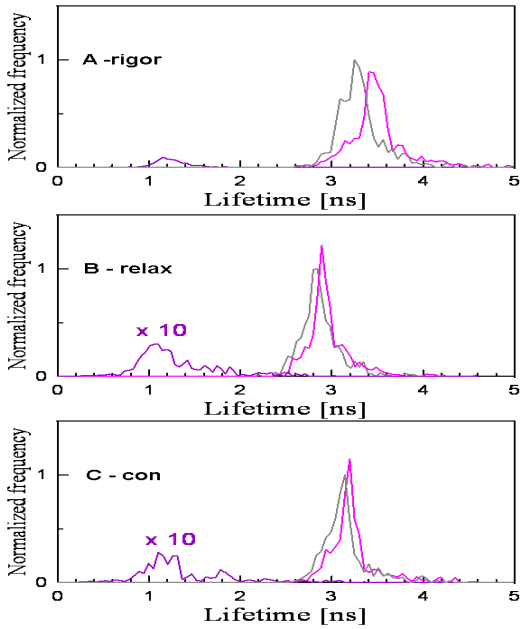

Fig. 19. *Normalized histogram of single-point lifetimes taken every 50 msec during 60 sec of data collection in rigor (A), relaxed (B) and contracted (C) Tg-D166V muscle. Colors are as depicted in* ***Fig. 12.***

DISCUSSION

In this study we compared the fluorescence lifetimes of Alexa488 labeled actin molecules in Tg-WT and Tg-D166V muscle myofibrils.

Single-point lifetime. Lifetime was measured 1,200 times every 50 msec for a total of 60 sec from an area fixed at the center of the I-band of rigor, relaxed and contracting muscle. Lifetime was measured from the frequency distributions. The number of actin monomers contributing to the signal was determined by DOL and by the size of the sampled area. The simple calculation outlined in the Materials & Methods suggests that there are ~20,000 G-actins in a typical half-sarcomere. Taking DOL of 1000 and the concentration of actin in muscle as 0.6 mM, we calculate that each half-sarcomere contains ≈ 20 fluorophores. The sampled area is diffraction limited by a 1.2 NA water objective and 470 nm laser wavelength, giving a diameter of the spot from which data is collected as ~0.3 μm. Thus the microscope resolves ($\pi \cdot 0.30^2$) = 0.28 μm^2 area. There are approximately 13 such areas in HS, each containing on average 20/13=1.6 fluorophores. However, this theoretical calculation most likely underestimates the number of fluorophores simply because we did not observe a step-wise photobleaching trait, which is characteristic of single molecule observations. There is a serious experimental difficulty in determining the dry weight of the mouse ventricle (see Materials & Methods). Therefore the most reliable way to estimate how many fluorophores are contributing to the change of lifetime in response to cross-bridge turnover is from the rate of arrival of photons. Typically, we observed ~16,000 photons arrive in 1 sec. We usually see ~4,000 photons arrive from a single

molecule in 1 sec (J. Borejdo, personal observation). We therefore estimate that in a single-point measurement on average ~4 fluorophores contribute to the signal.

In the present work, where we studied the RLC D166V mutation which was over-expressed at 90% in the Tg myocardium, this does not matter. In general, however, it is essential to have a technique capable of monitoring lifetimes of single molecules. Human patients are normally heterozygous for FHC mutations, so their myosin containing thick filaments are composed of wild type myosin heads interspersed with FHC mutant heads. Any large observational volume thus contains a mixture of WT and FHC molecules, making the comparison between kinetics of healthy and diseased muscle impossible. Therefore, the unambiguous determination of myosin cross-bridge kinetics requires that the experiments are carried out at the level of a single molecule to avoid averaging over ensembles of molecules with different kinetics.

It was assumed that during time t_s the cross-bridge bound to actin in the thin filament has lifetime τ_{rig} and that during time t_d the cross-bridge is free from actin and has lifetime τ_{rel}. This is because the environment and mobility of the fluorophore are significantly different when a cross-bridge is bound to or free from actin. It was observed that $\tau_{rig} > \tau_{rel}$. This difference is not expected to result from fluorescence quenching by amino acids of a cross-bridge when it is bound to actin during rigor, because quenching causes a decrease in lifetime. The most likely explanation for the observation that $\tau_{rig} > \tau_{rel}$ is that binding of cross-bridges stabilizes fluorophores attached to actin. Mobility of the dye may lead to a non-radiative depopulation of the excited state resulting in a decrease of lifetime. To check this hypothesis, we compared the lifetimes of mobile and immobilized Alexa488-phalloidin. The fluorophore was dissolved in

water or 100% glycerol to assure its mobility or immobility, respectively. The intensity decay curves were best fit by a sum of 3 exponentials. The amplitude averaged lifetimes in water and glycerol were 2.479±0.037 and 2.904±0.013 nsec, respectively, confirming the suggestion that the observed increase in lifetime during rigor is due to immobilization of the dye. This reasoning implies that the only factor contributing to a change in lifetime is binding of a cross-bridge to actin and not binding of ATP to myosin. This is because binding of ATP makes no difference to lifetime of fluorescein attached to myosin (2).

The accuracy of single point measurement was <26%. This low accuracy is perhaps due to the fact that myofibrils did not remain completely still during relaxation, and consequently data was not collected from a single position. In relaxation it is important that all troponin and tropomyosin molecules be fully functional. If even a small fraction of them is damaged, the muscle may oscillate due to contraction of sarcomeres containing non- functional regulatory proteins. This is unlikely to happen during contraction because Ca^{2+} and ATP are both present. Ishiwata et al. found that the myosin II motors show non-linear auto-oscillation, named SPOC (SPontaneous Oscillatory Contraction). For cardiac muscle it occurs when the activation level is intermediate between those of contraction and relaxation (32, 47). In our experiments, however, pCa was fixed at 4.

In addition, we have considered three possible explanations which could give rise to artifacts and concluded that none is likely:

1. It is impossible that lifetime is influenced by photobleaching because lifetime does not depend on intensity of fluorescence.

2. It is unlikely that measurements of lifetime are influenced by the dissociation of phalloidin from thin filaments because in a control experiment we first labeled 1 mg/ml (4 μM actin) of cardiac myofibrils with excess of unlabeled phalloidin. After brief incubation, we added 4 μM of fluorescent phalloidin in an attempt to displace bound phalloidin with fluorescent phalloidin. If the off-rate of phalloidin were fast, myofibril would have now become fluorescent. This was not the case, suggesting that the off-rate of phalloidin is slow. This is consistent with the fact that the dissociation of phalloidin from skeletal muscle actin is known to be slow (4.8×10^{-4} sec^{-1}), i.e. phalloidin spends on the average 2,000 sec on actin before dissociating.
3. It is impossible that Trp fluorescence of myofibrils contributes to the signal because Trp has practically no absorption at 470 nm and unlabeled myofibrils had no autofluorescence whatsoever (probably because the sample was only ~100 nm thick).

The low accuracy of measurements did not allow us to conclude that Ψ is statistically different in Tg-WT and Tg-D166V muscle. If it were possible to measure single-point lifetime of the same I-band in rigor, relaxed and contracted heart muscle, the accuracy of the measurement of one type of muscle (Tg-WT or Tg-D166V) would have been <1%. Unfortunately, such an experiment proved impossible. The exchange of bathing solution created a flow that often moved the myofibril beyond the field-of-view of the microscope. This means that in order to determine the absolute value of lifetimes, the measurements have to be done on a different I-band in a different myofibril. It should also be noted that from the records such as shown in **Fig. 17** it is possible, in principle, to measure the absolute amount of time cross-bridge spends attached and dissociated from actin (i.e. not only Ψ). At present, this signal is too noisy. Future work is needed to improve

it. Also, in the future it should be possible to design an experimental chamber to allow irrigation of myofibril with relaxing and contracting solutions so gently as to avoid any displacement.

It should be noted that phalloidin binding site is located at the contact region between three actin subunits. The observed changes of lifetime therefore reflect response to cross-bridge turnover of 3 actin monomers. Measuring changes of lifetime of these actins reflects changes of lifetime of a cross-bridge. Indeed, it has been shown that a 3-actin complex and a cross-bridge rotate in synchrony (57). Labeling actin has an important advantage in that it can be labeled specifically and stoichiometrically with fluorescent phalloidin. Further, phalloidin does not alter the enzymatic properties of muscle (13) and does not impair the regular structure of the myofibril.

Implications for heart muscle. In a parallel study, skinned and intact papillary muscle fibers from Tg-D166V mice were examined using a Guth Muscle Research System and the effects of the D166V mutation compared to Tg-WT and NTg (non-transgenic) mice (personal communication of Dr. D. Szczesna-Cordary). A large increase in the Ca^{2+} sensitivity of force and ATPase (ΔpCa_{50} higher than 0.25) measured simultaneously under isometric conditions was determined in skinned muscle fibers from Tg-D166V mice compared to control NTg and Tg-WT mice. This D166V mediated increase in the Ca^{2+} sensitivity of force and ATPase was shown to be due to a large decrease in the cross-bridge dissociation rate (g), expressed as the ratio of fiber ATPase/concentration of cross-bridges attached at all levels of force activation. Since $g \approx 1/t_s$, where t_s corresponds to time when a cross-bridge is attached to actin and generates force, this implies that t_s would have to increase in Tg-D166V muscle to result in a decreased g. As proposed by Huxley (17), the transition from the non-force-generating states to the force-generating states in muscle can be characterized by the cross-bridge attachment rate ($f \approx 1/t_d$) and

the rate of the cross-bridge return to the non-force-generating states ($g \approx 1/t_s$). In the present study we show that the duty cycle Ψ defined as a ratio of $t_s /(t_d+t_s)$ was the same in Tg-WT and in Tg-D166V myofibrils. Since the duty cycle $\Psi = t_s /(t_d+t_s)$ was not changed and t_s was predicted to increase in Tg-D166V muscle, this implies that in order for Ψ to remain constant, t_d would have to also increase and consequently the rate of cross-bridge attachment f would have to decrease.

Our results of no D166V mediated change in Ψ and predicted increases in t_s ($\approx 1/g$) and t_d ($\approx 1/f$) suggest that the rates of cross-bridge attachment and detachment are most likely decreased in Tg-D166V muscle compared to control Tg-WT. This hypothesis is supported by the measurements of prolonged force transients in Tg-D166V intact papillary muscle fibers compared to Tg-WT fibers (personal communication of Dr. D. Szczesna-Cordary). The slow force relaxation rate of the fibers could potentially result in diastolic dysfunction of the D166V mutated myocardium. Abnormal diastolic filling of the heart could also lead to a decreased stroke volume causing systolic dysfunction. These changes if severe enough would ultimately result in compensatory hypertrophy and could lead to sudden cardiac death as observed in the individuals harboring the D166V mutation (51).

CONCLUSIONS

We have shown that the environment of a single cross-bridge can be followed every 50 msec by measuring the fluorescence lifetime of actin monomer in an isometrically contracting muscle. By comparing relative contributions of lifetimes characteristic of relaxed and rigor muscle, we

determined that the lifetime and the fraction of cross-bridges bound to actin during contraction is similar for both Tg-WT and Tg-D166V muscle.

CHAPTER V

Faster Cross-bridge Kinetics Caused by the Familial Hypertrophic Cardiomyopathy R58Q Mutation in the Regulatory Light Chain of Myosin

INTRODUCTION

Mutations in genes that encode for the major contractile proteins of the heart underlie the genesis of Familial Hypertrophic Cardiomyopathy (FHC). FHC is an autosomal dominant disease characterized by ventricular hypertrophy, myofibrillar disarray and sudden cardiac death (SCD) (39). The most prevalent mutations occur in the beta-myosin heavy chain, myosin binding protein C, tropomyosin, troponin and actin (reviewed in (3, 39)). Less common but quite malignant FHC mutations have been observed in the ventricular regulatory (RLC) and essential (ELC) light chains of myosin (19, 51). The lack of therapeutic strategies in FHC highlights the importance of finding the pathogenetic mechanisms by which FHC mutations cause disease.

The R58Q mutation in RLC has been found in patients with various ethnic backgrounds and has been associated with a malignant disease phenotype including multiple cases of SCD [16, 46. Using a transgenic (Tg) animal model for the R58Q mutation expressed in the murine heart, we have previously shown that compared to the wild type (WT) mice, the R58Q mutant fibers were characterized by increased Ca^{2+} sensitivity of force, lower level of maximal force and impaired muscle relaxation (68). This potentially abnormal diastolic function determined in Tg-R58Q mouse papillary muscles was later confirmed by the echo-Doppler assessment showing prolonged deceleration times in Tg-R58Q mice compared with Tg-WT (1). We have also shown

an R58Q–dependent increase in the actin activated myosin ATPase activity and increased actin filament sliding velocity in the *in vitro* motility assays (24). The latter report confirmed, at the molecular level, the R58Q-dependent decrease in force generation (24, 68). Based on our previous findings we have hypothesized that the R58Q mutation of RLC may cause alterations in the kinetics of the acto-myosin interaction. Consequently, the focus of the current investigation was to determine the effect of R58Q on cross-bridge kinetics, using our recently described Single Molecule Detection (SMD) approach (51).

The kinetic information originating from measuring isometric force is a temporal average of trillions of individual impulses that myosin delivers to actin in each second. Averaging may cause a loss of this kinetic information. To extract myosin cross-bridge kinetics from the conventional force measurements it is necessary to employ of a specific model of muscle action utilizing the rates of cross-bridge association (f) and dissociation (g) (17). We have used this approach in our recent investigation of the effects of another RLC FHC mutation, D166V. We showed that the D166V mutation drastically decreased g, which resulted in compromised contractility of the D166V murine hearts (68). In parallel, using our recently developed single molecule detection (SMD), we demonstrated a D166V-dependent decrease in myosin cross-bridge kinetics at the level of single molecules (17). The SMD approach was based on the fact that when a myosin cross-bridge delivers a force impulse to actin, the adjoining segment of the thin filament changes orientation. The orientational changes were followed by polarization of fluorescence (P), which is a sensitive indicator of the state of muscle contraction (41).

P is defined as the ratio of parallel and perpendicular polarized intensities: $P=(I_V-I_H)/(I_V+I_H)$, where I_V and I_H are the orthogonal intensities of fluorescence obtained using vertical and

horizontal polarization of exciting light, respectively. The signals that were analyzed in the current work were the orthogonal intensities I_V or I_H, rather than P. This was because P, being a ratio of two noisy orthogonal intensities, was very noisy. Fortunately, over a short time period, with unchanged signal average, the I_V and I_H behave similarly to P [42]. Moreover, Barcellona et al. (7) have shown that the autocorrelation function of P approximates the autocorrelation function of polarized intensity.

Orthogonal intensities were obtained by measuring components of polarized fluorescence of rhodamine dipole attached to actin. In our experiments, about one of 100,000 actins contained in a cardiac myofibril from Tg-R58Q mouse hearts, were labeled with rhodamine-phalloidin. By using a small confocal aperture, we were able to limit the number of actin molecules under observation to 1-4. To minimize the noise and to obtain kinetic information originating from a single molecule, we used Fluorescence Correlation Spectroscopy (FCS) (18). It was advantageous to observe actin rather than the myosin molecules, because labeling of actin with fluorescent phalloidin does not alter the enzymatic properties of the actomyosin system (13, 48) and because labeling is stoichiometric allowing for the strict control of the degree of labeling. In addition, actin was labeled in a non-covalent manner and therefore rigidly, which is extremely important when orientation of a dipole moment of the probe is measured.

The SMD measurements ought to be carried out *ex vivo* due to molecular crowding that characterizes a dense muscle environment. The apparent concentrations of actin and myosin in muscle are ~0.6 and ~0.2 mM, respectively. Consequently, the access to proteins might be limited to only small molecules of solvent leading to over hydration *in vivo*, and which could be

overlooked in the *in vitro* measurements. Furthermore, myosin activity might depend on various cofactors and on the local geometry of the filament arrangements. It is thus important that the measurements are carried out under conditions that closely reproduce the *in vivo* conditions. In this communication, we report the measurements of the kinetics of the actin-myosin interaction in the *ex vivo* hearts captured at the single molecule level.

We demonstrate that the rate of changes of actin dipole orientation is significantly faster in isometrically contracting cardiac myofibrils from Tg-R58Q mice compared to control, Tg-WT preparations. We also demonstrate a lower force per cross-sectional area of muscle fiber in Tg-R58Q mice compared to Tg-WT. We conclude that the R58Q-dependent increase in the myosin cross-bridge kinetics and the lower level of force observed in R58Q mutated hearts are most likely responsible for the overall compromised cardiac function and inability of the mutated hearts to efficiently pump blood.

RESULTS

Imaging. A typical lifetime image of a rigor Tg-WT myofibril from the mouse heart labeled with fluorescent phalloidin is shown in **Fig. 20A** (all the fluctuation experiments were done using rhodamine-phalloidin -- Alexa488 phalloidin was only used for imaging). Note that the entire I-bands are labeled. In contrast, in skeletal muscle the fluorescent phalloidin labels only the overlap zone of the sarcomere (60). This is because of nebulin, which allows phalloidin to bind only to the pointed ends of actin filaments, restricting its binding to the middle of the I-band (4). Since there is no nebulin in cardiac muscle, the entire I-bands are stained. The H-bands appear

dark and this is because they contain no actin. The parallel (I_H) and perpendicular (I_V) polarization images are shown in **Fig. 20B** and **C**, respectively. They clearly show that fluorescence is highly anisotropic as it is expected from the aligned array of the polar actin filaments. For the quantitative measurement of orientation, it is important to know whether the probe is immobilized by the protein so that the transition dipole of the fluorophore reflects the orientation of the protein. **Fig 20D** shows that this is the case for the AP-labeled thin filaments. The decay of anisotropy, defined as $(I_H-I_V)/(I_{H+}2I_V)$ was best fitted with the exponential function $r(t)=R_\infty+a \cdot \exp(-t/\theta)$, where $R_\infty = 0.29$ is the value of anisotropy at infinite time, $a = 0.07$, is the amplitude of the anisotropy change, and $\theta = 1.3$ ns is the rotational correlation time. The short correlation time is due to rotation rate of AP, consistent with the rotation rates of a molecule with MW=1,250 kDa. The fact that the anisotropy did not decay to zero from the maximum value of $R_o = 0.35$, but decayed to a large asymptotic value of $R_\infty = 0.29$, shows that this constant anisotropy of fluorescence is contributed by the immobile actin filaments. The mobile fraction is contributed by (0.35-0.29)/0.35 = 17% of fluorophores. Thus, ~83% of fluorescent phalloidin is immobilized by F-actin. This is consistent with the fact that the probes attached to proteins through the interactions that stretch over the large surface areas, e.g. hydrophobic or Van der Waals interactions, are attached more rigidly than the probes attached by the covalent links. We conclude that fluorescent phalloidin is a good dye for monitoring anisotropy of actin protomers in cardiac myofibrils.

Number of detected actin molecules. The red circle in **Fig. 20A** indicates the projection of the confocal aperture on the image plane. Its diameter (1.2 μm) is equal to the diameter of the confocal pinhole (50 μm) divided by the magnification of the objective (40x). The Detection

Volume (DV) is equal to the surface area of the projection (1.1 μm^2) multiplied by the height of a myofibril. To calculate the number of fluorophores in DV, we recognize that the myofibril is labeled with 0.1 nM AP + 10 µM UP (unlabeled phalloidin), so only one in ~100,000 of actin monomers carries the fluorescent phalloidin. The length, width and height of a typical half-sarcomere (HS) are 1, 1, and 0.5 µm, respectively, and therefore the DV volume is ~5 x 10^{-16} L. Since the concentration of actin in muscle is ~0.6 mM (40), this volume contains ~2 actin monomers. This estimation carries a significant error arising from several factors, e.g. uneven labeling of muscle, uncertainty of myofibril thickness, and a possible underestimation of the diameter of the focused laser beam. We estimate this error to be no more than 100%. Thus, the actual number of observed fluorophores ranges from 1 to 4. This fits easily within the resolution of the FCS method (18).

Fig 20

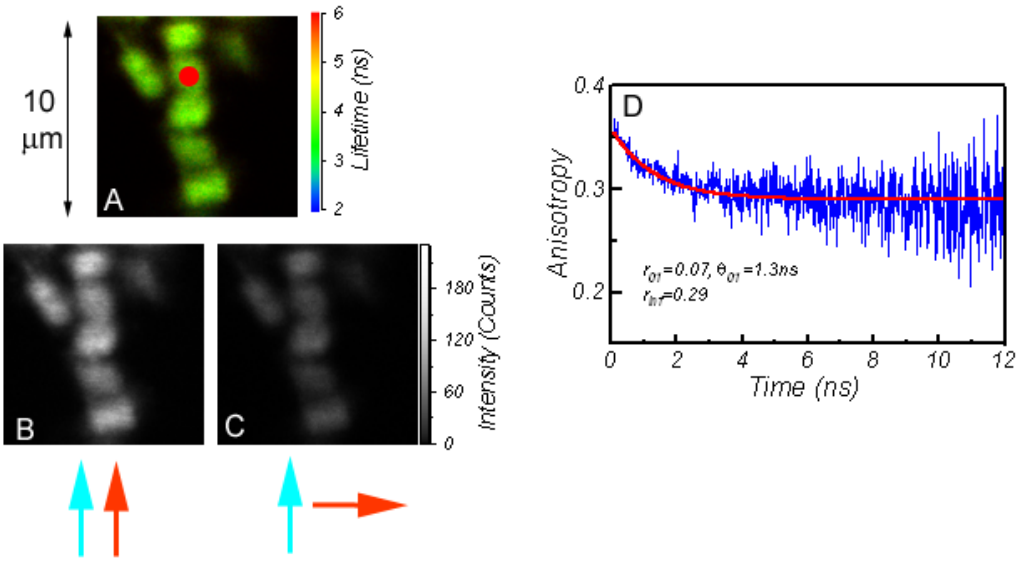

Fig. 20*. Lifetime (**A**) and polarization (**B**, **C**,) images of rigor Tg-WT myofibril from mouse ventricular muscle fibers. The color bar at right of lifetime image is the lifetime scale, with red corresponding to 6 ns and blue to 2 ns. The red circle is the projection of the confocal aperture on the sample plane. Its diameter (1.2 μm) is equal to the diameter of the confocal aperture (50 μm) divided by the magnification of the objective (40). The B/W intensity scale is 0-255, with 255 corresponding to white and 0 to black. Blue and red arrows indicate the direction of polarization of exciting and fluorescent light, respectively. The exciting light is polarized vertically. In this experiment only, myofibrils were labeled with 1 μM Alexa488-phalloidin.* ***D****. Decay of anisotropy of a typical I-band. Blue: experimental decay; red line: fit to the function* $r(t)=R_\infty+a \cdot exp(-t/\theta)$*, where* $R_\infty = 0.29$ *is the value of anisotropy at infinite time,* $a = 0.07$*, is the amplitude of the anisotropy change, and* $\theta = 1.3$ *ns, is the rotational correlation time. Data collected for 60 s. Data acquired with the PicoQuant Micro Time 200 confocal lifetime microscope. Excitation with a 470 nm pulse of light, emission through LP500 filter.*

Myofibrils. The signal utilized in this study was the intensity of polarized fluorescence, I_H or I_V. As mentioned above, the ideal signal would have been polarization of fluorescence, but it was too noisy being a ratio of two noisy orthogonal intensities. The intensity of polarized fluorescence was measured by positioning the laser beam at the center of the I-band and collecting the perpendicular and parallel components in ch1 and ch2, respectively. The laser beam was not scanned. After opening the laser shutter, the fluorescence intensity was initially high and after several seconds decayed to a steady state value of ~10K photons/s. **Figs. 21A** and **22A** show typical intensity data collected during 20 seconds from rigor and contracting cardiac myofibrils labeled with rhodamine-phalloidin (RP). The fluorescence signal was originating from 1-4 fluorophores.

Fig 21

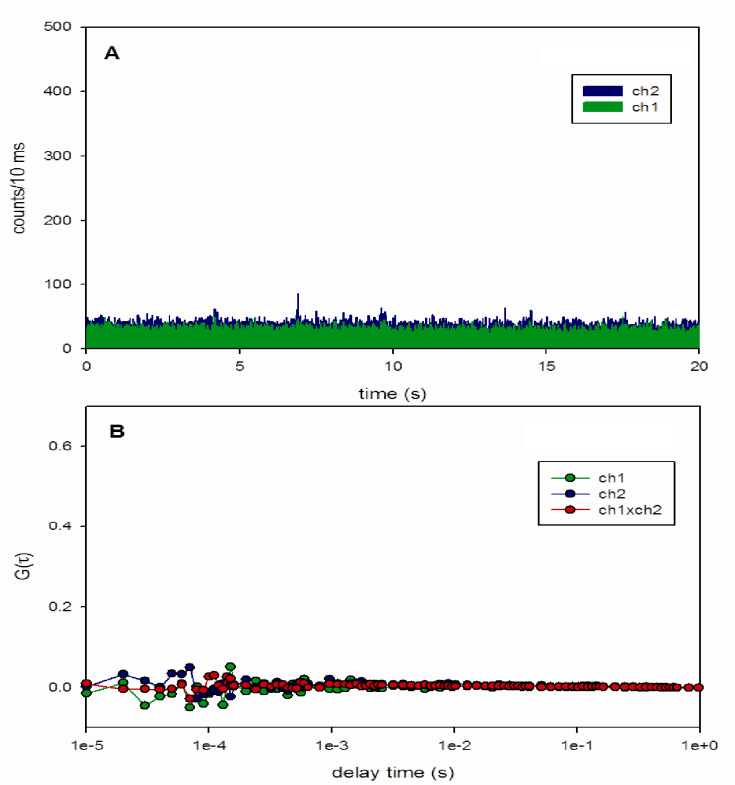

Fig. 21. ***A***. *The time course of polarized intensity of a rigor myofibril from the Tg-WT heart myofibril. The original data was collected every 10 μs, 1000 points were binned together to give time resolution of 10 ms. The vertical scale is the number of counts during 10 ms. Ch1 (green) and ch2 (blue) are the fluorescence intensities polarized perpendicular (I_V) and parallel (I_H) to the myofibrillar axis, respectively. Myofibrillar axis is vertical on the microscope stage.* ***B***. *The corresponding correlation functions. Laser polarization is vertical on the microscope stage.*

Fig 22

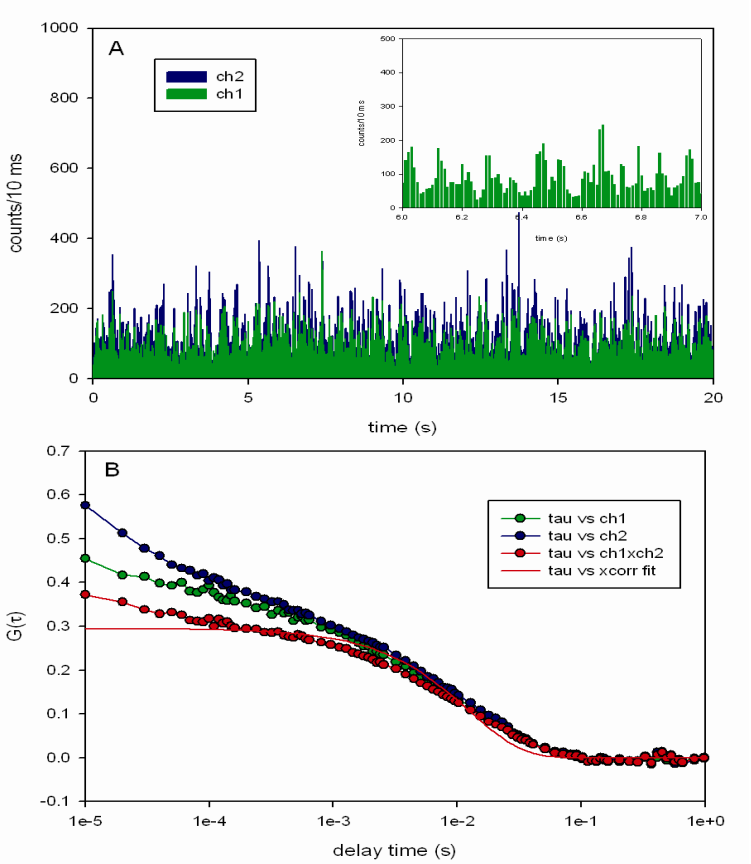

***Fig. 22**. **A**. The time course of polarized intensity of contracting myofibril from the Tg-WT heart myofibril. The vertical scale is the number of counts during 10 ms. Ch1 (green) is I_V and ch2 (blue) is I_H. Myofibrillar axis and laser polarization are parallel on the microscope stage. **B**. The corresponding correlation functions. The red line is the exponential fit to the cross-correlation function.*

Inset to **Fig. 22A,** shown at higher time resolution**,** demonstrates that it was possible to distinguish the individual impulses by inspection of the intensity traces. However, while the impulses were readily visible, it was difficult to extract from them the kinetic rates (such as the rate of rise and fall and the frequency), simply because they have variable shapes and duration. Also, the signal was noisy due to the impulses originating from 1-4 molecules amongst ~200,000

present in the HS and being bunched together. Nevertheless, kinetic information could be extracted from stochastic fluctuations by computing the correlation function of fluctuations. The correlation function at a given delay time τ is a sum of the products of the signal multiplied by a signal shifted by a delay time τ. If the signal is periodic, the autocorrelation function will also be periodic with the same periodicity as the original signal. At the same time, the autocorrelation of noise is zero, because there is no correlation between the value at a given time and its value at the later time. Cross-correlation eliminates any spurious events occurring in ch1 and not occurring in ch2. Thus, correlation greatly decreases the noise of the signal allowing for extracting the kinetic parameters from the signal that was a superposition of several events. The comparison of the correlation functions corresponding to the signals from Tg-WT myofibril in rigor and during contraction is shown in **Figs. 21B** and **22B**. The signal and the correlation functions obtained from contracting Tg-R58Q myofibril is shown in **Fig. 23**.

Fig 23

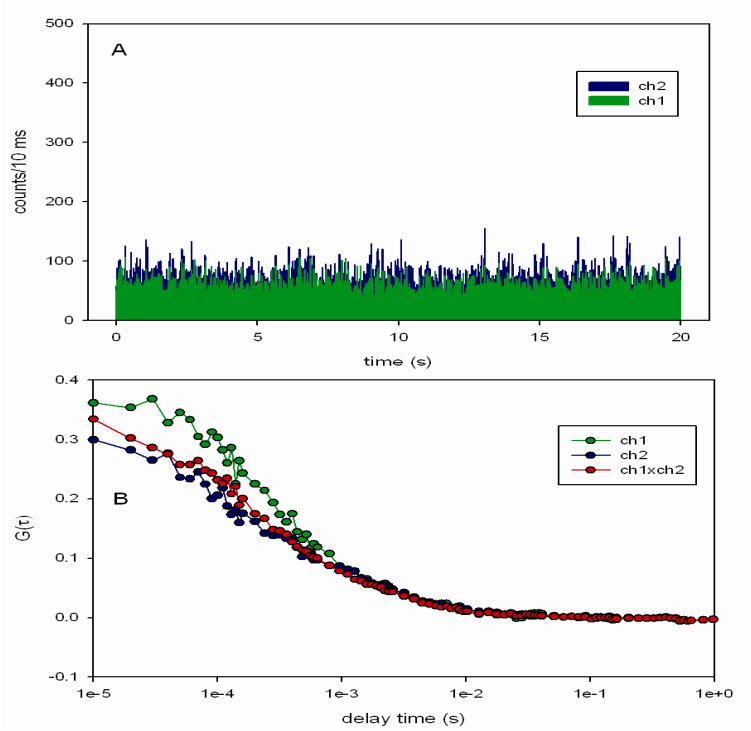

***Fig. 23**. The time course of polarized intensity (**A**) and correlation functions (**B**) of contracting R58Q mutated Tg-myofibril. Notations are like in the previous figures.*

The shape of the rotational autocorrelation function depends on the angle between the excitation and emission transition dipole moments, polarization of excitation and the presence of the emission polarizers. The expression for the rotational correlation function is very complex, but if the molecule were not to rotate during the excited state lifetime, the excitation and emission transition dipole moments are parallel. The muscle is excited with the polarized light and the emission is observed without polarizers. The rotational correlation function assumes an exponential form $G(\tau)=A+B \cdot \exp(-\tau/\tau_r)$, where A, B are constants, and τ_r is the rotational correlation time. The excited state lifetime of rhodamine is 4.08 ns and during such short time the actin filament does not rotate to any significant extent. Since the excitation and emission transition dipole moments of rhodamine are almost parallel above 470 nm, the decay of correlation function can be well described by a simple exponential function. This is illustrated in **Fig. 16B**, which shows the single exponential fit to the cross-correlation function. It is clear that τ_r adequately reflects the kinetics of the contracting heart muscle. We studied contraction of RP-labeled 30 different Tg-WT and 27 Tg-R58Q myofibrils. Two correlation functions (from ch1 and ch2) were obtained in each experiment for 60 measurements of WT muscle and 54 measurements of R58Q myofibrils. The mean rates ±SD were $k=1/\tau_r=169\pm96$ and 69 ± 13 s^{-1} for R58Q and WT myofibrils, respectively. The difference between the means was significant with t- and P- values of 2.109 and 0.102 (significance at 10% level), respectively. **Table 4** and **Fig. 24** summarize these results. There were no age-dependent differences in the kinetics measurements performed on myofibrils from 2.5, 5 and 13-month old male Tg-R58Q and age

and gender matched control Tg-WT mice. No differences were also observed between myofibrils from left and right ventricles or papillary muscles.

Fig 24

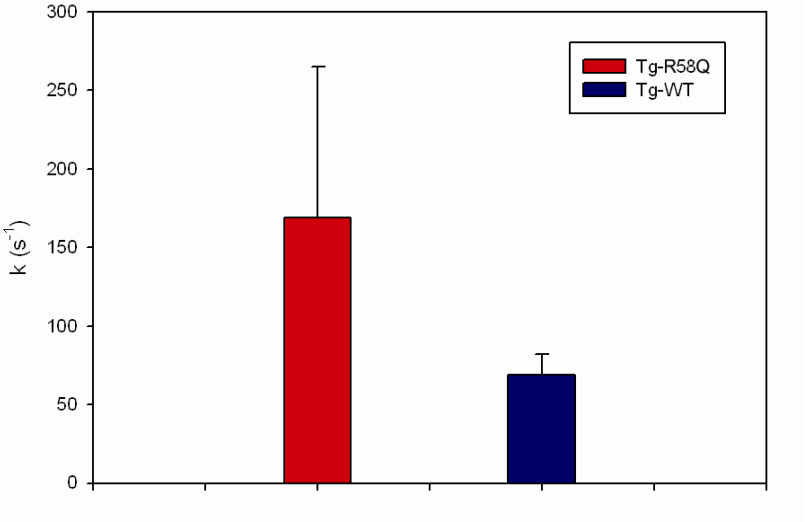

Fig. 24*. Comparison of the kinetic constant k extracted from data on 60 contracting Tg-WT (blue) and 54 contracting Tg-R58Q (red) heart myofibrils.*

Table 4.

The effect of the R58Q mutation on the rate of decay of the correlation function. N is the number of myofibrils tested.

Heart myofibrils	k (s^{-1})	N
Tg-R58Q	169±96	54
Tg-WT	69±13	60

Functional Studies in Skinned Cardiac Muscle Fibers. The functional consequences of the R58Q FHC mutation were also examined in glycerinated transgenic cardiac muscle fibers, the same which were used for the preparation of cardiac myofibrils for single molecule spectroscopy studies (above). In accord with our earlier report on fresh (not glycerinated) skinned muscle fibers (68), a significant decrease in the maximal force and a significant increase in myofilament Ca^{2+} sensitivity were observed in Tg-R58Q fibers compared with Tg-WT ($P<0.05$) (**Fig. 25**). Data are the average from n individual fibers ± SE. **Fig. 25A** shows a 2.5-fold decrease in maximal force measured in papillary muscle fibers from Tg-R58Q mice compared with Tg-WT ($P<0.001$). The average fiber diameter was about 120 μm. **Fig. 25B** shows a mutation dependent change in EC50 from 2.80±0.02 μM (Tg-WT) to 2.09±0.05 μM (Tg-R58Q). The Hill coefficient were n_H=2.47±0.10 for Tg-WT and n_H=1.97±0.04 for Tg-R58Q (**Fig. 25B**). Sixteen individual fibers from Tg-WT mice and thirty five from Tg-R58Q mice were examined, with ~ 4 fibers originating from the same mouse heart.

Fig 25

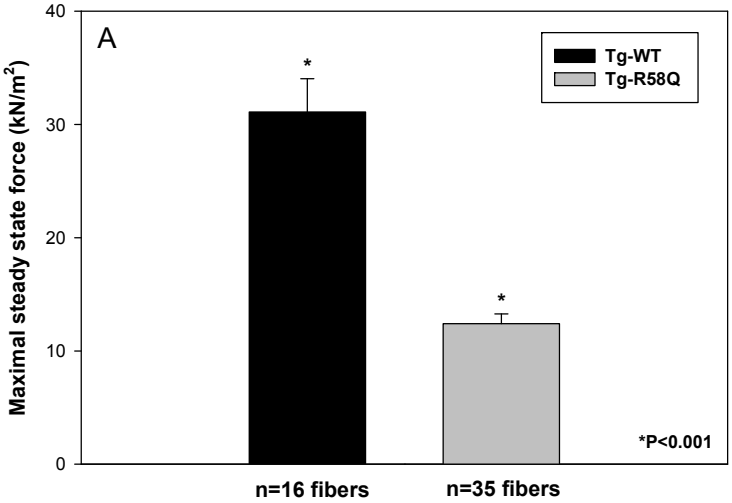

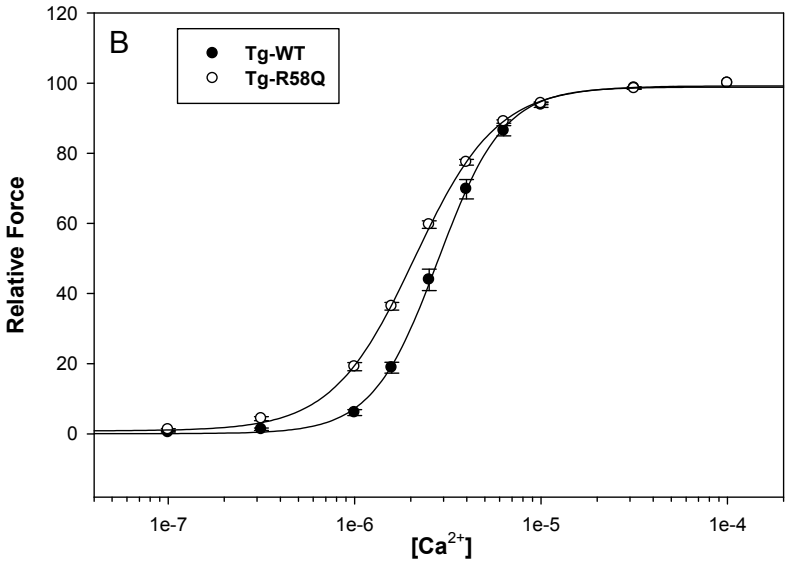

Fig. 25*. The effect of the R58QV mutation in myosin RLC on maximal force generation (**A**) and Ca^{2+} sensitivity of force (**B**) determined in Tg-R58Q glycerinated skinned papillary muscle fibers compared to Tg-WT. Data are expressed as mean of n experiments (n fibers isolated from mouse hearts) ± SE.*

DISCUSSION

In order to elucidate the effect of the FHC R58Q mutation on cardiac muscle performance at the molecular level, we measured the components of polarized fluorescence from cardiac myofibrils prepared from Tg-R58Q mouse hearts and compared it with the fluorescence originating from Tg-WT myofibrils. The signals were noisy, because they were contributed by a few molecules among ~200,000 present in the half-sarcomere. Fluorescence correlation spectroscopy was applied to reduce the noise and to extract the contribution of each single fluorophore. In our earlier studies with FHC muscle carrying the D166V mutation of RLC, the fluctuations were

well described by the ON-OFF binding and a dissociation of a myosin cross-bridge (17, 43). Anisotropy of actin was high when actin was immobilized by its binding to myosin and low when it was free (detached) from myosin (43). Most likely, the cross-bridge binding was able to inhibit bending motions of the whole filament rather than prevent the rotation of actin monomers, as there is no evidence that cross-bridge binding may prevent the rotation of G-actin. As a result, the signal was approximated by a rectangular wave with the "high" altitude of the wave corresponding to the high anisotropy of actin (when immobilized by binding to myosin), and the "low", expressed by low anisotropy (when freed (detached) from myosin) [17]. The corresponding correlation function was expressed as a series of triangles which were well reproduced by the experimental points.

In contrast, the correlation function of Tg-R58Q myofibrils used in the current investigation was not represented by a similar series of triangles. It was best approximated by the single exponential function. The kinetic parameter that could be extracted from correlation spectra was the rotational correlation time. Its reciprocal, k, is the rate with which actin rotates after being disturbed by a cross-bridge. This rotation does not occur when the muscle sarcomere is stretched beyond the overlap zone or in rigor, i.e. it reflects the rate of the interaction of actin with the cross-bridge. We showed a statistically significant difference between the rate obtained for Tg-R58Q myofibril compared to Tg-WT. We recognize that fitting of our data to a simple exponential decay function might be somewhat oversimplistic and that the actual events are probably more complex. Changes in myosin cross-bridge orientation and therefore in actin rotation most likely do not occur in a single reversible step (17). They probably occur in a series of smaller steps representing the mechanical steps associated with the well defined biochemical transitions. Moreover, the conditions for the exponential form of the correlation function are not

met because some rotation of the rhodamine moiety occurs during the excited state lifetime (**Fig. 20D**) and because the emission was observed through polarizers. Nevertheless, the best fitted exponential decay kinetics effectively reflects the difference between the rates observed for Tg-R58Q muscle and Tg-WT.

In this report, we demonstrate that the R58Q mutation of RLC leads to about 2.4-fold increase in the myosin cross-bridge kinetics, expressed by the higher values of k compared to the WT preparations (169 s^{-1} vs. 69 s^{-1}) (**Table 4**). Faster kinetics of the R58Q mutated cross-bridges occurs concurrently with a largely decreased force per cross-sectional area observed in Tg-R58Q vs. Tg-WT glycerinated skinned muscle fibers (**Fig. 25**). Faster kinetic rates of the R58Q cross-bridges are consistent with slightly increased myofibrillar ATPase rates observed in R58Q myofibrils compared to WT (0.64 s^{-1} vs. 0.56 s^{-1}). They are also in accord with our actin activated myosin ATPase rates obtained with transgenic mouse myocardium purified myosin from Tg-R58Q and Tg-WT mice (0.63 s^{-1} vs. 0.43 s^{-1}) (24). In addition, Tg-R58Q myosin also showed an increase in actin filament sliding velocity in an *in vitro* motility assay when compared to Tg-WT (2.17 $\mu m \cdot s^{-1}$ vs. 1.57$\mu m \cdot s^{-1}$) (24). Our results also show a large decrease in force observed in Tg-R58Q muscle fibers compared with Tg-WT fibers (**Fig. 25A**). These data suggest that the R58Q hearts may be subject to inefficient energy utilization that would ultimately lead to metabolite accumulation and compromised heart performance. Inefficient energy use by the R58Q mutant mice was also manifested in our earlier studies, where cardiac efficiency defined as a ratio of cardiac power to O_2 consumption was significantly compromised in Tg-R58Q mouse hearts compared with Tg-WT controls (1) In addition, we observed an

R58Q-dependent enhancement of ATPase activity at base (in pCa 8 solution) and incomplete relaxation ultimately leading to global diastolic dysfunction in Tg-R58Q animals (1).

Implications for R58Q based FHC disease. It has long been known that sustained or progressive demands on the heart can result in a series of compensatory responses including cardiac hypertrophy and myocardial remodeling. Elucidating the mechanisms of FHC-linked RLC mutations and how they might result in hypertrophic disease is a multilevel task and experiments have to be performed at the molecular, cellular and organ levels. The R58Q mutation of RLC is our most studied FHC mutation, which has been thoroughly characterized at the protein (24, 59) myofibrillar (1, 61), muscle fiber (68)and organ levels in RLC reconstituted preparations (61)or in a transgenic animal model (1, 24, 68). The Glutamine for Arginine substitution (R58Q) eliminated the capability of RLC to bind Ca^{2+} and only when R58Q-mutant was phosphorylated at Ser-15 with the Ca^{2+}-calmodulin MLCK, Ca^{2+} binding was restored (59). However, rescuing of Ca^{2+} binding function of RLC by its phosphorylation might be largely compromised in the R58Q myocardium as the downregulation of the phosphorylated form of RLC was recently observed in Tg-R58Q ventricular extracts (1). These results suggested that the R58Q mutation may play a role in alterations of myofilament calcium signaling. As we observed earlier (68) and in this report, the R58Q mutation results in an increase in the Ca^{2+} sensitivity of contraction (**Fig. 25B**). The myofilament calcium sensitivity is a function of two components: 1) k_{on}/k_{off} of Ca^{2+} binding to Troponin C (TnC), a major myofilament Ca^{2+} buffer, and 2) the kinetics of force generating myosin cross-bridges (60). Therefore, the observed leftward shift in the force–pCa relationship in Tg-R58Q myocardium could be due to slower R58Q cross-bridge kinetics or a decreased Ca^{2+} dissociation from TnC. The results of our current study showing faster R58Q-

dependent kinetics (**Table 4**) argue toward the R58Q induced effects in myocardial calcium homeostasis. Prolonged calcium transients measured in intact muscle fibres from Tg-R58Q mice (68) and diastolic dysfunction shown *in vivo* (1) fully support this notion. With regard to elevated cross-bridge kinetics observed in this report, the predicted physiologic effect of the R58Q RLC mutation would be inefficient ATP utilization for a given level of work and ultimate myocardial energy depletion. The R58Q-dependent increase in calcium sensitivity would be expected to produce a hypercontractile phenotype with increased use of ATP. Thus, energy expenditure through inefficient energy use would lead to increased turnover of ATP, particularly during stress. From the clinical standpoint, these R58Q-induced multilevel changes in cardiac contractility would lead to severe FHC phenotype including SCD, cardiac abnormalities observed in patients harboring this FHC RLC mutation.

CHAPTER VI

Single Molecule Kinetics in the Familial Hypertrophic Cardiomyopathy A13T Mutant Mouse Heart

INTRODUCTION

Clinical studies have revealed that the A13T mutation in the myosin RLC is associated with particular subtype of hypertrophy defined by mid left ventricular obstruction. Compared to the wild type (WT) mice, the A13T mutant fibers have increased affinity for Ca^{2+}, increased maximal actin-activated ATPase activity. (24). Current work, based on such determinations, suggests that FHC mutations cause alteration of kinetics of acto-myosin interaction, causing a heart to pump blood inefficiently (29, 68). However, isometric force is a temporal average of trillions of individual impulses that myosin delivers to actin in each second (49). Averaging causes a loss of kinetic information contained in the original signal, so that a specific model of muscle action (e.g (17)) is needed to extract kinetic information from the conventional measurements. In order to measure kinetics without the need for a specific model, it is necessary to observe individual impulses. The measurements should be carried out ex vivo, because molecular crowding is extreme in muscle. Concentration of actin and myosin in muscle is 0.6 and 0.2 mM, respectively (36) with the result that the access to proteins may be limited to only small solvents leading to over hydration (47). Further, myosin activity might depend on

cofactors and on the local geometry of the arrangement of filaments (12). It is thus important to carry out measurements under conditions that reproduce the in vivo conditions as closely as possible. In this communication, we measure the kinetics of acto-myosin interaction by studying few molecules of actin during steady-state contraction of ex vivo heart.

To visualize individual impulses, we observed sparsely labeled muscle through a small confocal aperture. We were able to limit the number of detected molecules to 1-4. To obtain kinetic information we used Fluorescence Correlation Spectroscopy (FCS) (18, 20). The signal that was studied was orientation of fluorescent dipole of a dye attached to a single molecule of actin or myosin. It is a sensitive indicator of a state of muscle contraction (16, 41). We observed orientation of actin rather than myosin, because labeling actin with fluorescent phalloidin does not alter enzymatic properties of skeletal muscle (13, 43), labeling is stoichiometric and thus allows strict control of the degree of labeling and labels actin non-covalently and therefore rigidly. Rigid binding is a must where orientation of a dipole moment of a probe is measured.
We report that the rate of changes of orientation is significantly slower in contracting cardiac myofibrils of transgenic (A13T) mice than of control transgenic wild type (WT) mice.

RESULTS

A typical lifetime image of a rigor Tg-WT myofibril from the right ventricle of mouse heart labeled with Alexa488-phalloidin is shown **Fig. 26A**. The entire I-bands are labeled, since there is no nebulin in cardiac muscle, entire I-bands are stained in contrast with skeletal muscle. H-bands are dark, because they contain no actin. For the quantitative measurement of orientation, it is important to know whether the probe is immobilized by the protein so that the transition dipole

of the fluorophore reflects the orientation of the protein. **Fig 26D** shows that this is the case for RP-labeled thin filaments. The decay of anisotropy, defined as $(I_{\parallel}-I_{\perp})/(I_{\parallel}+2I_{\perp})$, was best fitted by the exponential function $r(t)=R_{\infty}+a \cdot \exp(-t/\theta)$ where $R_{\infty} = 0.29$ was the value of anisotropy at infinite time, $a = 0.07$ was the amplitude of the anisotropy change and $\theta = 1.3$ ns was the rotational correlation time. The immobile fraction is contributed by (0.35-0.29)/0.35 = 17% of fluorophores. Thus 83% of fluorescent phalloidin is immobilized by F-actin.

Fig 26

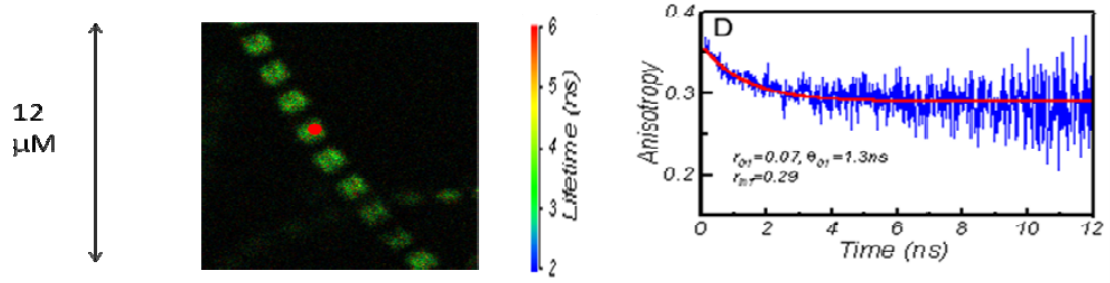

Fig. 26*. Lifetime (**A**) image of rigor Tg-WT myofibril from the mouse right ventricular muscle. The color bar at right of lifetime image is the lifetime scale, with red corresponding to 6 nsec and blue to 2 nsec. The red circle is the projection of the confocal aperture on the sample plane.* ***D****. Decay of anisotropy of the typical I-band. Blue: experimental decay; red line: fit to the function $r(t)=R_{\infty}+a \cdot \exp(-t/\theta)$. Data collected for 60 sec. Data acquired with the PicoQuant Micro Time 200 confocal lifetime microscope. Excitation with a 470 nm pulse of light, emission through LP500 filter.*

The red circle in **Fig. 26** indicates the projection of the confocal aperture on the image plane. The diameter of Detection Volume (DV) is (1.2 µm). This equals approximately the area of one half sarcomere (HS) which is 1 µm x 1 µm. Therefore the objective captures fluorescence from the

entire HS. To calculate number of fluorophiores in HS we recognize that the myofibril was labeled with 0.1 nM RP + 10 μM UP, so only one in 100,000 actin monomers carry fluorescent phalloidin. The volume of typical HS is 5 x 10^{-16} L. Since the concentration of actin in muscle is 0.6 mM [15], this volume contains ~2 actin monomers. Thus the actual number of observed fluorophores ranges from 1 to 4 even with 100% error. But even if it is 4, it falls well within resolution of FCS technique [39].

The polarized fluorescence intensity was measured by positioning the laser beam at the center of the I-band and collecting perpendicular and parallel components in ch1 and ch2, respectively. The laser beam was not scanned. After opening the laser shutter the fluorescence intensity was initially high and decayed after several seconds to a steady state value of ~10K photons/s. **Fig. 27A** and **28A** show typical intensity data collected during 20 seconds from rigor and contracting papillary myofibrils. The fluorescence was due to 1-4 fluorophores.

Fig 27

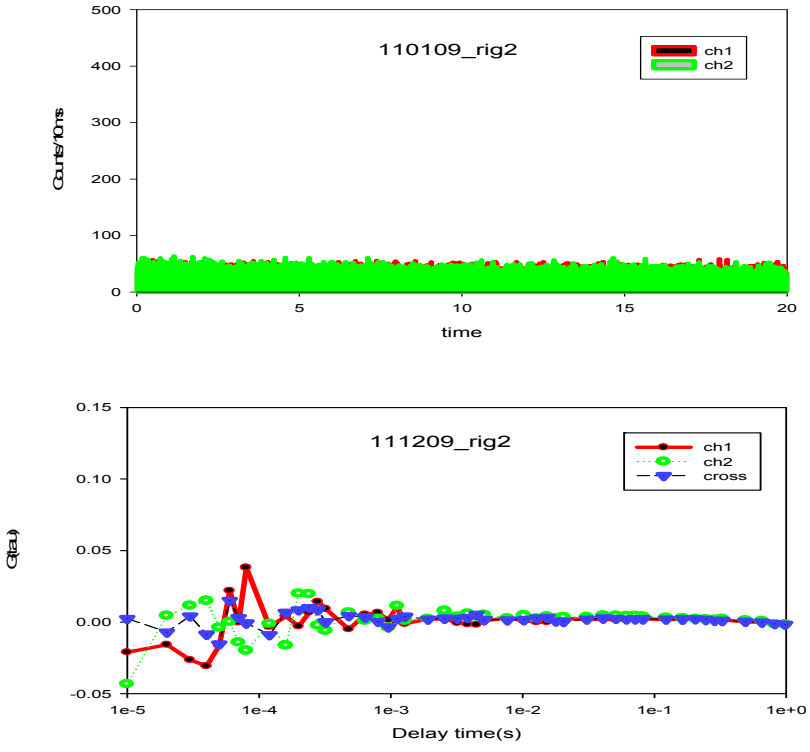

Fig. 27. A: *The time course of polarized intensity of rigor WT myofibril from papillary muscle of transgenic heart. The original data was collected every 10 μsec, 1000 points are binned together to give time resolution of 10 msec. The vertical scale is the number of counts during 10 msec. Ch1 (green) and ch2 (blue) are the fluorescence intensities polarized perpendicular ($I_{\perp}$) and parallel ($I_{\parallel}$) to the myofibrillar axis, respectively Myofibrillar axis is vertical on the microscope stage.* ***B****: The orresponding correlation functions. Laser polarization is vertical on the microscope stage.*

Higher time resolution can able to distinguish individual traces. However, while the impulses are readily visible, it is difficult to extract from them kinetic rates (such as the rate of rise and fall and frequency) because they have variable shape and duration. The signal is simply too noisy, impulses having originated from 1-4 molecules amongst 200,000 present in HS, and having been bunched together. Nevertheless, kinetic information can be extracted from stochastic fluctuations by computing a correlation function of the fluctuations. The correlation function at a given delay time τ is a sum of the products of a signal multiplied by a signal shifted by a delay time τ. If the signal is periodic, the autocorrelation function will also be periodic with the same periodicity as the original signal. At the same time the autocorrelation of noise is zero, because there is no correlation between value at a given time and its value any time later. Cross-correlation eliminates any spurious events occurring in ch1 and not occurring in ch2. Thus correlation greatly decreases noise in the signal. The correlation functions corresponding to the signal from Tg-WT heart papillary muscle in rigor and during contraction is shown in **Figs 27B** and **28B**.

Fig 28

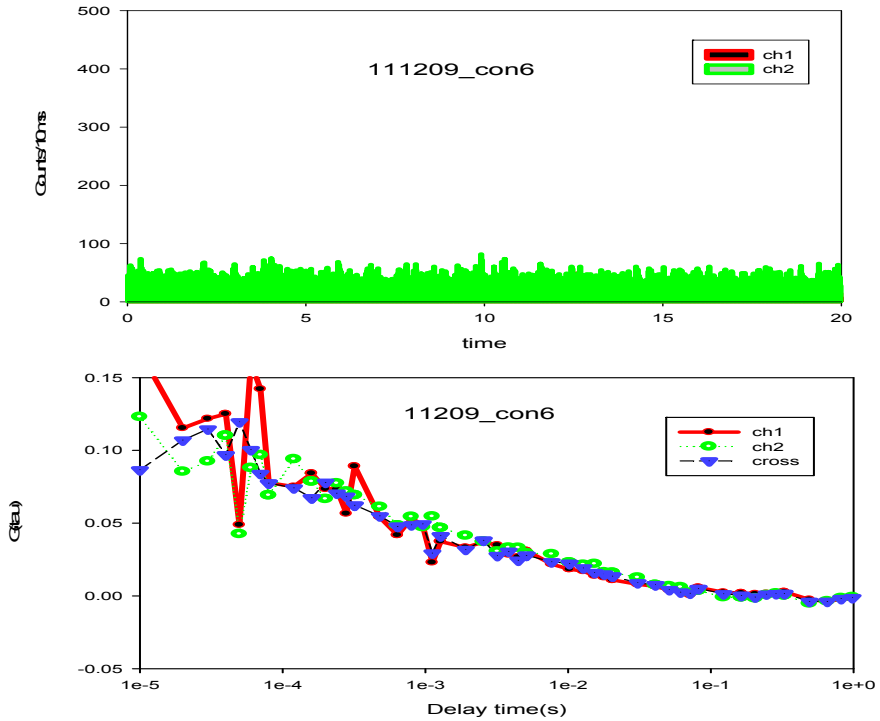

Fig. 28. A: *The time course of polarized intensity of contracting myofibril from WT papillary muscle of transgenic heart. The vertical scale is the number of counts during 10 msec. Ch1 (green) is* $I_{\perp}$ *and ch2 (blue) is* $I_{\parallel}$*. Myofibrillar axis and laser polarization are parallel on the microscope stage.* ***B****: The corresponding correlation functions. The red line is the exponential fit to the crosscorrelation function.*

The signal and correlation functions from A13T papillary muscle in rigor and contraction is shown in **Fig. 29 and Fig. 30**.

Fig 29

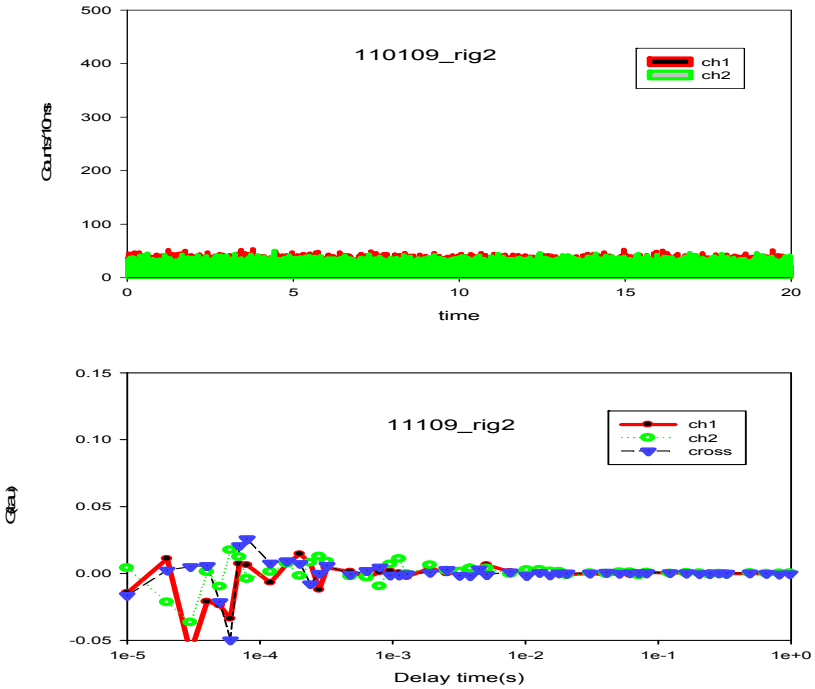

Fig. 29*. The time course of polarized intensity (**A**) and correlation functions (**B**) rigor myofibril. Notation like in previous figure, except that data is from A13Tmyofibril*

Fig 30

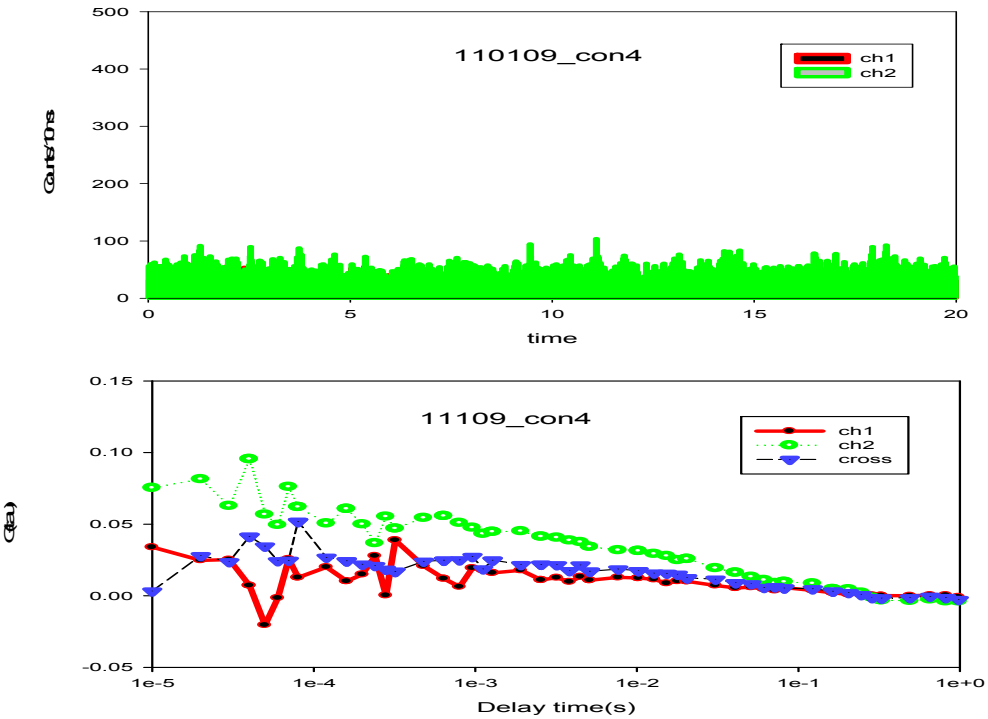

***Fig. 30**. The time course of polarized intensity (**A**) and correlation functions (**B**) of contracting myofibril. Notation like in previous figure, except that data is from A13Tmyofibril.*

The shape of the rotational autocorrelation function depends on the angle between the excitation and emission transition dipole moments, the polarization of the excitation, and the presence of emission polarizers. If the molecule does not rotate during the excited state lifetime, the excitation and emission transition dipole moments are parallel, muscle is excited with polarized light and the emission is observed without polarizers, the complex expression for the rotational correlation function assumes exponential form $G(\tau)=A+B \cdot \exp(-\tau/\tau_r)$ where A, B are constants and τ_r is the rotational correlation time (20). The excited state lifetime of rhodamine is 4.08 ns and during such a short time actin filament does not rotate to any significant extent. Since the excitation and emission transition dipole moments of rhodamine are almost parallel above 470 nm, the decay of correlation function is well described by a simple exponential. This is illustrated in **Fig. 28B**, which shows a single exponential fit to crosscorrelation function. It is clear that τ_r adequately reflects kinetics of contracting heart muscle. Two correlation functions (from ch1 and ch2) were obtained in each experiment for 25 measurements of WT muscle and 32 measurements of A13T muscle. The mean rates ±SD were 84±58 and 45±16 s^{-1} for mutated and WT heart, respectively. The difference between means was significant with t- and P- values at 3.5 and 0.0008, respectively. **Table 5** and **Fig. 31** summarize the results.

Table 5.

Effect of A13T mutation on the rate of decay of correlation function.

Heart muscle	k (s^{-1})
Tg-A13T	45±16
Tg-WT	84±58

***Fig. 31**. Comparison of kinetic constant k extracted from data on 22 contracting Tg-WT (blue) and 25 Tg-A13T (red) heart myofibrils.*

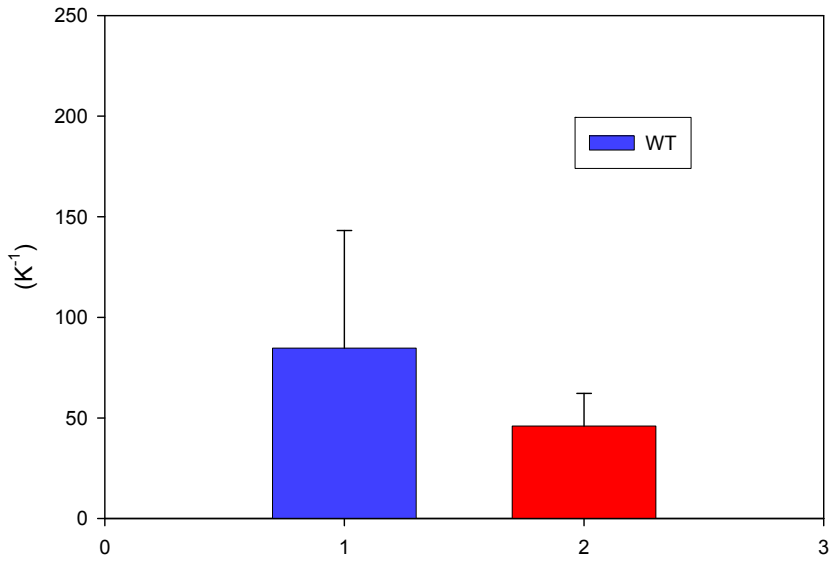

DISCUSSION

We measured polarized fluorescence signals to compare the kinetics of interaction of few molecules of actin with myosin in myofibrils prepared from Tg-WT and Tg-A13T hearts. The signals were noisy, because they were contributed by a few molecules among ~200,000 present in a half-sarcomere. To reduce the noise we applied FCS. The question arises what kinetic parameter does FCS spectrum represent? Correlation function of A13T muscles was not a series of triangles. It was best approximated by a single exponential function. The kinetic parameter extracted from the correlation spectra was the rotational correlation time. This parameter showed statistically significant difference between Tg-WT and Tg-mutated heart muscle. We recognize that fitting our data to simple exponential decay is a gross oversimplification of the actual events. The orientation change of myosin cross-bridges, and therefore of actin, does not occur in a single

reversible step, but as suggested by **Figs 28 and 30** probably occurs in a series of smaller steps. Moreover, it is reversed in a series of mechanical steps, each associated with definite biochemical transition (69). Finally, some rotation of the rhodamine moiety does occur during the excited state lifetime (**Fig. 26D**) and the emission is observed through polarizers. Nevertheless, exponential kinetics fits the data well and effectively reflects difference in kinetics of healthy and diseased heart. The kinetic parameter extracted from the experiments is most likely related Pi release (57). Thus the present work is consistent with the idea that FHC results from decreased efficiency.

In the model used here - transgenic mouse myocardium - the endogenous mouse ventricular RLC A13T is replaced by mutated human ventricular RLC in ~ 11% of cases. Therefore the probability of finding diseased acto-myosin in A13T sample is small. But the probability of finding diseased acto-myosin in human patients is not large. In human hearts 50% of myosin-containing thick filaments are composed of the non-mutant myosin heads interspersed with the FHC mutant heads, because patients are normally heterozygous for FHC disease. If the distribution of the healthy and diseased molecules is random, any collection containing more than few molecules carries high probability of containing a mixture of the healthy and diseased species. Therefore the probability of finding A13T-mediated cross-bridge kinetics in the experiments performed on heart biopsies from the patients carrying the A13T mutation would be 50:50. This emphasizes the value of our approach where only a few adjacent molecules are studied, because in conventional measurements averaging would prevent one from knowing whether a particular heart is affected by the disease.

Our studies suggest that the A13T mutation may lead to diastolic and systolic dysfunction through slower cross-bridge kinetics and ultimately result in a compensatory hypertrophy and sudden cardiac death as observed in the individuals harboring the A13T mutation in RLC

The results reported were obtained from right ventricle, left ventricle and papillary muscles. We did not attempt to discriminate between different types of cardiac muscle. It remains to be seen if different types of cardiac muscle behave in the same way.

CHAPTER VII

KINETICS OF A SINGLE CROSS-BRIDGE IN FHC MUSCLE MEASURED BY REVERSE KRETSCHMANN FLUORESCENCE

INTRODUCTION

This chapter focuses mainly on one of the most common FHC single-point-mutation, R58Q in a gene that encodes for the ventricular myosin regulatory light chain (RLC) (19, 51). Clinical studies have revealed that R58Q mutation in the myosin RLC - is associated with a malignant FHC disease phenotype (51).

Heart muscle contraction results from periodic interaction of myosin cross-bridges with actin, during which myosin delivers periodic force impulses to the thin filament. Current hypotheses, based on measurements of muscle force development, suggest that FHC mutations cause alteration of kinetics of this interaction, causing a heart to pump blood inefficiently (59). However, isometric force is a temporal average of trillions of individual force impulses. It is impossible to extract kinetic information from steady-state ensemble measurements. Averaging over many molecules will always mask individual impulses. However, kinetic information can be extracted from stochastic fluctuations of the signal from small ensemble of molecules. For such applications Fluorescence Correlation Spectroscopy (FCS) (19) is a method of choice. At the same time, it is important to perform experiments in a tissue because excluded volume effects, which come into play at high protein concentration, may play significant role during muscle contraction. Concentration of actin and myosin in muscle is extremely high. At high concentrations the access to proteins may be limited to only small solvents. As a result, proteins

in certain regions of a muscle cell may become over hydrated and behave differently than isolated proteins that are normally hydrated (52).

FCS is typically used together with confocal detection. This goes a long way towards achieving requirements of observing small number of molecules under ex vivo conditions. However, in confocal detection the axial dimension of the detection volume is of the order of few microns, large compared to the axial extent of the attached biomolecule. Moreover, a significant background is contributed by the reflection of the excitation light from the surface. Total Internal Reflection Fluorescence (TIRF) (70) resolved some of these problems and allowed application to myosin II and V in vitro (10, 62, 70). It is possible to further decrease axial dimension and avoid reflections by the use of Surface Plasmon Assisted Microscope (SPAM) (10). SPAM allows observing few molecules by producing extremely thin optical sectioning and by providing excellent background rejection. The axial dimension decrease is a consequence of the fact that the SPCE takes advantage of strongly restricted range for near field interactions (10, 22, 23). In SPCE the axial dimension is made small (ca 50 nm) by placing a sample on a thin metal film and illuminating it with the laser beam directly [reverse Kretschmann (RK) configuration] or through the metal layer via surface plasmons evanescent field [Kretschmann (KR) configuration]. Primarily, the thickness of the detection volume is defined by a distance-dependent fluorescence coupling to surface plasmons. This distance, typically less than 50 nm, is further reduced at a close proximity (below 10 nm) to a surface by fluorescence quenching by a metal. In KR mode the additional effect is due to evanescent wave distance dependent penetration depth that further reduces the thickness layer. The excellent background rejection is also enhanced by the fact that scattered excitation light is unable to penetrate the metal layer and enter the objective. An

additional benefit is the fact that fluorophores coupling to surface plasmons in the metal films strongly depend on fluorophore orientation. Emitting dipoles perpendicular to the surface couple very efficiently resulting in p-polarized emission on the other side of the film, and dipoles parallel to the surface do not couple (s-polarized modes are not supported by the surface plasmons). This nearfield based selection will have bigger effect than typically used photoselection and fluorescence polarization measurements. We used RK configuration because it avoids losses of intensity due to penetration of mirrored surface, it avoids losses inherent in a dichroic mirror, the exciting light need not to be polarized, and it is simpler and less expensive to implement.

A classical method of measuring muscle kinetics is to follow the changes of the orientation of fluorescent dipole of a dye attached to actin or myosin (12, 13, 41). However, we show here that coupling to surface plasmons is a more efficient process. We utilize this effect to detect by FCS subtle conformational changes occurring upon FHC point mutation. We call a simple extension of FCS technology to the case where orientational fluctuations strongly reflect on the observed SPCE signal the Surface Plasmons Correlation Spectroscopy (SPCS).

For observing few molecules it is preferable to focus on actin since it can be labeled with very low concentration of fluorescent phalloidin. Such labeling preserves the regular structure of a myofibril, phalloidin does not alter enzymatic properties of muscle (12, 48) and phalloidin labels actin stoichiometrically, which allows strict control of the degree of labeling. Finally, phalloidin attaches to actin non-covalently but strongly. Non-covalent binding is preferable in the case where changes in the orientation of dipole moment of a probe are measured. Non-covalent bonds

involve attachment over large surfaces through electrostatic and hydrogen links. Observing orientation of actin is a valid way of observing interaction with cross-bridges, because it has been known for a long time that actin changes orientation in response to cross-bridge binding (48, 71) and that those changes parallel changes of orientation of a cross-bridge (12) In this report we a present application of SPCS to clearly show that actin of transgenic heart muscle affected by R58Q mutation in RLC has different kinetic behavior than actin from transgenic wild type heart muscle.

PRINCIPLE OF THE METHOD

Let's first consider a conventional case (**Fig. 32A**) [the same argument applies when the light is incident at a sample from the bottom, either perpendicularly (confocal) or at a critical angle (TIRF)]. A muscle myofibril rests on a plain glass coverslip. The incident light (green) is incident on a sample from the top and excites red fluorescence of the labeled molecules. Fluorescence is collected by the objective through the immersion oil. However, some fluorophores are excited indirectly, by the light reflected from the surface of a coverslip or scattered by a sample (marked scattered excitation light). This light (far field fluorescence) is collected by an objective together with the main fluorescent light. To illustrate this effect, skeletal muscle myofibrils were labeled with 100 nM Alexa647-phalloidin (+10 μM unlabeled phalloidin acting as competition for actin) in the presence of the background in the form of 0.5 mM of Rhodamine 800. **Fig. 32B** shows that the fluorescence was completely dominated by the background and no image of myofibrils is discernible at all. **Fig. 32C** shows the Back Focal Plane (BFP) image. For the in-focus source, the microscope objective maps ray propagation angles into off-axis radial positions at the BFP. The result of the sine dependence for spherical refracting surfaces is that a ray originating from a source on-axis at the focal plane and

propagating at an angle θ with respect to the axis will cross the objective's BFP at an off-axis radial distance $r = nf \sin\theta$ where n is the refractive index of the medium (1.515) and f is the focal length of the objective [46]. **Fig. 32C** reveals that there is a weak peripheral ring, a diffuse interior and strong central spot. The ring is due to weak coupling even in the absence of metal, diffuse interior is the image and central spot arises because a significant amount of exciting light is able to pass to the detector (the detector is looking directly at the laser; all the light impinging on a sample at 0^o angle is passing through the center at BFP). Situation is quite different when a sample rests on a coverslip coated with a thin layer of noble metal (**Fig. 32D**). Incident light produces Surface Plasmons propagating along the surface of the metal. These plasmons couple with the light to excite fluorescence. Fluorescent light once again couples with the plasmons to emerge at the bottom of the coverslip at the Surface Plasmon Coupled Emission (SPCE) angle (which is smaller than SPR angle). Coupling is efficient only when the distance between metal and fluorophores is less than 50 nm. Fluorescence emanating from fluorophores closer than 10 nm to the surface is quenched by the metal. Thus, even though the exciting light does not produce evanescent wave, the RK/SPAM produces the effect similar to TIRF because only the fluorescence from molecules within 10 to 50 nm of the metal layer (indicated by a dashed line) can penetrate the metal layer via plasmon resonance. Moreover, scattered light (far field fluorescence) is reflected by the metal and is not collected by the objective. When the sample was observed by SPAM in RK configurations, the image was no longer dominated by the background (**Fig. 32E**). The BFP image of the rhodamine fluorophore on gold coated glass (**Fig. 32F**) is now doughnut-shaped, because the light emerging from the sample is contained within a cone with a well defined angle Θ. In conclusion: RK/SPAM provides excellent background

rejection, because it combines excitation volume comparable to TIRF with the fact that all the light scattered in a sample is unable to penetrate the metal (22).

Fig 32

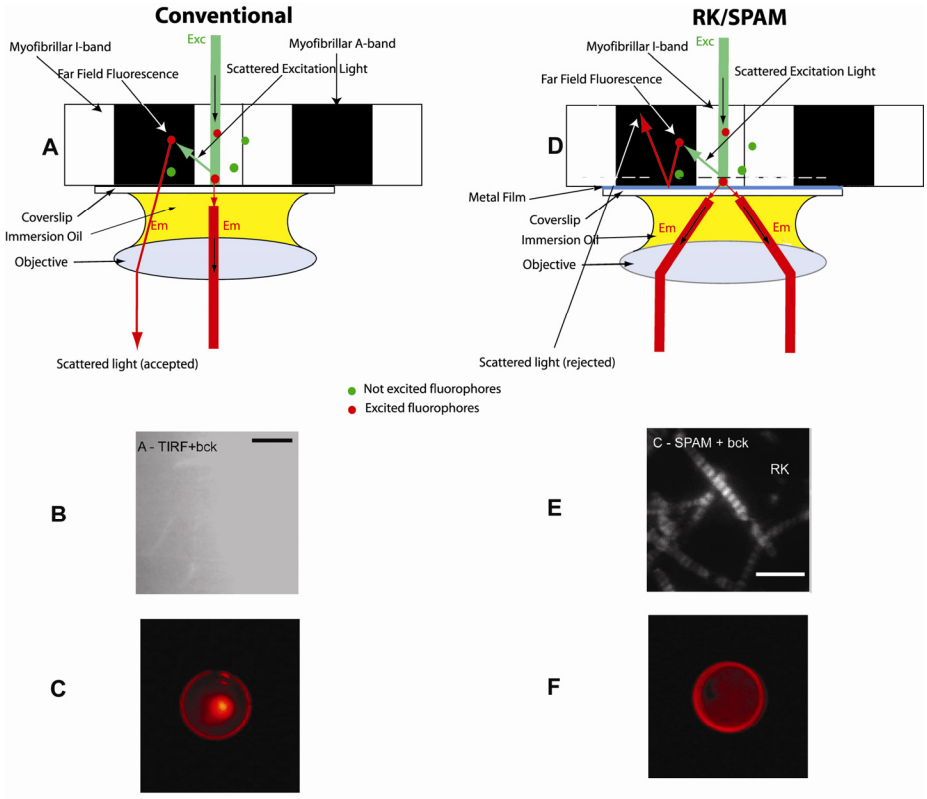

Fig. 32*. A concept of SPAM microscope. A cardiac myofibril is illuminated from above. In conventional microscope (**A**) all light, including scattered (background) light, is able to penetrate the coverslip. Green dots represent fluorophores that are out of the field of excitation. Red dots represent fluorophores that are in the path of direct or scattered excitation light. In RK/SPAM (**D**) sample is placed on a metal coated coverslip and excited with green light (right). The excitation energy from the excited fluorphore couples to the surface plasmons and radiates through the metal film (red) to the objective as a surface of a cone with half angle equal to the SPCE angle. Metal can be a thin layer of Al (20 nm thick) or Ag or Au (50 nm thick). The*

scattered light is unable to penetrate the coverslip and is radiated into free space. ***B*** *&* ***E****: The background rejection by SPAM. 0.5 mM Rhodamine 800 added as background obscures the image in ordinary TIRF (****B****). SPAM in RK configuration eliminates much of the background contribution (****E****). Myofibrils (0.1 mg/mL) were labeled with 100 nM Alexa647-phalloidin + 10 μM unlabeled phalloidin for 5 min at room temperature, then extensively washed with rigor buffer containing 50 mM KCl, 2 mM $MgCl_2$, 1 mM DTT, 10 mM TRIS pH 7.0. 633 nm excitation, 1.65 NA x100 Olympus objective, sapphire substrate, 1.78 Refractive Index immersion oil. The bars are 5 μm in B and 10 μm in E.* ***C*** *&* ***F****: The Back Focal Plane image of a sample in a microscope in conventional configuration (****C****) consists of weak outer ring and a diffuse interior with s strong center corresponding to imperfect blockage of exciting light. The BFP image of a sample in a microscope in RK configuration (****F****) consists of a strong ring corresponding to emission into free space in a cone.*

Another characteristic of SPAM is that fluorescence coupling to surface plasmons dramatically depends on the orientation of the fluorescent molecule transition moment. This is illustrated in **Fig. 33A** which compares, for SPCE and TIRF mode of detection, the power entering the microscope objective at different distances from the coverslip for different polar angles of the transition dipole. It is clear that at distances larger than 10 nm, more fluorescence is contributed by SPCE than TIRF. Not only is the power entering the objective higher for SPCE, but it is more sensitive than TIRF to changes in polar angle. **Fig. 33B** compares the sensitivity of SPCE vs. TIRF to change in angle. This makes the SPCE method particularly suited to the measurements of protein orientation changes. This is the method used here, i.e. fluctuations arise from changes in the degree of coupling as the dipole changes orientation. This is different than a classical

method of measuring orientation changes which follows anisotropy of fluorescent dipole of a dye attached to a molecule of interest (10).

Fig 33

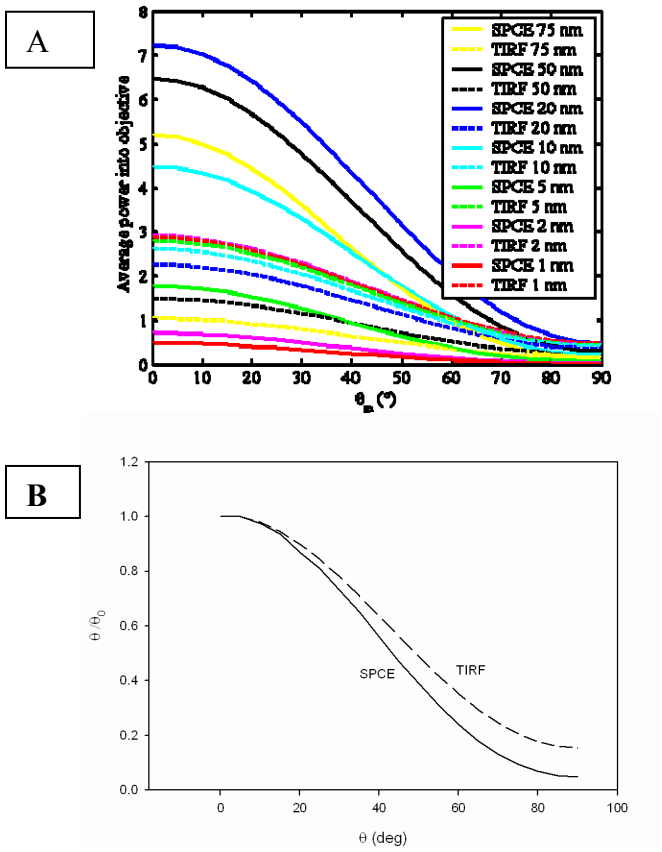

Fig. 33. ***A****: Power entering the objective at various distances from the surface of a coverslip.* ***B****: the SPCE (solid line) and TIRF (broken line) power entering objective at various polar angles. Curves normalized to power at* $\theta=0^{o}$.

RESULTS

Photon flux from a single chromophore. To estimate this number, we measured signal from a freely diffusing chromophore (the same as labeling muscle) is the absence of photobleaching. We used 50 nM rhodamine which translates to an average of 100 molecules in the 3 fL volume Detection Volume (DV) at any time. No overall bleaching occurs because fluorophores spend

only limited amount of time in the DV. These 100 molecules gave parallel (I_H) and perpendicular (I_V) intensities on gold of I_H= 7,125±1,040 and I_V= 6,442±1,721 photons/10 ms for the total photon rate I_{Tot} = 20,407 photons/10ms. Therefore the average number of observed photons per fluorophore in 10 ms was ~200/10 ms.

***Polystyrene spheres*.** In order to show that the method is superior to conventional confocal technique of measuring motions of protein-sized particles, we compared Brownian motion of 100 nm polystyrene spheres. **Fig. 34** compares typical RK-SPAM FCS experiments of 0.1 μm fluoro-spheres diffusing on glass, gold-coated-glass and gold-coated-sapphire coverslips. Typical time course of a signal from spheres diffusing on gold-glass coverslip is shown in **Fig. 34A.** The parallel (I_H) and perpendicular (I_V) intensities are shown in the blue and red, respectively. The average counts were I_H= 1746±694 and I_V= 2189±785 photons/10ms, respectively. The total photon rate was $I_{Tot}=I_V +2*G*I_H$ = 5681 photons/10ms ≈ 600 Kcounts/s, where G is the correction factor (0.98). **Fig. 34B** compares correlation function of spheres diffusing on glass (red), gold-coated-glass (green) and gold-coated-sapphire (blue). For spheres diffusing on glass, the magnitude of the correlation function at zero delay time is equal to the inverse of the number of particles in the detection volume and gives ~ 22 spheres in the DV. Since the confocal volume is ~3 fL the concentration of spheres is 7 x 10^{12}/mL, close to the number estimated by Molecular Probes (100x dilution of the stock concentration of 3.6 x 10^{13} /mL). **Fig. 34B** shows also that the magnitude of correlation function at zero delay time of spheres diffusing on gold-coated glass was nearly 4 times larger than for spheres diffusing on glass. This is consistent with the fact that gold coating decreases DV by quenching fluorescence near the metal surface (26) Inset to **Fig. 34B** shows that the decay of the correlation function is the fastest for spheres diffusing on gold-

coated-sapphire and the slowest for glass. This is due to the fact that experiments on sapphire were carried out using high aperture objective (NA=1.65) which has the thinnest depth-of-focus, and the fact that gold coating decreases DV. Since the correlation function was noisy for gold-coated-sapphire, we used gold-coated-glass for the rest of the experiments. The decay of correlation occurs between 10^{-3} and 10^{-2} s, consistent with earlier results obtained for a 100 nm diameter sphere with a diffusion coefficient of 4.12×10^{-12} m^2/s [50] diffusing along Z-axis through a distance of 36 nm (27).

Fig 34

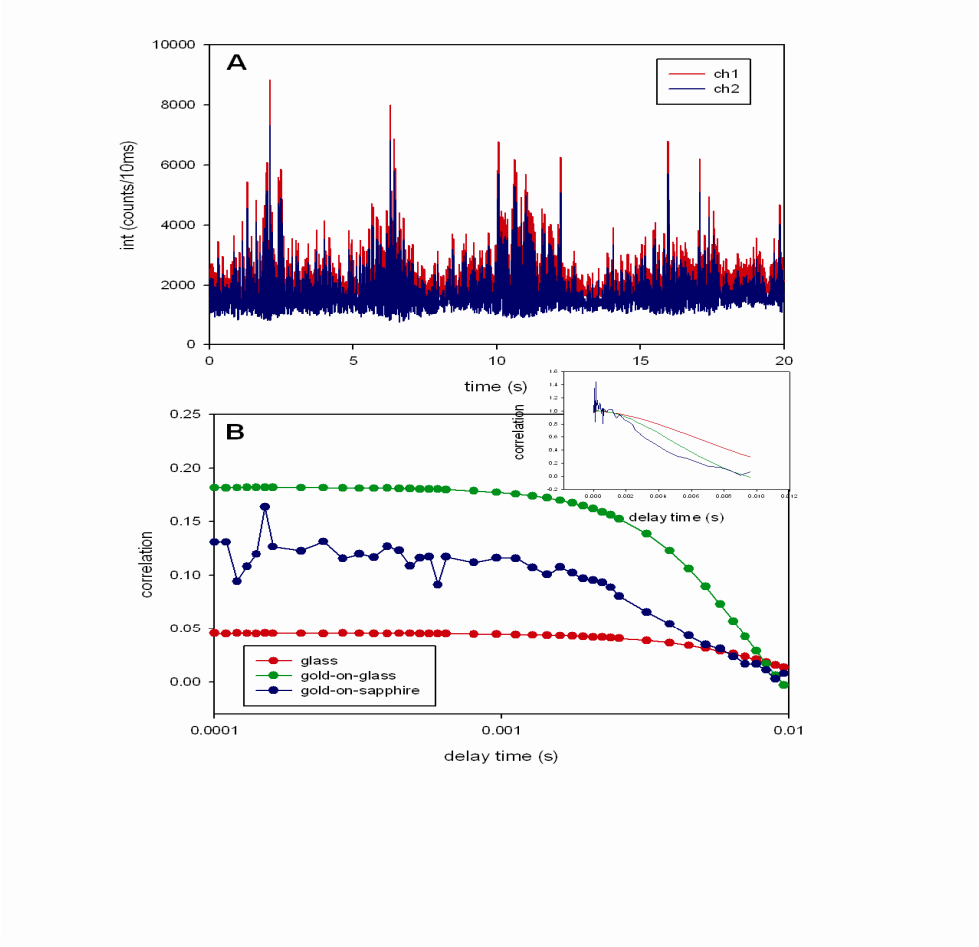

Fig.34. *RK-SPAM FCS experiments using fluorescent spheres diffusing on glass, gold-coated-glass and gold-coated-sapphire coverslips.* ***A*** *- Typical time course of a signal from 0.1 μm spheres diffusing on gold-glass coverslip. The total photon rate was ≈ 600 Kcounts/s.* ***B*** *- correlation function of spheres diffusing on glass (red), gold-coated-glass (green) and gold-coated-sapphire (blue). The average number of spheres in DV was 6, 8 and 22, respectively. Inset - the decay of the correlation function is the fastest for spheres diffusing on gold-coated-sapphire and the slowest for glass. The incident power 150 μW.*

Contracting heart muscle. The myofibril was labeled with 10 nM RP + 10 μM UP. Thus only one in 1,000 actin monomers carried fluorescent phalloidin. The length, width and height of a typical half sarcomere (HS) are 1, 1, and 0.5 μm, respectively and therefore its volume is 5×10^{-16} L. Since the concentration of actin in muscle is 0.6 mM [17], this volume contains ~200,000 actin monomers. Therefore there are ~ 200 fluorophores per HS. The diameter of DV (0.9 μm) is equal to the diameter of the confocal pinhole (50 μm) divided by the magnification of the objective (60x). Therefore the objective captures entire fluorescence from one HS (200 fluorophores). Since the signal from a freely diffusing chromophore is 200 photons/10 ms, in the absence of photobleaching we would have observed 200x200=40K counts/10 ms. In fact, the signal (**Fig 35A**) was many folds smaller: the average counts on gold were I_V= 28±8 and I_H=72 ±17 photons/10ms for the total photon rate I_{Tot} = 174 photons/10ms. This shows that photobleaching is a significant factor in our experiments. In contrast to free diffusion, where fluorophores spend only hundreds of μseconds in DV, in our experiments muscle is immobilized on a coverslip and each fluorophore is exposed to light for a few minutes required to focus and measure. This causes bleaching of most of the fluorophores in muscle, and by the time the

measurement is taken only the few remaining ones give rise to the observed signal. **Fig. 35B** is the control intensity trace of muscle in rigor, when no mechanical activity occurs.

Histogram of photocounts during contraction and rigor is shown in insets to **Fig. 35A** and **B,** respectively. In all experiments the Gaussian curve used to fit the data was asymmetrical during contraction. In the example shown in inset to **Fig. 35**, the fit to the function $f=aexp(-.5((x-x_o)/b)^2)$ gave $R^2=0.985$ for ch2 during rigor and $R^2=0.922$ for ch2 during contraction. The contraction data also failed normality test (Test Failed with P = 0.0007). The normality test checks whether the data passed or failed the test of the assumption that the source population is normally distributed around the regression, and the P value calculated by the test. Rigor data, in contrast, passed the test with P = 0.3755. Failure of the normality test can indicate the presence of outlying influential points or an incorrect regression model. This may indicate that contraction is a multi-step process, as originally proposed (27).

Fig 35

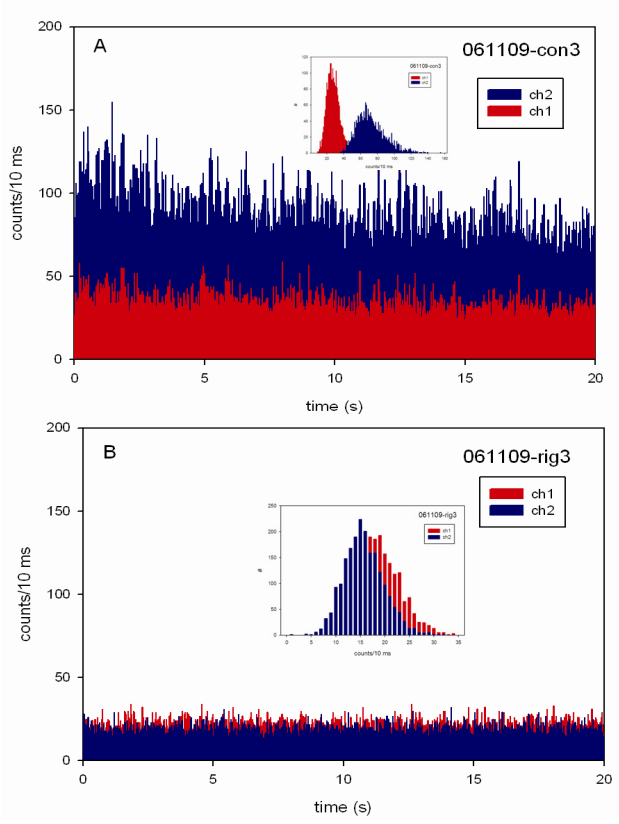

***Fig. 35**. Comparison of the time traces of 50 nM rhodamine B on glass (**A**) and on gold-coated glass (**B**). Parallel (I_H) and perpendicular (I_V) intensities shown in the blue and red, respectively. The average counts on glass were I_H= 3,903±712 and I_V= 3929±603 photons/10ms; the total photon rate I_{Tot} = 11,578 photons/10ms. The average counts on gold were I_H= 7,125±1040 and I_V= 6442±1721 photons/10ms; the total photon rate I_{Tot} = 20,407 photons/10ms. The incident laser power 150 μW. Insets show histograms of counts during contraction **(A)** and rigor **(B)**. The Gaussian curve used to fit the data is asymmetrical in A.*

Not surprisingly, the signals were very noisy because they originated from >>200 molecules among ~200,000 present in half-sarcomere. A standard way to reduce contribution of noise in a signal is to compute its autocorrelation function. The correlation functions computed from the signal shown in **Fig. 35** is plotted in **Fig. 36**. The expression for rotational autocorrelation function is very complex. Even in the simplest case – the rotational diffusion on glass - it depends on the angle between the excitation and emission transition dipole moments, the polarization of the excitation, and the presence of emission polarizers. In the simplest case, where the molecule does not rotate during the excited state lifetime, the excitation and emission transition dipole moments are parallel, muscle is excited with polarized light and the emission is observed without polarizers, the complex expression for the rotational correlation function assumes exponential form $G(\tau)=B\exp(-\tau/\tau_r)$ where B is a constant and τ_r is the rotational correlation time (17). The excited state lifetime of rhodamine is 4.08 ns (20) and during such a short time actin filament does not rotate to any significant extent. Since the excitation and emission transition dipole moments of rhodamine are almost parallel above 470 nm, the decay of correlation function is well described by a simple exponential. Pre-exponential constant B is

taken as a measure reflecting kinetics of contracting heart muscle. While this scheme is an oversimplification of the actual events (see Discussion), constant B reflects clearly a difference between WT and mutated muscle. The experiment was repeated 4 times for Tg-WT and 5 times for Tg-mutated hearts. **Fig. 37** summarizes the results and shows that there is statistically significant (t=-3.16, P=0.034, paired-test) difference between WT and mutated myofibrils. Correlation function of the rigor control shows no decay at all (**Fig. 36B**).

Fig 36

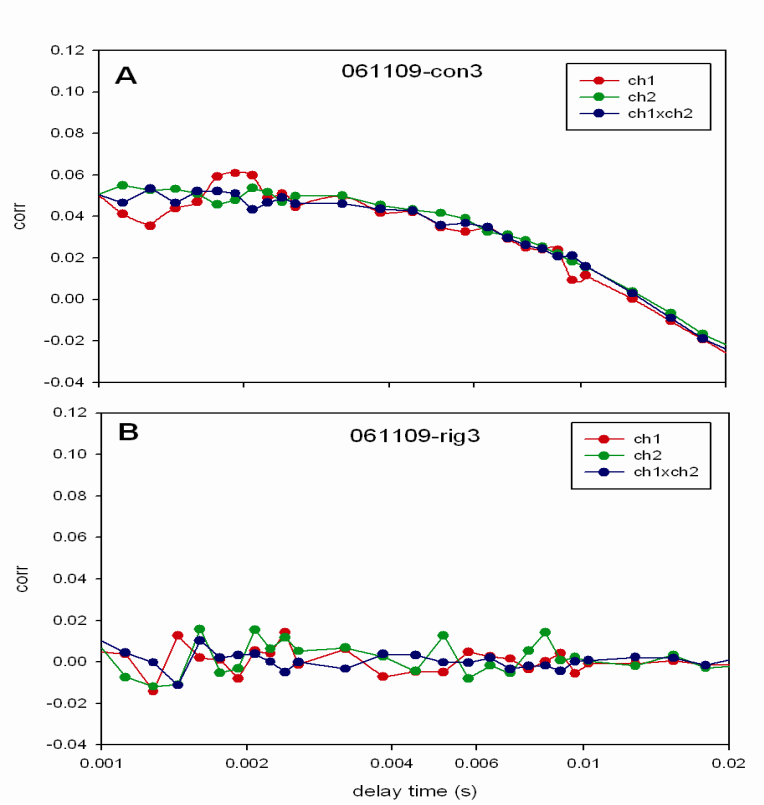

***Fig. 36**. Correlation function of Tg-R58Q myofibrils. A – contracting myofibrils, B – rigor myofibrils. ● -autocorrelation function of ch1 (I_H), ● - ch2 (I_V), ● - cross-correlation ch1 x ch2.*

Fig 37

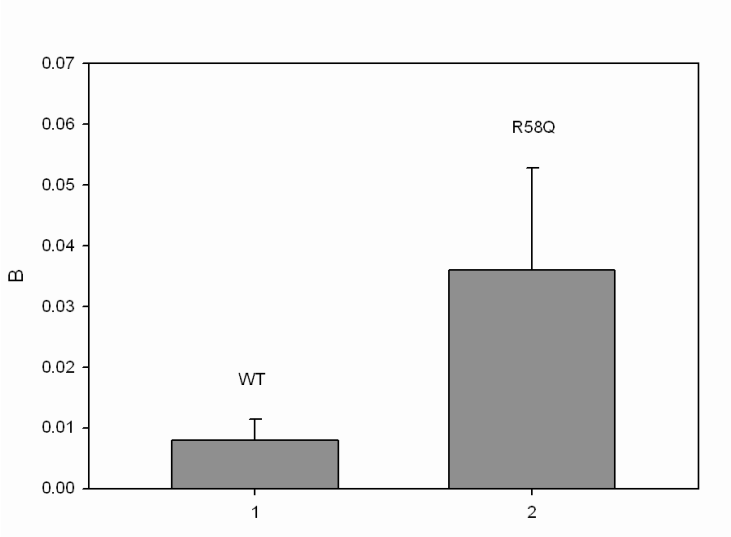

Fig. 37. *Pre-exponential constant B from a fit of WT (left) and mutated (right) myofibrils. The error bar is SD. N=5 for R58Q, 4 for WT.*

DISCUSSION

SPAM can be built in two configurations: Reverse Kretschmann (RK) configuration as described above, when the laser beam strikes a cell directly, and in Kretschmann configuration (KR) where the laser beam strikes a sample from below at SPR angle. RK has the advantages that it avoids losses of intensity due to penetration of mirrored surface, it avoids losses inherent in a dichroic mirror, and it is simpler and less expensive to implement. The RK/SPAM method has three additional characteristic features that make it particularly suitable for FCS:

1. it has excellent background rejection, made possible by the fact that scattered excitation light is unable to penetrate the metal layer and enter the objective (**Fig 32**). In SPAM, the scattered excitation light, which is a predominant problem in FCS measurements in tissue, is unable to penetrate the coverslip which acts as a simple mirror. In conventional detection, however, scattered light has no difficulty penetrating the coverslip and entering the objective.

2. the coupling of the fluorescence is strongly distance dependent and extends only to about fifty nanometers into a sample, smaller than 100-200 nm characteristic of TIRF (**Fig. 33**). It is further reduced at close proximity (below 10 nm) to a surface by quenching by a metal. Thus using SPAM, detection of signal is confined to a window of 10 nm above the surface to 50 nm above the surface of the metal plate. This property of only detecting light that originates from this 40 nm wide window is a main factor in reducing the background signal. In effect, RK-SPAM is equivalent to TIRF excitation without the need to produce evanescent wave.

3. fluorescence coupling to surface plasmons dramatically depends on the orientation of the molecule transition moment, i.e. the method is particularly suited to measurements of protein orientation changes. This feature has been exploited here.

In addition, it is important to note that coupling very well preserves spectral properties of fluorophores (40).

We applied RK/SPAM to study an important biological problem – a Familial Hypertrophic Cardiomyopathy (FHC). It is a serious heart disease that often leads to a sudden cardiac death

(39). The disease is associated with single point mutations which occur in sarcomeric proteins. We are interested specifically in mutation in a genes that encodes for the ventricular myosin regulatory light chain (RLC) (19, 51). In particular we studied R58Q mutation in the myosin RLC. Heart muscle contraction results from periodic interaction of myosin cross-bridges with actin, during which myosin delivers periodic force impulses to the thin filament. It is believed that FHC mutations cause alteration of kinetics of this interaction, causing a heart to pump blood inefficiently (58). We used RK-SPCE to compare the kinetics of interaction of actin with myosin in myofibrils prepared from Tg-WT and Tg-R58Q hearts. The signals were noisy, because they were contributed by a small fraction of ~200,000 actins present in a half-sarcomere. To reduce the noise we applied FCS. The question arises what kinetic parameter does FCS spectrum represent? In FHC muscle carrying D166V mutation in RLC, the fluctuations were well described by ON-OFF binding and dissociation of a myosin cross-bridge. Anisotropy of actin was high when it was immobilized by binding to myosin and low when it was free (detached) from myosin (43). Cross-bridge binding probably inhibited bending modes of the whole filament rather than preventing rotation of the actin monomer because there is no evidence that cross-bridge binding prevents rotation of G-actin (71). As a result, a signal was approximated by a rectangular wave, a "high" of a wave corresponding to high anisotropy of actin when it was immobilized by binding to myosin and "low" by low anisotropy when it was free (detached) from myosin. Corresponding correlation function was a series of triangles which were well reproduced by an experiment. In contrast, correlation function of R58Q muscles was not a series of triangles. It was best approximated by a single exponential function. The kinetic parameter extracted from the correlation spectra was the amplitude of correlation function. This parameter showed statistically significant difference between Tg-WT and Tg-mutated heart muscle. We

recognize that fitting our data to simple exponential decay is a gross oversimplification of the actual events. The orientation change of myosin cross-bridges, and therefore of actin, does not occur in a single reversible step, but as suggested by asymmetry of histogram shown in inset to **Fig. 35A**, it probably occurs in a series of smaller steps. Moreover, it is reversed in a series of mechanical steps, each associated with definite biochemical transition (26, 46). Finally, some rotation of the rhodamine moiety does occur during the excited state lifetime (unpublished data) and the emission is observed through polarizers. Nevertheless, exponential kinetics effectively reflects difference in kinetics of healthy and diseased heart. The fact that the amplitude is increased in mutated muscle is consistent with the fact that ATPase rate and the maximal velocity of actin translation in the in-vitro motility assay was larger for R58Q myosin in comparison with WT myosin (38). At the same time, maximal force developed by mutated muscle was not increased, suggesting a decrease in the efficiency of ATP utilization. Thus the present work is consistent with the idea that FHC results from decreased efficiency.

The diagnosis of the disease in human patients is made more complex by the fact that humans are normally heterozygous for FHC disease. Consequently, 50% of their myosin-containing thick filaments are composed of the non-mutant myosin heads interspersed with the FHC mutant heads. We therefore anticipate that 50% of experiments using human tissue would exhibit R58Q-mediated cross-bridge kinetics, and 50% of experiments would exhibit WT-mediated cross-bridge kinetics. On the other hand diagnosis in humans would be made easier by the fact that MYL2 gene expression occurs both in the heart and in the slow skeletal muscle. The biopsies for diagnosis could be therefore obtained from the soleus muscle of the R58Q patients. This could be advantageous not only because biopsied samples are easy to obtain, but also because of the

regular sarcomere organization of the skeletal muscle myofibrils make the experiments easier to perform.

CHAPTER VIII

Summary and Conclusion

Despite significant clinical advances in the treatment of various cardiovascular diseases, mortality rates remain high. FHC is a serious heart disease that often leads to sudden cardiac death (SCD) at young age (1). Expertise in single molecule fluorescence and thorough understanding of skeletal muscle contraction at molecular level is the motivation behind pursuing this challenging project. This research is aimed at elucidating the molecular mechanisms leading to hypertrophic cardiomyopathy in individuals carrying mutations in myosin Regulatory Light Chain (RLC).

We hypothesized that mutations in the regulatory light chain of myosin will alter the cross-bridge kinetics leading to the compromised heart function in FHC individuals. Specifically, I looked at the changes in single molecule of actin during contraction and rigor in myofibrils. During rigor state there is no change in fluorescence intensity fluctuations because there is no change in actin orientation. However, during contraction fluorescence intensity fluctuates depending upon orientation changes of actin driven by myosin filaments. Fluorescence correlation spectroscopy is the preferred technique here to determine the impaired actin and myosin filament cross-bridges in FHC mutations.

Before working with mutant mouse myocardium, I optimized the technique for single molecule actin kinetics in rabbit skeletal muscle. Studies on skeletal muscle lead to the determination of right concentration of rhodamine phalloidin for kinetics assays without problems of photo

bleaching up to ~20seconds. Experiments on skeletal muscle indicated that labeling actin with rhodamine phalloidin offers strict control of molar ratio of concentration of the dye and is ideal for single molecule kinetics (11, 12). We see high anisotropy when a cross-bridge strongly attaches to actin ON-time (t_{ON}) and low anisotropy associated during the OFF-time (t_{OFF}).

The objective of this study is to monitor kinetics of cross bridge in transgenic mouse hearts which carry disease-causing mutations in the RLC of myosin against healthy controls

A relatively convenient and independent way of monitoring the cross bridge kinetics is to follow the environment of a single cross-bridge every 50 msec by measuring the fluorescence lifetime of actin monomer in an isometrically contracting muscle. By comparing the relative contributions of lifetimes, we determined that the lifetime and the fraction of cross-bridges bound to actin during contraction are similar for both Tg-WT and Tg-D166V muscle (43).

Fluorescence anisotropy measurements determined the rate of cross-bridge attachment and detachment during contraction for Tg-WT right ventricle is one fold higher than Tg-D166V mutated right ventricle. The overall cross-bridge turnover rate for Tg-WT is one fold higher than Tg-D166V ventricle.

The kinetic rate 2.4 fold larger in contracting cardiac myofibrils of Tg-R58Q mice compared to control Tg-wild type (WT). The R58Q-induced increase in myosin cross-bridge kinetics, occurring simultaneously with lower levels of force generation, significantly contributes to the inability of the R58Q mutated hearts to efficiently pump blood. R58Q hearts may be prone to

inefficient energy utilization that would ultimately lead to metabolite accumulation and compromised heart performance. These conclusions may well result in improved risk assessment ultimately lead to development of cardiomyocyte and myosin light chain specific treatments.

Studies on A13T mutation indicated decreased cross bridge turnover rate in myosin cross-bridge kinetics with regard to wild type. The slow force relaxation rate of the fibers could potentially result in diastolic dysfunction of the A13T mutated myocardium. These changes, if severe enough, would ultimately result in compensatory hypertrophy and could lead to sudden cardiac death.

Kinetics of a single cross bridge measured by Reverse Kretschmann Fluorescence addressed the typical problems encountered in FCS measurements and allows observing few molecules by producing extremely thin optical sectioning and by providing excellent background rejection. These studies consistent with the idea that FHC results from decreased efficiency of heart to pump blood. The conclusions drawn here and the techniques mentioned here might be used for the development of novel diagnostic tool for earlier detection of the disease (42).

Future studies would involve studying the cross bridge kinetics of various other pathological mutations in FHC and understanding the disease pathology at single molecule level and translate these studies to cellular level. Translation of single molecule studies to cellular level will help to understand the mechanism of action of individual mutations to cause FHC (52, 54, 65).

Further complete picture of cross bridge kinetics can be obtained by measuring transient kinetics of Single Cross Bridge. This can be achieved by the sudden release of ATP from a caged precursor by rapid UV pulse. Electron Microscopic CCD camera can be used to collect the signal

after the flash of UV pulse. These transient kinetics data will answer the efficiency of dissociation and binding of a cross-bridge from thin filaments, ADP release from the active site of single cross-bridges of transgenic cardiac myofibrils from FHC mice versus ADP release from myosin of healthy transgenic controls.

Finally techniques like silver island films (SIFs), SIFS on metal or Monolayers of silver nanoparticles would be of great interest to study these kinetics since these are well known for decreased photobleaching while enhanced fluorescence intensity (45, 47).

This project addresses the disease pathology, scope for improved risk assessment and may ultimately lead to the development of specific treatments. The results of our studies significantly contribute to the development of targeted cellular therapeutics to treat FHC related cardiac dysfunction. In addition, the single molecule experiments and methods will have numerous applications in monitoring ligand receptor interactions in live cells, involvement of protein molecules in internalization of bacteria by cells, conformational fluctuations of DNA and in detection of viruses at an early phase of infection.

REFERENCES

1. Abraham, T. P., Jones, M., Kazmierczak, K., Liang, H. Y., Pinheiro, A. C., Wagg, C. S., Lopaschuk, G. D., and Szczesna-Cordary, D. (2009) Diastolic Dysfunction in Familial Hypertrophic Cardiomyopathy Transgenic Model Mice. Cardiovasc. Res. 82, 84-92.

2. Aguirre, R., Gonsoulin, F., and Cheung, H. C. (1986) Interaction of Fluorescently Labeled Myosin Subfragment 1 with Nucleotides and Actin. Biochemistry. 25, 6827-6835.

3. Alcalai, R., Seidman, J. G., and Seidman, C. E. (2008) Genetic Basis of Hypertrophic Cardiomyopathy: From Bench to the Clinics. J. Cardiovasc. Electrophysiol. 19, 104-110.

4. Ao, X., and Lehrer, S. S. (1995) Phalloidin Unzips Nebulin from Thin Filaments in Skeletal Myofibrils. J. Cell. Sci. 108 (Pt 11), 3397-3403.

5. Ashrafian, H., Redwood, C., Blair, E., and Watkins, H. (2003) Hypertrophic Cardiomyopathy:A Paradigm for Myocardial Energy Depletion. Trends Genet. 19, 263-268.

6. Baker JE, Brosseau C, Joel PB, Warshaw DM. 2002. The biochemical kinetics underlying actin movement generated by one and many skeletal muscle myosin molecules. Biophys J. 82(4):2134–2147.

7. Barcellona, M. L., Gammon, S., Hazlett, T., Digman, M. A., and Gratton, E. (2004) Polarized Fluorescence Correlation Spectroscopy of DNA-DAPI Complexes. Microsc. Res. Tech. 65, 205-217.

8. Barreiro, O., Zamai, M., Yanez-Mo, M., Tejera, E., Lopez-Romero, P., Monk, P. N., Gratton, E., Caiolfa, V. R., and Sanchez-Madrid, F. (2008) Endothelial Adhesion Receptors are Recruited

to Adherent Leukocytes by Inclusion in Preformed Tetraspanin Nanoplatforms. J. Cell Biol. 183, 527-542.

9. Bonne, G., Carrier, L., Richard, P., Hainque, B., and Schwartz, K. (1998) Familial Hypertrophic Cardiomyopathy: From Mutations to Functional Defects. Circ. Res. 83, 580-593.

10. Borejdo, J., Calander, N., Gryczynski, Z., and Gryczynski, I. (2006) Fluorescence Correlation Spectroscopy in Surface Plasmon Coupled Emission Microscope. Opt. Express. 14, 7878-7888.

11. Borejdo, J., Muthu, P., Talent, J., Akopova, I., and Burghardt, T. P. (2007) Rotation of Actin Monomers during Isometric Contraction of Skeletal Muscle. J. Biomed. Opt. 12, 014013.

12. Borejdo, J., Shepard, A., Dumka, D., Akopova, I., Talent, J., Malka, A., and Burghardt, T. P. (2004) Changes in Orientation of Actin during Contraction of Muscle. Biophys. J. 86, 2308-2317.

13. Bukatina, A. E., Fuchs, F., and Watkins, S. C. (1996) A Study on the Mechanism of Phalloidin-Induced Tension Changes in Skinned Rabbit Psoas Muscle Fibres. J. Muscle Res. Cell. Motil. 17, 365-371.

14. Calander, N., Muthu, P., Gryczynski, Z., Gryczynski, I., and Borejdo, J. (2008) Fluorescence Correlation Spectroscopy in a Reverse Kretchmann Surface Plasmon Assisted Microscope. Opt. Express. 16, 13381-13390.

15. Dumka, D., Talent, J., Akopova, I., Guzman, G., Szczesna-Cordary, D., and Borejdo, J. (2006) E22K Mutation of RLC that Causes Familial Hypertrophic Cardiomyopathy in Heterozygous Mouse Myocardium: Effect on Cross-Bridge Kinetics. Am. J. Physiol. Heart Circ. Physiol. 291, H2098-106.

16. Hopkins SC, Sabido-David C, van der Heide UA, Ferguson RE, Brandmeier BD, Dale RE, Kendrick-Jones J, Corrie JE, Trentham DR, Irving M and others. 2002. Orientation changes of the myosin light chain domain during filament sliding in active and rigor muscle. J Mol Biol. 318(5):1275-91.

17. Huxley AF. 1957. A hypothesis for the mechanism of contraction of muscle. Prog. Biophys. Biophys. Chem. 7:255-318.

18. Elson, E. L. (2001) Fluorescence Correlation Spectroscopy Measures Molecular Transport in Cells. Traffic. 2, 789-796.

19. Flavigny, J., Richard, P., Isnard, R., Carrier, L., Charron, P., Bonne, G., Forissier, J. F., Desnos, M., Dubourg, O., Komajda, M., Schwartz, K., and Hainque, B. (1998) Identification of Two Novel Mutations in the Ventricular Regulatory Myosin Light Chain Gene (MYL2) Associated with Familial and Classical Forms of Hypertrophic Cardiomyopathy. J. Mol. Med. 76, 208-214.

20. Foldes-Papp, Z. (2006) What it Means to Measure a Single Molecule in a Solution by Fluorescence Fluctuation Spectroscopy. Exp. Mol. Pathol. 80, 209-218.

21. Garcia, D. I., Lanigan, P., Webb, M., West, T. G., Requejo-Isidro, J., Auksorius, E., Dunsby, C., Neil, M., French, P., and Ferenczi, M. A. (2007) Fluorescence Lifetime Imaging to Detect Actomyosin States in Mammalian Muscle Sarcomeres. Biophys. J. 93, 2091-2101.

22. Gomes, A. V., and Potter, J. D. (2004) Molecular and Cellular Aspects of Troponin Cardiomyopathies. Ann. N. Y. Acad. Sci. 1015, 214-224.

23. Gordon, A. M., Homsher, E., and Regnier, M. (2000) Regulation of Contraction in Striated Muscle. Physiol. Rev. 80, 853-924.

24. Greenberg, M. J., Watt, J. D., Jones, M., Kazmierczak, K., Szczesna-Cordary, D., and Moore, J. R. (2009) Regulatory Light Chain Mutations Associated with Cardiomyopathy Affect Myosin Mechanics and Kinetics. J. Mol. Cell. Cardiol. 46, 108-115.

25. Gryczynski, I., Malicka, J., Jiang, W., Fischer, H., Chan, W. C., Gryczynski, Z., Grudzinski, W., and Lakowicz, J. R. (2005) Surface-Plasmon-Coupled Emission of Quantum Dots. J Phys Chem B. 109, 1088-1093.

26. Gryczynski, Z., Gryczynski, I., Matveeva, E., Malicka, J., Nowaczyk, K., and Lakowicz, J. R. (2004) Surface-Plasmon-Coupled Emission: New Technology for Studying Molecular Processes. Methods Cell Biol. 75, 73-104.

27. Gryczynski, Z. K. (2008) FCS Imaging--a Way to Look at Cellular Processes. Biophys. J. 94, 1943-1944.

28. Heineke, J., and Molkentin, J. D. (2006) Regulation of Cardiac Hypertrophy by Intracellular Signalling Pathways. Nat. Rev. Mol. Cell Biol. 7, 589-600.

29. Hernandez, O. M., Housmans, P. R., and Potter, J. D. (2001) Invited Review: Pathophysiology of Cardiac Muscle Contraction and Relaxation as a Result of Alterations in Thin Filament Regulation. J. Appl. Physiol. 90, 1125-1136.

30. Herrmann, C., Lionne, C., Travers, F., and Barman, T. (1994) Correlation of ActoS1, Myofibrillar, and Muscle Fiber ATPases. Biochemistry. 33, 4148-4154.

31. Herrmann, C., Sleep, J., Chaussepied, P., Travers, F., and Barman, T. (1993) A Structural and Kinetic Study on Myofibrils Prevented from Shortening by Chemical Cross-Linking. Biochemistry. 32, 7255-7263.

32. Ishiwata, S., Shimamoto, Y., Suzuki, M., and Sasaki, D. (2007) Regulation of Muscle Contraction by Ca2+ and ADP: Focusing on the Auto-Oscillation (SPOC). Adv. Exp. Med. Biol. 592, 341-358.

33. Keren, A., Syrris, P., and McKenna, W. J. (2008) Hypertrophic Cardiomyopathy: The Genetic Determinants of Clinical Disease Expression. Nat. Clin. Pract. Cardiovasc. Med. 5, 158-168.

34. Lakowicz, J. R., Malicka, J., Matveeva, E., Gryczynski, I., and Gryczynski, Z. (2005) Plasmonic Technology: Novel Approach to Ultrasensitive Immunoassays. Clin. Chem. 51, 1914-1922.

35. Lankford, E. B., Epstein, N. D., Fananapazir, L., and Sweeney, H. L. (1995) Abnormal Contractile Properties of Muscle Fibers Expressing Beta-Myosin Heavy Chain Gene Mutations in Patients with Hypertrophic Cardiomyopathy. J. Clin. Invest. 95, 1409-1414.

36. Lionne, C., Iorga, B., Candau, R., and Travers, F. (2003) Why Choose Myofibrils to Study Muscle Myosin ATPase? J. Muscle Res. Cell. Motil. 24, 139-148.

37. Lips, D. J., deWindt, L. J., van Kraaij, D. J., and Doevendans, P. A. (2003) Molecular Determinants of Myocardial Hypertrophy and Failure: Alternative Pathways for Beneficial and Maladaptive Hypertrophy. Eur. Heart J. 24, 883-896.

38. Lowey, S. (2002) Functional Consequences of Mutations in the Myosin Heavy Chain at Sites Implicated in Familial Hypertrophic Cardiomyopathy. Trends Cardiovasc. Med. 12, 348-354.

39. Maron, B. J. (2002) The Young Competitive Athlete with Cardiovascular Abnormalities: Causes of Sudden Death, Detection by Preparticipation Screening, and Standards for Disqualification. Card. Electrophysiol. Rev. 6, 100-103.

40. Matveeva, E. G., Gryczynski, Z., Malicka, J., Lukomska, J., Makowiec, S., Berndt, K. W., Lakowicz, J. R., and Gryczynski, I. (2005) Directional Surface Plasmon-Coupled Emission: Application for an Immunoassay in Whole Blood. Anal. Biochem. 344, 161-167.

41. Morales MF. 1984. Calculation of the polarized fluorescence from a labeled muscle fiber. Proc Nat Acad Sci USA 81:145-9.

42. Mettikolla, P., Calander, N., Luchowski, R., Gryczynski, I., Gryczynski, Z., and Borejdo, J. (2010) Kinetics of a Single Cross-Bridge in Familial Hypertrophic Cardiomyopathy Heart Muscle Measured by Reverse Kretschmann Fluorescence. J. Biomed. Opt. 15, 017011.

43. Mettikolla, P., Luchowski, R., Gryczynski, I., Gryczynski, Z., Szczesna-Cordary, D., and Borejdo, J. (2009) Fluorescence Lifetime of Actin in the Familial Hypertrophic Cardiomyopathy Transgenic Heart. Biochemistry. 48, 1264-1271.

44. Morimoto, S. (2008) Sarcomeric Proteins and Inherited Cardiomyopathies. Cardiovasc. Res. 77, 659-666.

45. Muthu, P., Gryczynski, I., Gryczynski, Z., Talent, J. M., Akopova, I., and Borejdo, J. (2008) Decreasing Photobleaching by Silver Nanoparticles on Metal Surfaces: Application to Muscle Myofibrils. J. Biomed. Opt. 13, 014023.

46. P.Muthu,P.Mettikolla , R. Luchowski, I. Gryczynski, Z. Gryczynski, D. Szczesna-Cordary, and J. Borejdo, Single Molecule Kinetics in the Familial Hypertrophic Cardiomyopathy D166V Mutant Mouse Heart. Journal of Molecular and Cellular Cardiology. xxx (2009) xxx–xxx.

47. Muthu, P., Talent, J. M., Gryczynski, I., and Borejdo, J. (2008) Cross-Bridge Duty Cycle in Isometric Contraction of Skeletal Myofibrils. Biochemistry. 47, 5657-5667.

48. Prochniewicz-Nakayama, E., Yanagida, T., and Oosawa, F. (1983) Studies on Conformation of F-Actin in Muscle Fibers in the Relaxed State, Rigor, and during Contraction using Fluorescent Phalloidin. J. Cell Biol. 97, 1663-1667.

49. Rayment, I., Holden, H. M., Whittaker, M., Yohn, C. B., Lorenz, M., Holmes, K. C., and Milligan, R. A. (1993) Structure of the Actin-Myosin Complex and its Implications for Muscle Contraction. Science. 261, 58-65.

50. Reedy, M. C. (2000) Visualizing Myosin's Power Stroke in Muscle Contraction. J. Cell. Sci. 113 (Pt 20), 3551-3562.

51. Richard, P., Charron, P., Carrier, L., Ledeuil, C., Cheav, T., Pichereau, C., Benaiche, A., Isnard, R., Dubourg, O., Burban, M., Gueffet, J. P., Millaire, A., Desnos, M., Schwartz, K., Hainque, B., Komajda, M., and EUROGENE Heart Failure Project. (2003) Hypertrophic Cardiomyopathy: Distribution of Disease Genes, Spectrum of Mutations, and Implications for a Molecular Diagnosis Strategy. Circulation. 107, 2227-2232.

52. Rivero, J. L., Serrano, A. L., Barrey, E., Valette, J. P., and Jouglin, M. (1999) Analysis of Myosin Heavy Chains at the Protein Level in Horse Skeletal Muscle. J. Muscle Res. Cell. Motil. 20, 211-221.

53. Rodriguez, J. E., McCudden, C. R., and Willis, M. S. (2009) Familial Hypertrophic Cardiomyopathy: Basic Concepts and Future Molecular Diagnostics. Clin. Biochem. 42, 755-765.

54. Roopnarine, O. (2003) Mechanical Defects of Muscle Fibers with Myosin Light Chain Mutants that Cause Cardiomyopathy. Biophys. J. 84, 2440-2449.

55. Schaub, M. C., Hefti, M. A., Zuellig, R. A., and Morano, I. (1998) Modulation of Contractility in Human Cardiac Hypertrophy by Myosin Essential Light Chain Isoforms. Cardiovasc. Res. 37, 381-404.

56. Schiaffino, S., Gorza, L., Sartore, S., Saggin, L., Ausoni, S., Vianello, M., Gundersen, K., and Lomo, T. (1989) Three Myosin Heavy Chain Isoforms in Type 2 Skeletal Muscle Fibres. J. Muscle Res. Cell. Motil. 10, 197-205.

57. Shepard, A. A., Dumka, D., Akopova, I., Talent, J., and Borejdo, J. (2004) Simultaneous Measurement of Rotations of Myosin, Actin and ADP in a Contracting Skeletal Muscle Fiber. J. Muscle Res. Cell. Motil. 25, 549-557.

58. Szczesna, D. (2003) Regulatory Light Chains of Striated Muscle Myosin. Structure, Function and Malfunction. Curr. Drug Targets Cardiovasc. Haematol. Disord. 3, 187-197.

59. Szczesna, D., Ghosh, D., Li, Q., Gomes, A. V., Guzman, G., Arana, C., Zhi, G., Stull, J. T., and Potter, J. D. (2001) Familial Hypertrophic Cardiomyopathy Mutations in the Regulatory Light Chains of Myosin Affect their Structure, Ca2+ Binding, and Phosphorylation. J. Biol. Chem. 276, 7086-7092.

60. Szczesna, D., and Lehrer, S. S. (1993) The Binding of Fluorescent Phallotoxins to Actin in Myofibrils. J. Muscle Res. Cell. Motil. 14, 594-597.

61. Szczesna-Cordary, D., Guzman, G., Ng, S. S., and Zhao, J. (2004) Familial Hypertrophic Cardiomyopathy-Linked Alterations in Ca2+ Binding of Human Cardiac Myosin Regulatory Light Chain Affect Cardiac Muscle Contraction. J. Biol. Chem. 279, 3535-3542.

62. Szczesna-Cordary, D., Guzman, G., Zhao, J., Hernandez, O., Wei, J., and Diaz-Perez, Z. (2005) The E22K Mutation of Myosin RLC that Causes Familial Hypertrophic Cardiomyopathy

Increases Calcium Sensitivity of Force and ATPase in Transgenic Mice. J. Cell. Sci. 118, 3675-3683.

63. Szczesna-Cordary, D., Jones, M., Moore, J. R., Watt, J., Kerrick, W. G., Xu, Y., Wang, Y., Wagg, C., and Lopaschuk, G. D. (2007) Myosin Regulatory Light Chain E22K Mutation Results in Decreased Cardiac Intracellular Calcium and Force Transients. FASEB J. 21, 3974-3985.

64. Takagi, Y., Shuman, H., and Goldman, Y. E. (2004) Coupling between Phosphate Release and Force Generation in Muscle Actomyosin. Philos. Trans. R. Soc. Lond. B. Biol. Sci. 359, 1913-1920.

65. Tardiff, J. C. (2005) Sarcomeric Proteins and Familial Hypertrophic Cardiomyopathy: Linking Mutations in Structural Proteins to Complex Cardiovascular Phenotypes. Heart Fail. Rev. 10, 237-248.

66. Thierfelder, L., Watkins, H., MacRae, C., Lamas, R., McKenna, W., Vosberg, H. P., Seidman, J. G., and Seidman, C. E. (1994) Alpha-Tropomyosin and Cardiac Troponin T Mutations Cause Familial Hypertrophic Cardiomyopathy: A Disease of the Sarcomere. Cell. 77, 701-712.

67. Toprak E, Enderlein J, Syed S, McKinney SA, Petschek RG, Ha T, Goldman YE, Selvin PR. 2006. Defocused orientation and position imaging (DOPI) of myosin V. Proc Natl Acad Sci U S A. 103(17):6495-9. Epub 2006 Apr 13.

68. Wang, Y., Xu, Y., Kerrick, W. G., Wang, Y., Guzman, G., Diaz-Perez, Z., and Szczesna-Cordary, D. (2006) Prolonged Ca2+ and Force Transients in Myosin RLC Transgenic Mouse Fibers Expressing Malignant and Benign FHC Mutations. J. Mol. Biol. 361, 286-299.

69. Warrick, H. M., and Spudich, J. A. (1987) Myosin Structure and Function in Cell Motility. Annu. Rev. Cell Biol. 3, 379-421.

70. Warshaw DM, Hayes E, Gaffney D, Lauzon AM, Wu J, Kennedy G, Trybus K, Lowey S, Berger C. 1998. Myosin conformational states determined by single fluorophore polarization. Proc Natl Acad Sci U S A 95(14):8034-8039.

71. Yanagida T, Oosawa F. 1978. Polarized fluorescence from epsilon-ADP incorporated into F-actin in a myosin-free single fiber: conformation of F-actin and changes induced in it by heavy meromyosin. J Mol Biol. 126(3):507-24.